Two supramolecular methods for detecting a cancer metabolite with cucurbituril

by

Wei Li
Diploma, British Columbia Institute of Technology, 2012
B.Sc., Jilin University, 1988

A Thesis Submitted in Partial Fulfillment
of the Requirements for the Degree of

MASTER OF SCIENCE

in the Department of Chemistry

Supervisory Committee

Two supramolecular methods for detecting a cancer metabolite with cucurbituril

by

Wei Li
Diploma, British Columbia Institute of Technology, 2012
B.Sc., Jilin University, 1988

Supervisory Committee

Dr. Fraser Hof, Department of Chemistry
Supervisor

Dr. Alexandre Brolo, Department of Chemistry
Departmental Member

Dr. Reuven Gordon, Department of Electrical & Computer Engineering
Outside Member

Abstract

Supervisory Committee
Dr. Fraser Hof, Department of Chemistry
Supervisor
Dr. Alexandre Brolo, Department of Chemistry
Departmental Member
Dr. Reuven Gordon, Department of Electrical & Computer Engineering
Outside Member

The enzyme spermidine/spermine N1-acetyltransferase (SSAT) is a candidate biomarker for various cancers as its activity in cancerous tissues is significantly increased. An artificial molecule, amantadine, is exclusively acetylated by SSAT to acetylamantadine (AcAm), levels of which in urine can serve as a proxy biomarker for malignancy. Current method of AcAm detection is laborious, time-consuming, and lacks the possibility of transforming to a point-of-care device. In this thesis, two different approaches were applied to detect AcAm in deionized water and in human urine using optical methods. The first one was fluorescence-based indicator displacement assay using cucurbit[7]uril as the receptor molecule. The second was programmed gold nanoparticle disaggregation with cucurbit[7]uril as a molecular linker.

Table of Contents

List of Figures

List of Schemes

Abbreviations

Ala	Alanine
1,8-ANS	1-Anilinonaphthalene-8-Sulfonic Acid
Abs	Absorbance
AcAm	Acetyl amantadine
Am	Amantadine
AuNP	Gold nanoparticle
BzAm	Benzoyl amantadine
BER	Berberine
CB7	Cucurbit[7]uril
CBn	Cucurbit[n]uril
dF	Change of fluorescence intensity
GC	Gas chromatography
GC20	20 nm gold nanoparticles
Gly	Glycine
dH_2O	Deionized water
IDA	Indicator displacement assay
Iso-Leu	Isoleucine
LC	Liquid chromatography
Leu	Leucine
LLE	Liquid-liquid extract
LSPR	Localized surface plasmon resonance
MB	Methylene blue

MS	Mass spectrometry
Phe	Phenylalanine
Pro	Proline
RhB	Rhodamine B
RhG	Rhodamine G
SERS	Surface enhanced Raman spectrum
SPE	Solid phase extraction
SSAT	Spermidine/spermine N_1-acetyltransferase
TO	Thiazole orange
Trp	Tryptophan
Val	Valine

Acknowledgments

I would like to express my deepest gratitude to my supervisor Professor Fraser Hof for giving me such a wonderful opportunity to work in the group. I appreciate his continuous guidance, support, and encouragement throughout my study. He taught me not only science but also how to be a scholar. I am very grateful to Professor Reuven Gordon for his help and guidance, and I am very grateful to Professor Alex Brolo for his encouragement and directions. I would like to thank Professor Peter Wan for his generous help as well.

I would like to thank all who have inspired, encouraged, and supported me during my study at University of Victoria in the past three years. I would like to thank all of my wonderful group members.

I would like to thank my parents for their love and support. My dad has been inspiring, encouraging and supporting me to pursue my dreams. I would like to thank my wife and my two beautiful daughters for their love and support. Without their support, it would be impossible for me to complete my study. Especially, I would like to thank the little one, Angelina, now 7 years old of age, for her understanding. Angelina often says this to me when I am about to leave home for school after dinner: “Don’t go, daddy. I want you to stay because I do not see you often … … now you go, you go early so that you come back home early”.

Dedication

To Mom and Dad

and

Rachel and Angelina, my lovely daughters, and their Mom

Chapter 1: Introduction

1.1 Background

Cancer is a leading cause of death worldwide.[1] The number of new cancer cases is expected to increase 40% in the next 15 years in Canada due to aging and growing population.[2] Among all cancers, lung cancer is the most commonly diagnosed in this country (excluding non-melanoma skin cancers) and it accounts for 14% of all new cases of cancer. It is the leading cause of death from all cancers for both men and women in Canada and worldwide.[2,3] Cancer has become a major threat to the public health worldwide[4] and it is a burden to the society, therefore cancer has to be controlled.

1.2 Early cancer detection through cancer biomarker

Methods of controlling the impact of cancer include preventive measures, advancement of treatments and early cancer detection. Early detection of cancers before they become metastatic and incurable can increase the chances for effective therapy and therefore the survival rate, and decrease suffering.[5]

Cancer detection methods can be categorized into four groups, namely imaging, endoscopy, cell morphology examination from a suspicious tissue sample, and analysis of a cancer biomarker conducted at a medical laboratory. This thesis focuses on biomarker detection, therefore other detection methods will be addressed only briefly. Cell morphology examinations are performed on blood films or stained tissue sections made from biopsy or cytology specimens. They are regarded as the gold standard for cancer detection.[6] However, the process is time consuming and the images of cells or tissues are difficult to grade in a reproducible manner.[6] There has been tremendous progress in

imaging technology in recent years, such as mammograms, x-ray computed tomography (x-ray CT) and magnetic resonance imaging (MRI).[7] There is limit to its sensitivity, as tumors that are less than 1 cm can be detected only on rare occasions.[8] In addition, fluorescence imaging proves to be an appealing technology for the detection of cancer at the cellular level,[9] which can provide fast cancer screening. The drawback of this technique is that the conventional fluorescent dyes go through photo bleaching process easily and sufficient target-to-background ratio is hard to achieve.[10] Therefore finding ways to prevent fluorescent dyes from photo bleaching and to enhance their optical properties is an on-going effort.[10,11]

Cancer biomarker refers to a molecule secreted by a cancerous tumor or a specific molecular response of the host to the presence of cancer. Cancer biomarkers can be DNA, mRNA, proteins, or metabolites. Protein biomarkers include enzymes, glycoproteins, oncofetal antigens and receptors.[12] Despite intensive research efforts, some cancer biomarkers remain too insensitive or nonspecific for effective cancer detection.[13] For example, prostate specific antigen (PSA) is used as a biomarker for prostate cancer, however, it is not very specific. In one study, about half of the tumors with the PSA value ranged from 0 to 4.0 ng/mL (generally considered to be the normal range[14]) had aggressive features, which should be diagnosed and treated.[15] On the other hand, a false-positive test result may occur when a man's PSA level is elevated but he actually does not have cancer. Most men with a positive PSA result (> 4.0 ng/mL) do not have prostate cancer; only about 25% of men having an elevated PSA value actually have the cancer, which is confirmed by prostate biopsy study.[16] U.S. Preventive Services Task Force (USPSTF) believes that PSA-based screening for prostate cancer may benefit a small number of men but will bring

harm to many others. Most positive PSA test results lead to biopsy which brings about moderate or major harms to 33% of men; treatment may result in complications such as serious cardiovascular events, erectile dysfunction, and even death.[17] USPSTF recommends against PSA-based screening for prostate cancer.[17]

As far as lung cancer detection is concerned, no molecular biomarkers for early stage cancers have been discovered that have clinical usefulness.[18] Therefore, development of cancer biomarkers with good sensitivity, selectivity and stability is desirable, challenging and urgently needed.[5]

1.2.1 Polyamines and SSAT

Polyamines (putrescine, spermidine, and spermine) exist as aliphatic polycations at biological pH. They play vital roles in both eukaryotic and prokaryotic cell growth, differentiation, ion channel activity[19] and other functions. They interact with many macromolecules producing cellular effects.[20] Their metabolic pathways are highly regulated and their concentrations inside cells are rigorously controlled.[19] In general, rapid growing cells contain high concentrations of polyamines. Concentrations of polyamines in certain types of cancer cells are also elevated.[21]

Spermidine/spermine N^1-acetyltransferase (SSAT) is an enzyme that carries out spermidine/spermine acetylation reaction on the aminopropyl moieties in vivo (Figure 1.1).[22] SSAT is a GCN5-related N-acetyltransferase (GNAT) superfamily of acetyltransferase. The GNAT enzyme contains a conserved fold and in solution it presents as a homodimer. It catalyzes the transfer of acyl groups from acetyl-CoA to the primary amines. Acetylation reduces the positive charges on the polyamines and their ability to bind to acidic macromolecules is changed and so are their functions. SSAT is involved in the

process of cellular polyamine degradation and removal.[23] The concentrations of acetylated polyamines, namely N^1-acetylspermidine and N^1-acetylspermine are small inside normal cells, as they are exported from the cells once produced. However in some tumor cells significant quantities of acetylated polyamines are detected.[21] Therefore there is a link between normal cell growth and neoplastic growth based on the state of polyamine metabolism.[20]

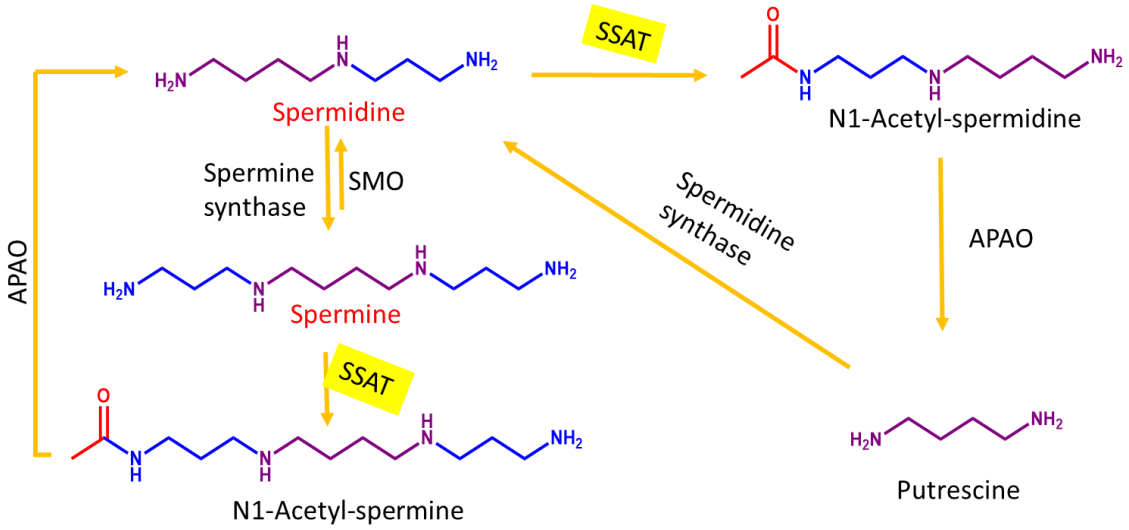

Figure 1.1 Polyamine acetylation catalyzed by SSAT.

The levels of acetyl spermidine in urine from cancer patients increased. This suggests the increased SSAT activity. Therefore SSAT is a candidate biomarker for various cancers.[24,25] Quantification of SSAT can be achieved by enzyme-linked immunosorbent assay (ELISA),[26] but the procedure requires highly-skilled operators and is expensive, time-consuming with minimal signal amplifications. Also, this analysis requires extraction

of a tissue sample in order to measure SSAT levels, because SSAT is not an excreted enzyme.

1.2.2 AcAm is a proxy biomarker for SSAT

Amantadine (1-adamantylamine or 1-aminoadamantane) is a synthetic molecule that is a competent substrate for SSAT. Amantadine is a colorless, stable, achiral, polycyclic aliphatic primary amine with a symmetrical molecular structure. It is a weak base and positively charged at physiological pH. It is an approved drug, and has been used for the prophylaxis and treatment of influenza A infection for decades.[27, 28] It has more recently been used to provide symptomatic relief for Parkinson's disease.[29]

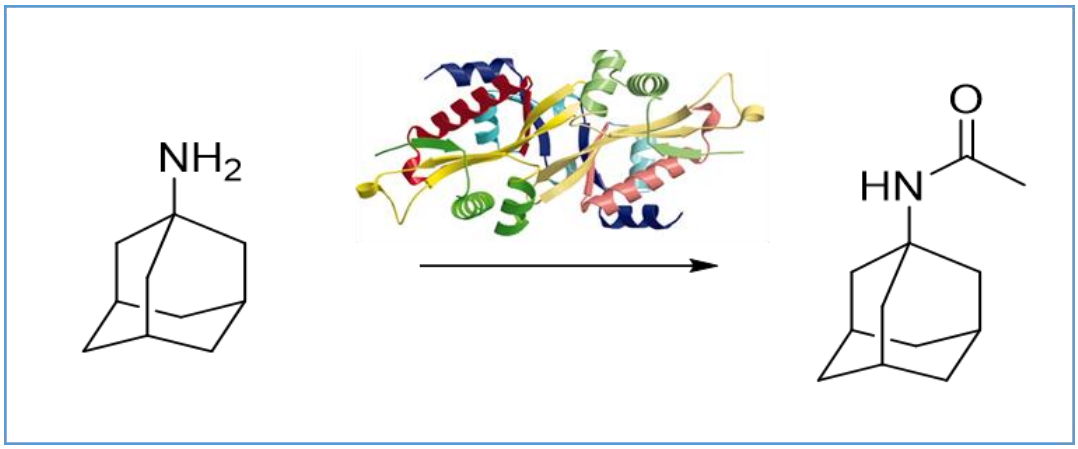

Figure 1.2 SSAT catalyzes acetylation of Am to AcAm.

Acetyl amantadine is the product of the metabolism of amantadine by SSAT, and it is excreted in the urine after being formed elsewhere in the body. A study in mice showed that the drug metabolite is exclusively produced in vivo by SSAT and by no other acetyl transferases.[29] Because amantadine is exclusively acetylated by SSAT to acetylamantadine, as depicted in Figure 1.2, and the enzyme is upregulated in cancer cells,

as depicted in Figure 1.3, there is an association between the presence of AcAm in urine at the nanograms per milliliter level and SSAT enzymatic activity in the body.[30] This correlation is a very important piece of information because amantadine acetylation can serve as a diagnostic tool to measure the activities of SSAT,[29] thus detection and quantification of AcAm in urine has been proposed as a screening method for cancers.[30] The proposal has been made that acetyl amantadine levels in urine can serve as a proxy biomarker for malignancy.[31]

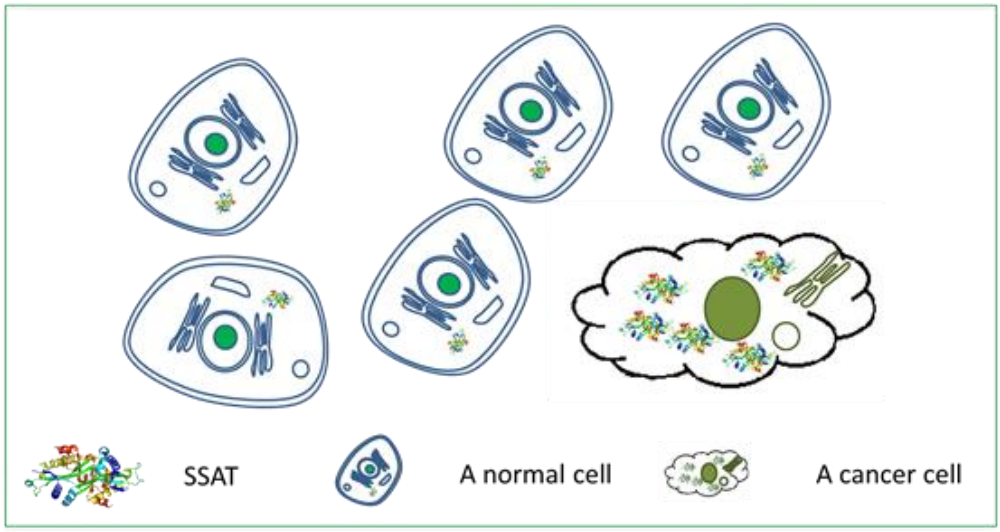

Figure 1.3 SSAT is up-regulated in cancer cells.

1.2.3 Current method of detection of AcAm

1.2.3.1 Urinalysis

Laboratory medicine originated from the analysis of human urine 6000 years ago, which was called uroscopy until the 17th century and now called urinalysis.[32] Urine is readily available (a healthy adult generates 600 – 1600 mL urine daily) and easily collected with no invasive procedures involved.[33] Urine contains more than 2600 different

metabolites.[34] It also contains proteins, sodium, potassium, calcium, chloride and epithelial cells. Bilirubin, nitrite, hemoglobin, glucose, ketones may be present. Leucocytes, erythrocytes, bacteria, casts and crystals are often seen as well. Urinalysis, either macroscopically or microscopically, is of great importance for diagnosis and screening purposes.[33]

In a modern medical laboratory, to be cost-effective, urinalysis starts with the reagent strip (dipstick) analysis of well mixed urine. If the results indicate any one of the following tests to be positive, then a microscopic examination will be conducted on the sediment obtained after centrifugation at relative centrifugal force (**RCF**) of 400 for 5 minutes:[35]

1. Protein
2. Blood
3. Leucocyte esterase
4. Nitrite
5. Bilirubin

Urine levels of sodium, potassium, chloride, urea, creatinine, and albumin are tested using expensive clinical chemistry analyzers by certified technologists as well. A clinical chemistry analyzer is an automated instrument which hosts an array of basic manual laboratory techniques and procedues.[36] Sample (serum, plasma, and body fluids including urine) and reagents are mixed in the reaction vessels, where chemical reactions occur. Detection techniques include electrochemistry, immunoassay, and spectrophotometry. For example, the first step for the detection of serum iron is to release ferric ion from a transport protein, transferrin, by decreasing the pH of the sample. The second step is to reduce ferric

iron to ferrous iron. The third step is to have ferrous iron to react with a chromogen, such as ferrozine.[37] The system monitors the absorbance change, which is directly proportional the iron concentration in the sample.[36]

Urine drug screen can be performed either qualitatively by using a point-of-care device (test kit) or quantitatively by using a chemistry analyzer. These tests are all performed on the supernatant from a spun-urine at 400 RCF for 5 minutes to get rid of formed elements and other interfering substances. The urine sample preparation process is illustrated in Figure 1.4.

Adequate sample preparation is very important for quantitative bioanalysis.[38] The chemical compositions and physical appearance of urine vary from patient to patient; for the same patient it changes as well depending on the state of health, the medications the patient takes, and the food the patient eats. Interfering matrix compounds, such as salts, proteins and liquids should be removed before analysis to improve the sensitivity, selectivity and reliability. There are a couple of sample preparation techniques that can be employed including protein precipitation, liquid-liquid extraction (LLE) and solid-phase extraction (SPE). Centrifugation is the first step of sample preparation. Organic solvents used in urine sample preparation include dichloromethane to remove lipids, acetonitrile to remove proteins.[39,40] LLE and SPE are both time-consuming and labor-intensive.

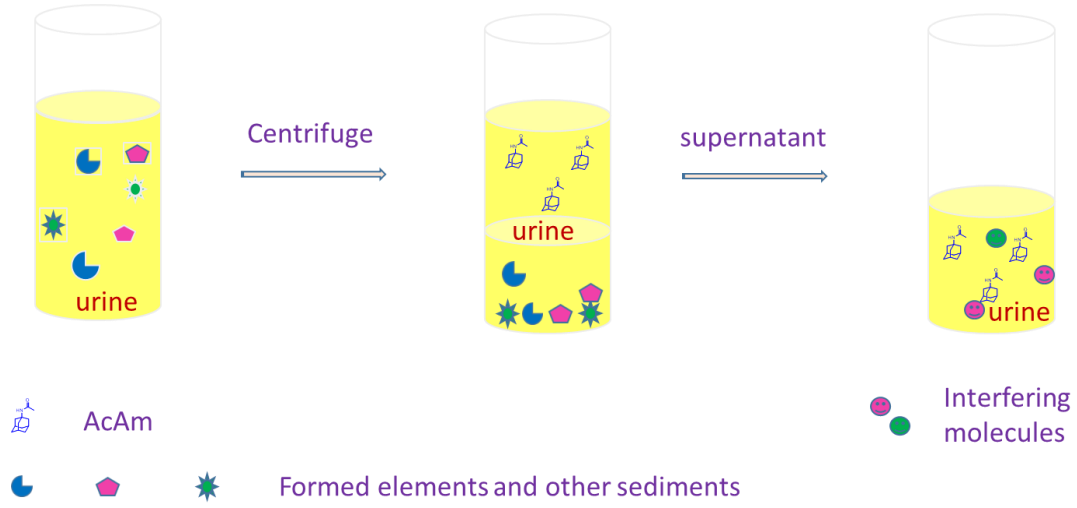

Figure 1.4 A general process of urine sample preparation for testing.

1.2.3.2 AcAm detection

The proposed threshold values for a positive test for AcAm in urine are 10 ng/mL for North American subjects and 1 ng/mL for Chinese subjects.[30] The level of AcAm in Chinese subjects is lower, which implies that the SSAT activity is lower due to genetic reasons. Therefore, development of detection techniques for AcAm in urine with detection limit being 1 ng/mL with desired specificity, sensitivity, and reproducibility is very important in early cancer detection.

The current method for AcAm detection and quantification in urine involves solid phase extraction (SPE) and liquid chromatography with tandem mass spectrometry (LC-MS/MS), with a limit of detection of about 10 ng/mL.[24] LC-MS/MS is a very powerful analytical tool in organic compound analysis which has very high sensitivity and selectivity, however it is not that tolerant of matrix effect, which are mainly due to endogenous composition of biological samples.[41] These substances will be co-eluting with the analyte of interest and interfere with the ionization process. Therefore sample

preparation is a key step to remove or minimize the presence of the interfering components that cause matrix effect.[38,42]

There are two significant problems with the current technique. SPE provides good sample clean-up but the process is very laborious.[43] LC-MS/MS is an expensive equipment setup and requires highly skilled people to operate. This method lacks the possibility of transforming to a point of care device. Therefore alternative methods of AcAm detection and quantification that are rapid, cost-effective, sensitive, and easy to use and with the possibility of generation of a point of care device have been sought after. Importantly, the aforementioned problems with SPE/LC-MS/MS analysis are actually shared by many other analytical processes that rely on LCMS. It is possible that new methods for rapid AcAm detection would also provide solutions that are more broadly applicable in a clinical setting.

1.3. Methods of chemical analysis

1.3.1 Principles of some optical analysis

Chemical sensors are molecules that are designed to change their properties upon interacting with other molecules. A chemical sensor contains a binding subunit (receptor) and a signaling subunit (reporter). When an analyte interact with the binding subunit of the sensor, a change in the microenvironment perturbs the properties of the signaling subunit that registers the alteration of the spectroscopic, redox or some other properties of the system, which can be interpreted as sensor versus analyte response.[44,45] The role of the signaling subunit is to translate the chemical information at the molecular level with a measurable signal.[46] One way of attaching the signaling subunit to the receptor is through covalent bonds, which may be difficult to fulfil; another is by reversible non-covalent forces including hydrogen bonding and electrostatic attractions.

Depending on the sensing mechanism, chemical sensors can be categorized into optical, electrochemical, and mechanical sensors, etc. Optical chemical sensors are based on either light absorption, emission or scattering techniques.[47] The advantages of using optical methods include ease of use, fast, cheap, satisfactory accuracy and precision, adequate specificity and sensitivity, and ready adaptability to automation.[48] They are also often non-toxic in use and can be applied to point-of-care diagnostics.

Molecular vibrations may be detected and measured either in an IR spectrum or in a Raman spectrum. Raman scattering is intrinsically weak, but surface enhance Raman scattering (SERS) finds broad applications in chemical sensing and biosensing.[9, 49] The ultraviolet and visible spectra of organic compounds are produced by the electron transitions between different energy levels.[50]

Absorption techniques used for optical sensors are either colorimetric or spectroscopic in nature. Colorimetric sensors are developed to detect the color change induced by the analyte; spectroscopic sensors are built to detect the intrinsic molecular absorption properties of the analyte.[51] Fluorescence and colorimetric detection techniques will be the focus of this thesis.

1.3.1.1 Principle of spectrophotometric analysis

According Beer's law, absorbance is linearly related to the concentration of the analyte in solution as expressed by equation below,

$$A = - \log (I_S/I_0) = - \log T = abc \qquad (1)$$

where a is molar extinction coefficient with units of $L \cdot mol^{-}1 \cdot cm^{-1}$, b is light path in centimeters, and c is concentration of the absorbing compound with units of $mol \cdot L^{-1}$.[47] T

= $I_S/I_{0,}$ where T is transmittance of light, I_S the intensity of transmitted light for analyte in solution, and I_0 is the intensity of incident light.

1.3.1.2 Principle of spectrofluorometric analysis

Some molecules or atoms absorb radiation at one wavelength and emit some of the energy at a longer wavelength (lower energy). In luminescence spectroscopy, we are interested in the effect of the exciting radiation on the sample, while in absorption spectroscopy, we are interested in the effect that the sample produces on the incident radiation. In luminescence spectroscopy, we are focused on choosing the excitation wavelengths that would produce the most luminescence from the sample. Fluorescence is one kind of luminescence. See Figure 1.5 for luminescence energy level diagram. S_0 is the singlet state at the ground level; S_1 is the first excited singlet state; T_1 is the first excited triplet state; A is the absorption process; RVD is the radiationless vibrational deactivation process; Q is the quenching process; F is the fluorescence process from the first excited singlet state; P is the phosphorescence process and RC is the radiationless crossover process.

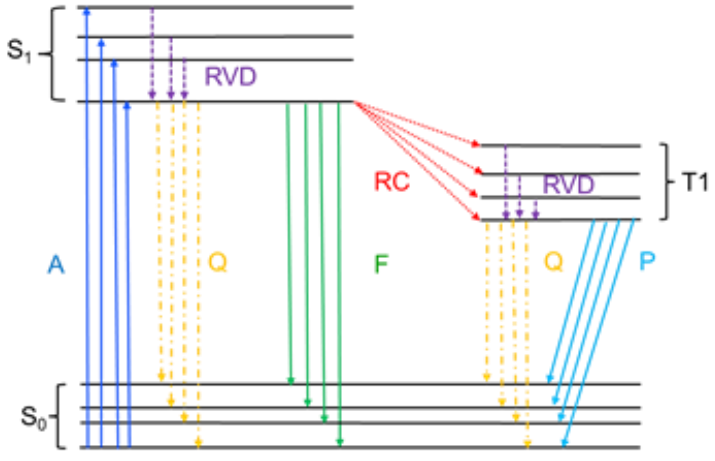

Figure 1.5 Luminescence energy level diagram.

Spectrofluorometry is a more sensitive technique than absorbance measurements. It can be 100 to 1000 times greater than the sensitivity of absorbance measurements through the use of more intense light sources, better filtering techniques, and sensitive emission photometers.[36]

Despite the many advantages that optical methods have on chemical and biochemical analysis, using optical methods to detect AcAm in urine faces some challenges. AcAm has no chromophore, thus it cannot be detected directly by optical methods; photochemistry in complex media, such as urine, is challenging due to the existence of interfering substances; The reproducibility in complex samples is low.

1.3.1.3 Supramolecular tools in optical sensing

Supramolecular chemistry is very helpful to address the above challenges. Macrocyclic molecules such as cyclodextrins (CDs) and cucurbiturils (CBs) have strong binding affinities with AcAm. In complex media, the macrocycles would capture AcAm, thus isolating it from the interferences and protecting it from the quenchers and denaturants.

1.3.2. Supramolecular configurations for spectrofluorometric sensing

1.3.2.1 Indicator displacement assay

In an indicator displacement assay (IDA), the analyte competes with the indicator (chromophore or fluorophore) for the binding pocket of a supramolecular host molecule. Displacement of the indicator from the binding pocket would cause a signal alteration, the degree of which relates to the concentration of the analyte that is present in the system. Schematic representation of IDA is shown in Figure 1.6. The molecular components of the sensor assemblies must be placed with specific orientations in order for the system to work.[52]

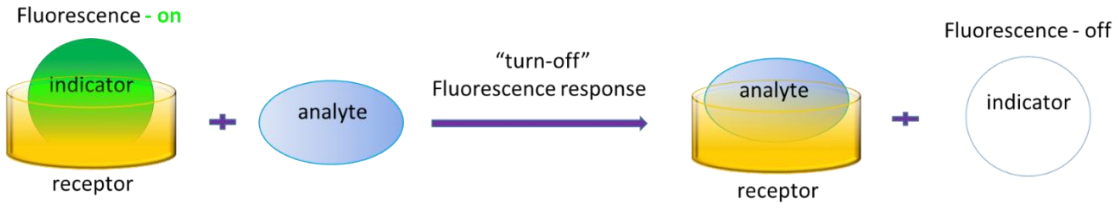

Figure 1.6 Schematic representation of IDA.

The advantages of IDA include: a) different indicators can be tested against one specific receptor molecule in order to find the best indicator/receptor pair; b) because the entire sensing system does not contain extra covalent bond, one can focus on selecting/designing of the receptor molecular first based on the analyte of interest, and choosing an indicator at a later stage; c) the assay works well in both aqueous and organic solvents.[45] It would be helpful to keep in mind that when designing an assay, the binding affinity between the analyte and the receptor should be comparable to that between the indicator and the receptor,[53] otherwise the correlation between the signal change and the analyte concentration would not be suitable for the analyte detection.

IDA has become a standard molecular sensing strategy and many agents have been analyzed using this method, where most of the synthetic receptors are used as recognition subunit,[53] and the colorimetric and fluorescent molecules as the signaling subunit. IDA is not only capable of determining absolute analyte concentrations, it can also be used to monitor analyte concentrations in real-time.[54]

One of the earlier examples of IDA was reported by Inouye in 1994 for the detection of acetylcholine.[55] The receptor chosen was calixarene, the indicator dye was a pyrene-modified N-alkylpyridinium cation. Anslyn's group has developed many chemosensors using the principle to detect molecules such as citrate[56], tartrate,[57] glucose-6-phosphate,[58]

inositol-1,4,5-triphosphate,[59] gallate,[60] heparin,[61] and nitrate.[45] Carboxy and phospho sugars were also detected using the method.[62] The same group recently introduced a mechanically controlled IDA at the air-water interface.[63]

1.3.2.2 Fluorescence based IDA

Fluorescence based indicator displacement assay using macrocycles of cyclodextrin, calixarene, cyclophane, and cucurbiturils (Figure 1.7) as receptor molecules is frequently employed.[54]

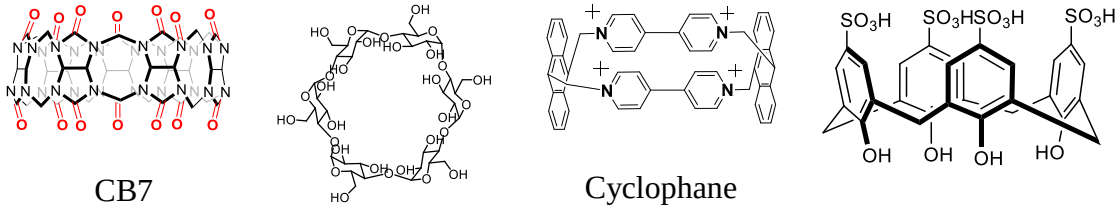

Figure 1.7 Structures of macrocycles.

Using 4-Sulfocalix[4]arene (CX4) as the supramolecular host, lucigenin (LCG) as the fluorescent dye to construct a macrocyclic/fluorescent dye ensemble in a supramolecular tandem membrane assay, Nau was able to monitor the transport of unlabeled protamine, an antimicrobial peptide, through a bacterial transmembrane protein. [64] The working principle is illustrated in Figure 1.8. Macrocyclic host/dye ensemble encapsulated inside a liposome (left) and transport of an analyte through a channel protein into liposome (right). The analyte binds to the macrocycle displacing the dye either turning on or off fluorescence response.

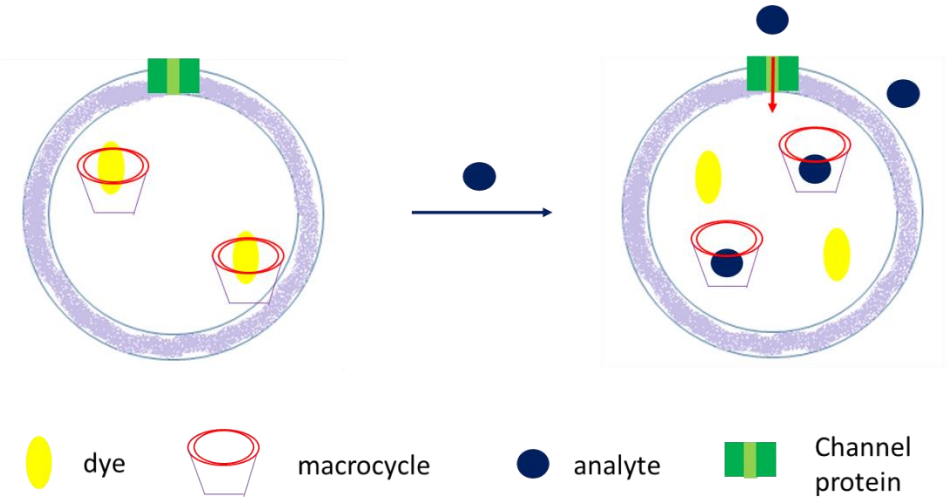

Figure 1.8 Working principle of a supramolecule tandem membrane assay.

For the assay data shown in Figure 1.9, CX4/LCG ensemble was first encapsulated in the liposomes, then OmpF (a channel protein) was added. When protamine was added to the system, fluorescence increased dramatically. This demonstrated that the channel protein helped protamine pass through the lipid bilayer of liposomes. Figure 1.9 also shows results of various control experiments.

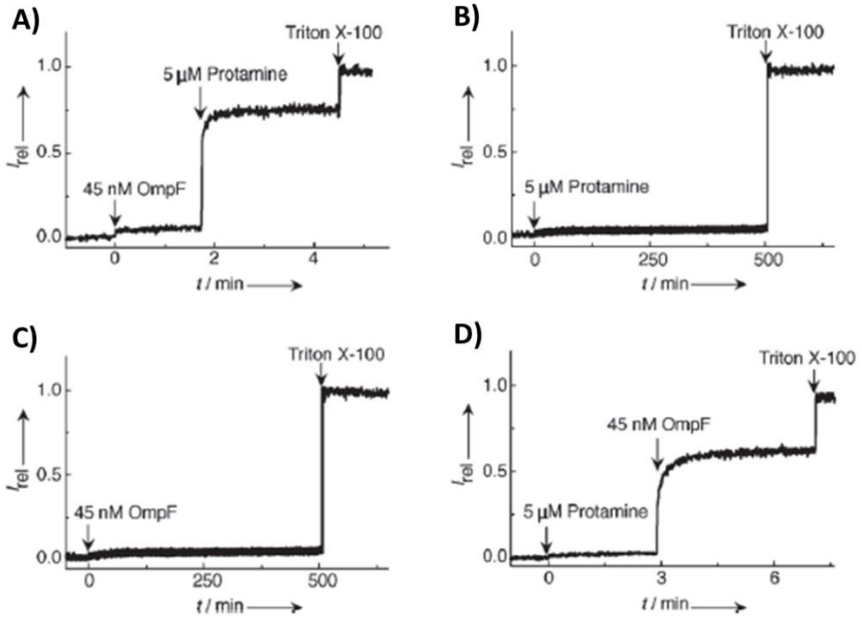

Figure 1.9 Supramolecular tandem membrane assays monitoring protamine translocation. A-D) Fluorescence intensity of CX4/LCG loaded liposomes upon addition of A) 45 nM OmpF (a channel protein) then 5 µM protamine, B) 5 µM protamine, C) 45 nM OmpF, D) 5 µM protamine, then 45 nM OmpF. Reprinted from *Angewandte Chemie International Edition* 2014, *53* (10), 2762-2765, with permission from Wiley.

This method provides micromolar sensitivity and is transferrable to other unlabeled organic analytes, such as natural metabolites, toxins and drugs, which can be recognized by the host molecule. The advancement of IDA technique has also enabled it to measure bioorganic analytes inside live cells.[65]

1.3.3 Colorimetric technique

Colorimetric analysis is simple, fast and cost-effective. The same as the other chemical sensors, a colorimetric sensor consists of a binding site and a signaling site. The modulation created by the interaction of the binding site with the analyte is transferred into color change on the signaling site.[66] The efficiency of the two components are critical in

order to construct a sensor with good response time, signal-to-noise ratio (S/N), sensitivity, and selectivity.[67]

1.3.3.1 Localized surface plasmon resonance

A number of atoms or molecules (10^6 atoms or fewer) bond together to form nanoparticles. The size of nanoparticles ranges from 1 – 100 nm, which is in-between that of individual atoms and bulk materials.

Metallic nanoparticles possess unique optical, electronic, chemical, and magnetic properties that are different from those of the individual atoms and the bulk materials.[68] When the oscillating electromagnetic field of light interacts with noble nanoparticles, the conduction electrons of the nanoparticles undergo a coherent oscillation, which is in resonance at a particular light frequency. This phenomenon is called localized surface plasmon resonance (LSPR) oscillation.[69] The conduction electrons exist as electron gas that moves away from its equilibrium position when interacting with an external light field (Figure 1.10). Surface polarization charges are thus induced that pull the electron gas back to its equilibrium position generating collective oscillation of the free electrons.[70] At the LSPR frequency, the electric field intensity is strongly enhanced as well with molar extinction coefficients as high as 10^{11} M^{-1}•cm^{-1}.[71]

Plasmonic nanoparticles are good signaling moieties. The properties of the nanoparticles to absorb and scatter light have been applied in the detection of metal ions, small molecules, nucleic acids, proteins, and microorganisms.[67] This technique is sensitive, robust, and easy to use. Just like any other methods, shortcomings exit with LSPR detection as well: 1) for small molecules it would require a large number of the molecules to coat the nanoparticle surface in order to get good signal, and 2) for the detection of analytes in

complex biological media, such as serum or urine, interferences are present due to biofouling of the nanoparticle surface.[71]

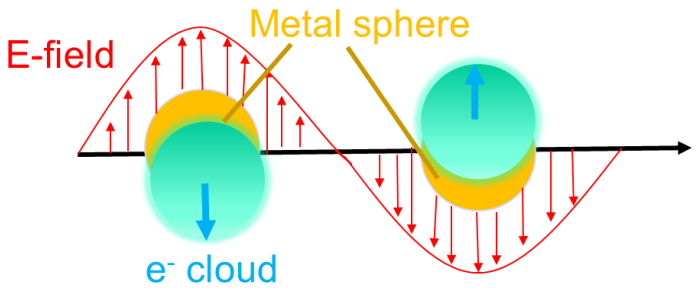

Figure 1.10 Schematic representation of plasmon oscillation for a sphere. It illustrates the displacement of the conduction electron charge cloud relative to the nuclei.

1.3.3.2 Colloidal gold nanoparticles for optical sensing

Not all materials have surface plasmons, but only those with a negative real and small positive imaginary dielectric constant do. Copper, silver and gold all belong to Group 11 in the periodic table. Copper is less stable, therefore silver and gold nanoparticles (AuNPs) are used more often in optical sensing.[69]

Plasmonic nanoparticles are highly dispersible in aqueous media to form colloidal nanoparticles with intense color which is due to the interaction of surface plasmons with light.[72] The study of the optical properties of colloidal gold started in the middle of 1800s.[73]

Plasmon absorption of colloidal AuNPs depends on their size, shape, aggregate morphology, dieletric properties, as well as surface modification and refractive index of the medium and temperature.[74]

AuNPs can be regarded as non-molecular chromophores with very good light collecting capability due to their extremely high molar extinction coefficients.[75] Spherical

AuNPs show different colors in solution as the core size varies from 1 to 100 nm. Their intense absorption peaks are present from 500 to 550 nm as the result of surface plasmon band of the nanoparticles, which is absent in nanoparticles with diameter smaller than 2nm and in bulk materials.[76] For example, the color of 20 nm AuNPs is ruby red due to their strong absorption of green light at 520 nm.[68]

As the distance between the AuNPs deceases, particle–particle coupling at the near-field starts to dominate producing 1) a strong enhancement of the localized electric field within the interparticle spacing ("hot spot") and 2) a strong red shifts of the LSPR frequency.[77]

AuNPs have been widely applied in optical sensing. Colorimetric detection based on nanoparticles is one of the most powerful and simple sensing techniques available.[77] The quantification of DNA by Mirkin and Letsinger's group based on the color change due to the AuNPs aggregation is considered as a milestone discovery.[78,79] They have also been applied for the detection of alkali metals, heavy metals, ions, as well as proteins, nucleic acids, and neutral molecules.[67]

AuNPs are also used for neutral molecule sensing, for example, glucose sensing[80,81] and cocaine sensing. The mechanism and results of cocaine sensing are depicted in Figure 1.11.[82,83] AuNPs are functionalized with aptamers, and aptamer linkers link the nanoparticles to form aggregates producing a color change from ruby red to purple. When cocaine molecules are added to the solution, the AuNP aggregates disassemble and the color of the changes from purple to ruby red. The intensity of the color depends on the concentration of cocaine. The linear range for cocaine is from 50 to 500 μM. The type of colorimetric sensor is simple and cheap to design and operate (Figure 1.12).

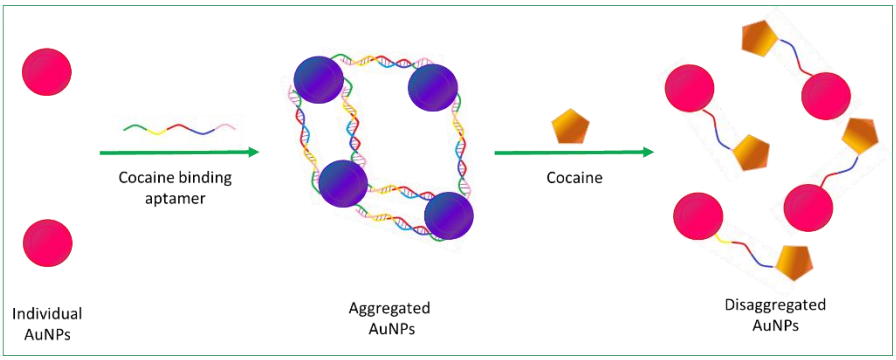

Figure 1.11 Schematic representation of the colorimetric detection of cocaine. It is based on cocaine-induced disassembly of nanoparticle aggregates linked by a cocaine aptamer.

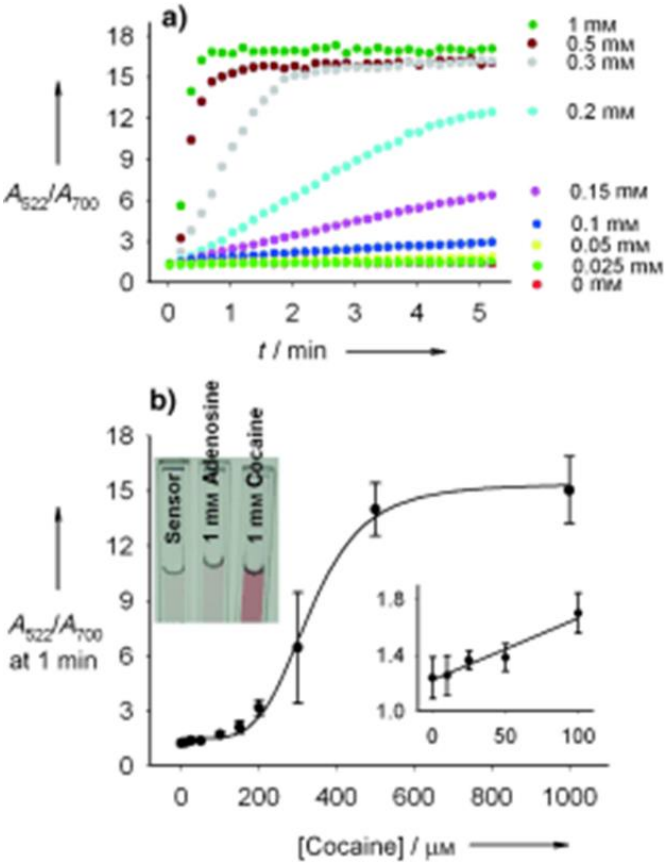

Figure 1.12 Cocaine detection kinetics and its quantification. A) Kinetics of the color change of the cocaine sensor. B) Quantification of cocaine concentration by monitoring the absorbance ratio one minute after the addition of cocaine. Reprinted from *Advanced drug delivery reviews* 62.3 (2010): 316-328, with permission from Elsevier.

A urine-based colorimetric assay of heavy metal ion, such as Hg^{2+}, using AuNPs sensing platform was developed with good sensitivity.[84] (Figure 1.13 and Figure 1.14). Nitrogen-rich components in urine are adsorbed onto the surface of AuNPs with the color remaining ruby red. The main nitrogen-containing molecules in normal urine include urea, uric acid and creatinine[85] (Figure 1.15 for structures), they have similar functional sites as thymine and melamine.[84] However, neither uric acid nor creatinine functionalized AuNPs are linked by Hg^{2+} which is due to the binding sites reduction on uric acid or creatinine for the metal ions because some of those are used onto binding AuNPs.[84]

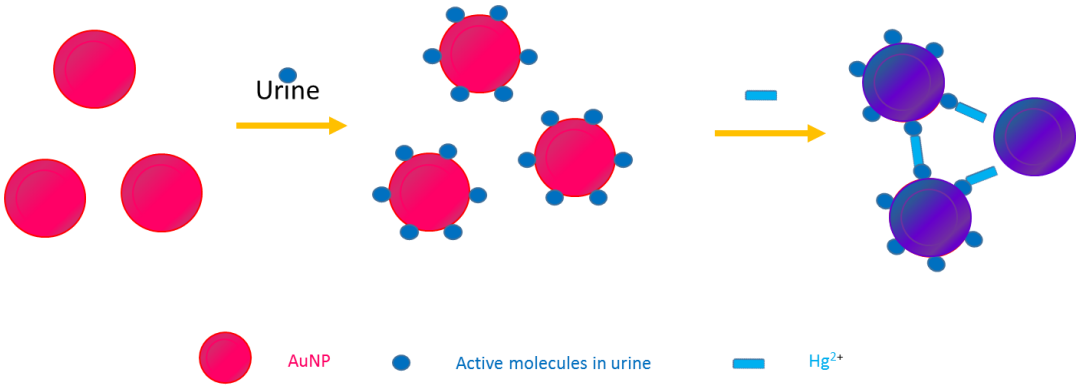

Figure 1.13 Schematic of the colorimetric detection of Hg^{2+}. It is based on simply mixing urine and AuNPs. Nitrogen rich substances from urine are adsorbed to the citrate ions capped AuNPs surface with little color change. Addition of Hg^{2+} causes crosslinking-induced aggregation of AuNPs with an instant red-to-blue color change.

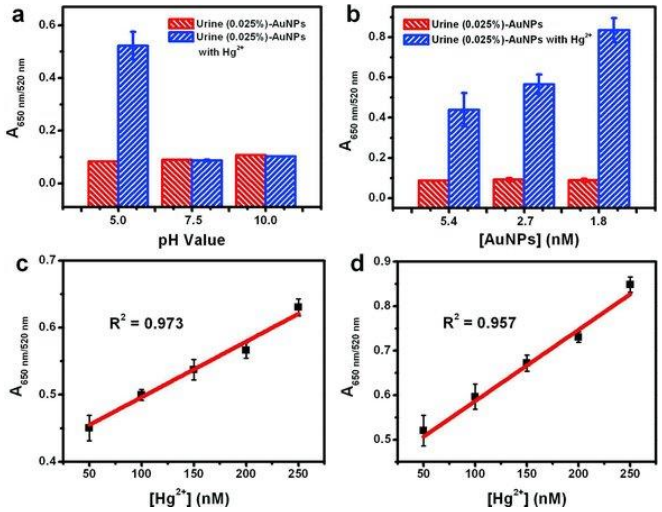

Figure 1.14 Relationship between absorbance and various parameter. (a) A650nm/520nm changes in urine (0.025%)–AuNPs in the absence and presence of Hg^{2+} (500 nM) with different pH values; (b) A650nm/520nm changes in urine (0.025%)–AuNPs with different concentrations of AuNPs (1.8, 2.7, and 5.4 nM) in the absence and presence of Hg^{2+} (500 nM) at pH 5.0; and (c, d) linear plots of A650 nm/520 nm of the urine (0.025%)–AuNPs (1.8 nM) vs. Hg^{2+} concentration (50–250 nM) in tap water and lake water. Reprinted from *Small* 9.24 (2013): 4104-4111, with permission from Elsevier.

In order for Hg^{2+} to link the AuNPs, the particles have to be capped by more than one nitrogen-containing molecules to compensate for the loss of binding sites on the nitrogen-containing molecules, such is the case when AuNPs are applied to humane urine. These nitrogen-containing molecules (Figure 1.15) interact with Hg^{2+} through coordination chemistry (Figure 1.16).[84]

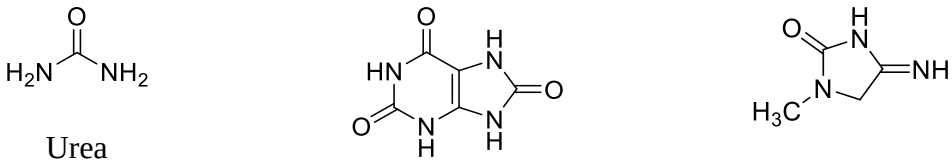

Urea

Uric acid

Creatinine

Figure 1.15 Structures of nitrogen-containing molecules in urine.

The color of the solution changes from ruby red to blue instantly. This plasmonic colorimetric detection of Hg^{2+} offer good selectivity with detection limit being about 100 nM.[84] This study used nitrogen-rich compounds in urine, a biological waste, to cap the AuNP surface to sense mercury cations obtaining good results. This colorimetric technique is based on color change when AuNPs aggregate.

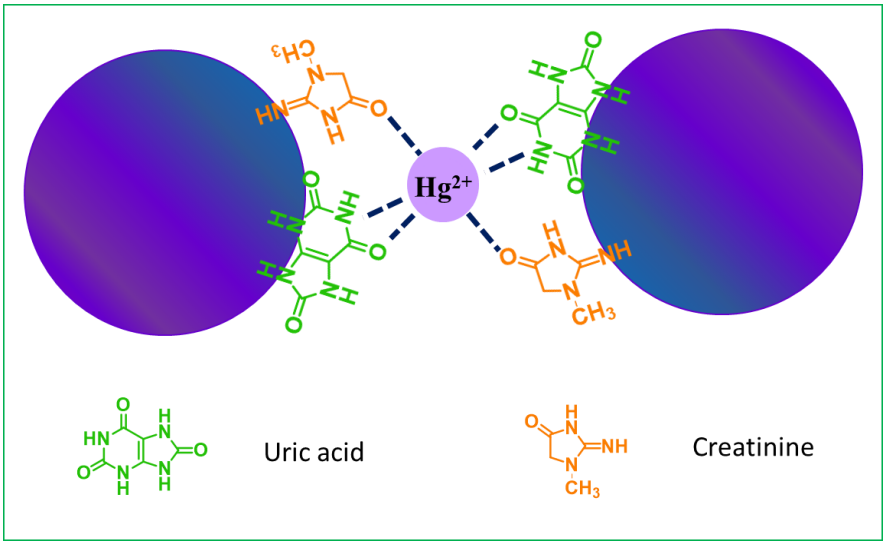

Figure 1.16 Coordination chemistry between $Hg^{2+}$and nitrogen-containing molecules.

How to construct a surface-bound biosensing system using colloidal nanoparticles? The key factors that regulate such systems include: 1) the modes how biomolecules are bio-conjugated to the nanoparticles, 2) the signaling methods applied, and 3) the analyte-receptor interacting mechanism.[86] The signal derived from AuNPs' unique optical properties is modulated by the presence of a target analyte, which makes AuNPs very good signal transducers. Figure 1.17 illustrates the detection of a protease enzyme that cleaves a linker peptide through the color change of the AuNP solution.[86]

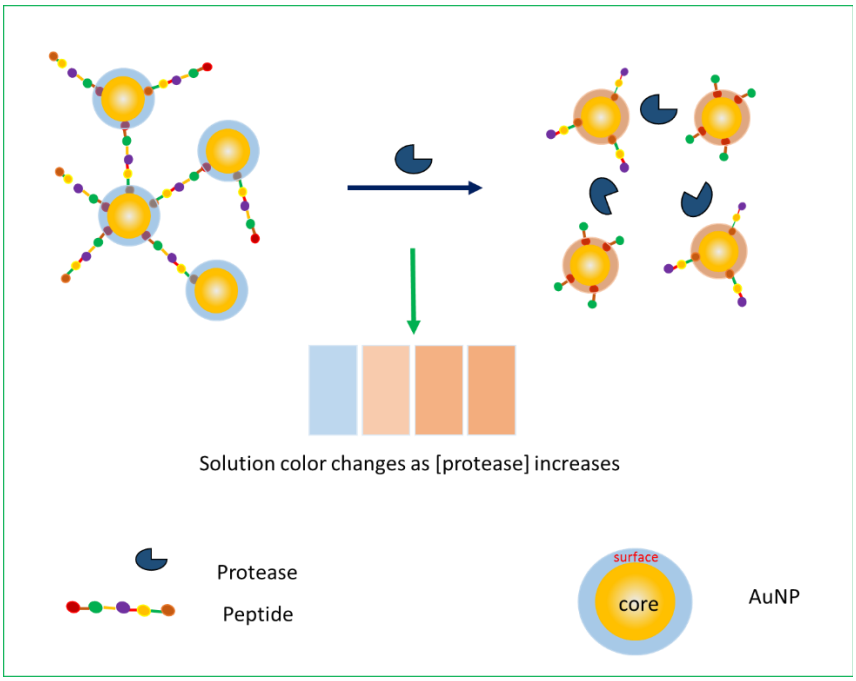

Figure 1.17 Plasmonic AuNP biosensor for protease detection.

The molecular recognition moiety of the bio-conjugated molecules on nanoparticle surface interacts with the analytes to render a physical or chemical response that modulates the particle-derived signal. The intrinsic redox properties of certain biomolecules can be utilized by nanoparticle biosensors to measure pH. In Figure 1.18, dopamine is oxidized to quinone under basic pH. Quinone can quench quantum dots by charge transfer.

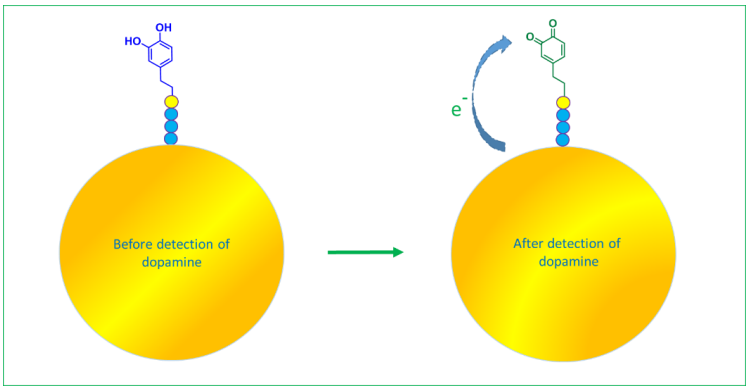

Figure 1.18 Quinone quenches quantum dots by charge transfer.

Surface capping of the nanoparticles are necessary in order to minimize nonspecific binding;[69] In addition, it reduces the interparticle distance thus increases the coupling efficiency, enhances the optical field strengths in the interstitial spaces.

1.3.3.3 CB7 used as capping agent for AuNPs

Aggregates of metal nanoparticles generate enhanced local electromagnetic fields confined in the interparticle space (hot spot), making them ideal for sensing purposes.[87] The control of the interparticle distance with subnanometer precision is very critical in order to obtain reproducible hot spot for reliable signals.[88] Molecules inducing the nanoparticle aggregations in solution include DNA, biotin-streptavidin, and multivalent thiols, all fail to define the rigidity of the linking process. They also restrict the access of the analytes to the hot spot they construct, thus make them not practical for sensing purposes. Methods of producing aggregation by organic monolayer-capping and "salting" both fail to control the gap of the neighboring nanoparticles.[88]

CBs are good capping agents for AuNPs. CBs bind to the metallic surface through their carbonyl groups at the portals of the molecules[89] to fix the interparticle separation precisely at 0.9 nm, the distance between the two portals of any CB molecule (Figure 1.19).[90,91] Analyte of interest binds to the CB molecules, which makes the analyte to be in the center (hot spot) of the intense confined electric field for optimal sensing, such as in SERS[88]

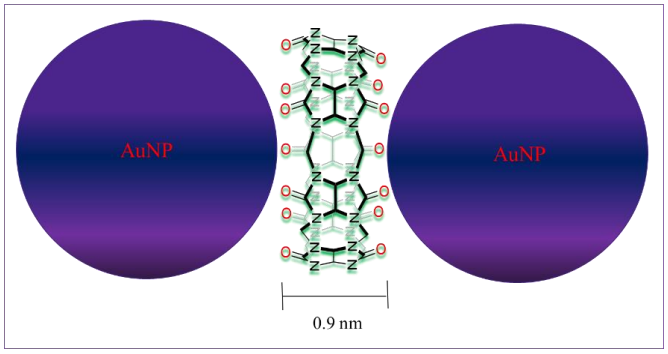

Figure 1.19 CB7 links AuNPs.

1.3.3.4 Host-guest control over nanoparticle aggregation

As stated earlier, aggregation of the AuNPs causes the resonance wavelength of the electron oscillations shifts to the red region. On the contrary, disaggregation of the particles shifts the electron oscillations back to the blue region. Both of the phenomena are used for sensing, but reports of plasmonic sensors which reply on the disassembly of the particle aggregates are fewer,[92] with cocaine sensing being one of them.[82]

To summarize, colloidal AuNPs form very good sensing platform. AuNPs have to be capped with biomolecules in order to have specific binding with the analyte. Most of the sensing mechanisms are based on the red shift of the resonance wavelength which correspond to the aggregation of the AuNPs, a few are on the blue shift of the resonance wavelength due to the perturbation of the aggregates by the analyte. Both models are simple and cheap to perform offering good sensitivity and selectivity.

1.4. A brief description of research methods for my thesis

The goal of my thesis research is to develop simple, fast, cost-effective, selective and sensitive methods for the detection of AcAm, a proxy cancer biomarker, in urine using optical techniques with the aid of supramolecular tools. I report on my efforts using both the IDA and colorimetric method using AuNPs.

Chapter 2: Fluorescence based IDA with CB7 as receptor for the detection of AcAm

This Chapter reports the AcAm detection using fluorescent dye based IDA with CB7 as receptor in both water and urine.

I proposed the indicator displacement assay (IDA) for the detection of AcAm. I conducted all of the experiments, collected and analyzed all of the data. I synthesized acetyl amantadine (AcAm).

2.1 Introduction

2.1.1 Cucurbiturils

CBs form a family of synthetic host molecules which have exceptionally high binding constants with their guests.[93] As early as 1905, cucurbit[6]uril was reported to bind indicator dyes such as congo red and methylene blue. Among all CBs, CB7 has been used as a receptor molecule in indicator displacement assay most frequently.

CB7 (Figure 2.1) is a pumpkin-shaped molecule and has the most water solubility (20-30 mM) among cucurbiturils.[93,94] Its molecular structure is highly symmetrical and rigidly constructed with seven glycoluril units linked by methylene groups. The upper and lower portals of the molecule are made of carbonyl groups where the oxygen atoms are tilted inwards to allow the passage only of complementary guest molecules.[95] The cavity is hydrophobic, which is about 200 $Å^3$ in volume with very low chemical reactivity and polarizability due to a few factors which include no C-H bonds pointing inside, no easily ionizable electron pairs, and the existence of only strong polar bonds.[95] It forms 1:1 complexes with a wide range of molecules,[95,96,97] including aromatic compounds.[98] CB7

can form host-guest complexes with certain chromophoric guest molecules, which are isolated from the bulk solvent. The fluorescent properties can be affected by the change of the microenvironment.[97]

CB7 molecules are able to encapsulate neutral or positively charged molecules by positioning cationic sites along with the electronegative portals or by encapsulating the hydrophobic moiety inside the hydrophobic cavity, where the driving force is the release of high-energy water molecules.[99] The binding strength between CB7 and amantadine (Am) is extremely strong with binding constant being $(4.2 \pm 1.0) \times 10^{12}\ M^{-1}$, obtained using a competitive titration method.[100,101] This indicates a very good complementarity of the host and the guest.[102] At the start of this work, AcAm had not been studied as a guest for CB7 before. I assumed that its similar adamantane core would fit well within CB7 and would drive efficient binding, and that the replacement of the NH_3^+ group in Am with NHAc group in AcAm would have only a small negative affect on binding to CB7.

2.1.2 CB7 as IDA receptor

Inclusion of fluorescent dyes by CB7 can improve the efficiency of fluorescence emission due to a combination of a few factors including the encapsulation in a rigid confined environment which decreases the radiationless decay. CB7 itself is transparent in the visible range of spectrum and does not quench the fluorescence at the concentrations in the mM range.[97] Certain analytes would compete with the dye molecule for the hydrophobic cavity to produce binding-dependent spectral changes.[103]

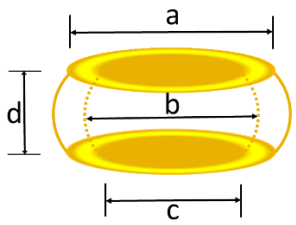

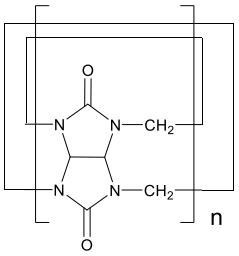

CBn: n = 5, 6, 7, 8

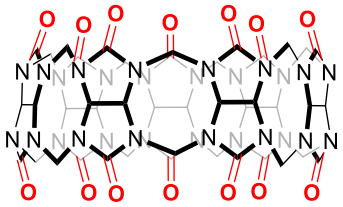

CB7

		CB5	CB6	CB7	CB8
Outer diameter (Å)	**a**	13.1	14.4	16	17.5
Cavity (Å)	**b**	4.4	5.8	7.3	8.8
	c	2.4	3.9	5.4	6.9
Height (Å)	**d**	9.1	9.1	9.1	9.1
Cavity volume ($Å^3$)		82	164	279	479

Figure 2.1 Structural parameters of CBs

Examples of CB7-dye assembles include those summarized by Nau,[104] and many more. Many have been used for IDA-based detection schemes. For instance, the CB7-palmatine pair has been constructed and studied for the detection of various substances including ranitidine, nizatidine, cimetidine, L-cysteine, L-phenylalanine, and astemizole.[105,106,107,108] The CB7-methylene blue assembly was used for the detection of nicotine in cigarettes.[109]

CB7-coptisine ensemble was used to detect amantadine and rimantadine in urine by Wu's group.[39] The limit of detection of the method for amantadine and rimantadine in

their pharmaceutical forms and in urine ranges from 1.2 ng/mL to 1.3 ng/mL.[39] The energy-minimized configurations of CB7-amantadine and CB7-rimantadine are displayed in Figure 2.2 and the IDA spectra are shown in Figure 2.3. The urine sample was treated prior to analysis with 4 M sodium hydroxide solution and dichloromethane to remove lipids.[40]

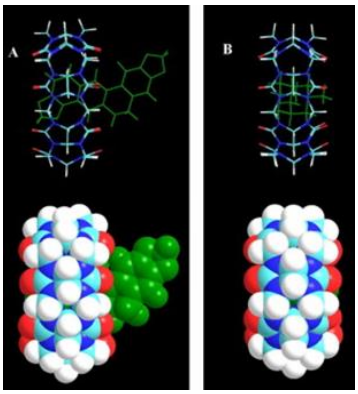

Figure 2.2 Energy-minimized structures of host-guest complexes. A: CB7–coptisine, B: CB7–amantadine. Color codes: coptisine and amantadine, green; CB7, oxygen, red; nitrogen, blue; carbon, light blue. Reprinted from *Spectrochimica Acta Part A: Molecular and Biomolecular Spectroscopy* 98 (2012): 275-281, with permission from Elsevier.

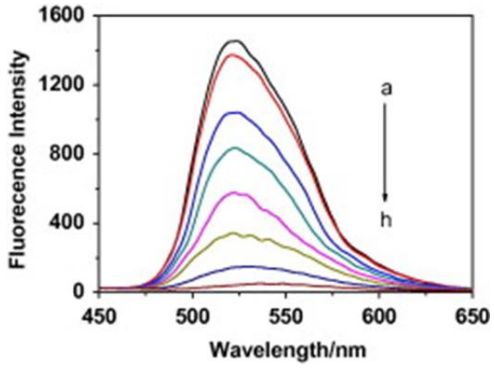

Figure 2.3 Fluorescence spectra of CB7-coptisine in the presence of amantadine. The concentrations of amantadine (μM) ranged from (a) 0 to (h) 2.66. C_{CB7} was 1.00 μM, $C_{coptisine}$ was 1.00 μM, while pH was set to 3.0. $\lambda_{ex}/\lambda_{em}$ = 358/522 nm. Reprinted from *Spectrochimica Acta Part A: Molecular and Biomolecular Spectroscopy* 98 (2012): 275-281, with permission from Elsevier.

Among the indicator dyes, berberine chloride demonstrates very good fluorescence enhancement upon binding to CB7. Berberine (BER) is a quaternary ammonium salt, a natural product which belongs to the isoquinoline alkaloids. The fluorescence intensity of the dye molecule increases significantly when it is inside the hydrophobic cavity of CB7 due to a significant change of its microenvironment.[104] The CB7-berberine system has been used to detect labetalol[110], ethambutol[111], and dibucaine.[112]

Rhodamine B (RhB) belongs to the group of xanthene dyes, which possesses a high fluorescence quantum yield $\Phi_F = 0.31$.[113] In acidic solutions RhB remains as a cation with emission maximum at 568 nm while in neutral solutions RhB is a zwitterion due to the deprotonation of the carboxylic group (pKa = 3.2) with emission maximum at 583 nm.[113,114] The binding of RhB to CB7 has been studied before with binding constant being $1.6 \times 10^5\ M^{-1}$.[115] It has been reported that CB7 has the ability to disrupt RhB aggregate formation on glass substrates through host-guest interactions with RhB.[116]

To summarize, IDA with cucurbit[7]uril as the receptor and a fluorescent dye as the indicator is a very sensitive optical technique for the analysis of a wide range of small molecules that have good binding affinity with CB7.

2.1.3 Goals to achieve in this Chapter

Amantadine has very good binding affinity with CB7 with the adamantyl group merged deeply inside the hydrophobic cavity while the amine group poking outside of and yet staying very close to the hydrophilic portal made of carbonyl oxygen atoms. Comparing with amantadine, acetylamantadine retains the bulky and hydrophobic adamantyl group. It is non-fluorescent. I predict that AcAm would be detected and quantified by using the fluorescence based IDA with very good selectivity and limit of detection in water.

I will use CB7 and a fluorescent dye to construct IDA ensemble, namely CB7-berberine and CB7-Rhodamine B pairs to detect AcAm in both deionized water and urine.

2.2 Experimental methods

2.2.1 Synthesis of AcAm

All reactants were used as received without further purification. Adamantamine is from Tokyo Chemical Industry Co. Ltd., HPLC grade dichloromethane is from EMD Chemicals, triethylamine and acetic anhydride are both from Anachemia.

The synthetic procedure is based on a paper published in 2011[117]. Adamantamine (2.00 g, 10.7 mmol) was dissolved in 30 ml dichloromethane under nitrogen atmosphere. Triethylamine ((3.77 g, 37.5 mmol) was added to the mixture drop-wise. The resulting solution was stirred for 5 minutes at room temperature. After an addition of acetic anhydride (2.17 g, 21.3 mmol), the solution was stirred for one hour at room temperature. After an addition of water, the aqueous layer was extracted. The organic extract was dried over sodium sulfate, and filtered. A rotary evaporator was used to evaporate the solvent. High vacuum was applied to afford N-Acetyl Adamantanamine as white solid. The yield was 57%. The NMR spectrum is listed in Appendix 1 in order to support identity and >95% purity of this well-known compound. GC-MS was also used to characterize the compound (Appendix 2). The MS spectra of AcAm was run against NIST library version 2.0 built on August 11, 2008. It was the 1st hit with 77.3% reverse match and 30% probability. All other compounds showed significant differences.

^{1}H NMR (300 MHz, DMSO-d6): 7.20 (br, 1H), 1.94-2.02 (m, 3H), 1.86-1.92 (m, 6H), 1.72 (s, 3H), 1.56-1.62 (m, 6H).

2.2.2 Binding constant determinations

Both of CB7 and Rhodamine B were purchased from Sigma-Aldrich. Berberine chloride was purchased from Fluka Analytical. All chemicals were used as obtained. Stock solutions were prepared in dH_2O. Samples were prepared directly in NUNC 96 black-well plates with optically clear bottom. Fluorescence intensity was measured using a SpectraMax® M5 / M5e Microplate Reader.

2.2.2.1 K_{HI} determination - direct titrations for dye-CB7 affinities

I start with assuming that it is a 1:1 binding between the dye indicator I and the host molecule H.

At equilibrium,

$$H + I \rightleftharpoons HI \tag{2}$$

$$K_{HI} = \frac{[HI]}{[H][I]} \tag{3}$$

Where [HI], [H], and [I] are equilibrium concentrations. K_{HI} is determined by measuring the fluorescence of a set of solutions with constant fluorescent indicator concentration, $[I]_{total,}$ and increasing host concentration, $[H]_{total}$.

Unbound I is weakly fluorescent; bound I, HI, is fluorescent with enhanced intensity.

$$[H]_{total} = [H] + [HI] \tag{4}$$

$$[I]_{total} = [I] + [HI] \tag{5}$$

$$\frac{1}{F - F0} = \frac{1}{(F\infty - F0)K_{HI}[H]} + \frac{1}{(F\infty - F0)} \tag{6}$$

Where F_0 is the fluorescence intensity of indicator I in the absence of the host H, $F\infty$ is the fluorescence intensity when all of the indicator molecules are complexed with the host. F is the measured fluorescence intensity at each [H][118].

A straight line is obtained when plotting $1/(F-F_0)$ against 1/[H], which indicates that indeed a 1:1 complex is formed between the indicator and the host.

$$\text{Slope} = \frac{1}{(F\infty - F0)K_{HI}} \qquad (7)$$

The value of the slope can be obtained, and K_{HI} can be obtained from equation (6).[118]

Solutions of RhB and CB7 were prepared in dH_2O in glass vials. Solutions for fluorescence measurement were prepared by mixing directly in a 96-well plate. 100 μL of 0.005 mM RhB solution was pipetted into wells of 96-well plate, 100 μL of various concentrations of CB7 stock solution was then added. Final [RhB] = 2.5 μM. Final concentrations of CB7 ranged from 0 to 10 μM. Excitation wavelength used for RhB was 554 nm. Data was collected at room temperature.

Experiments for berberine were carried out similarly.

2.2.2.2 K_{HG} determination - competition titrations to determine analyte-CB7 affinities

Binding constant K_{HG} is determined by curve fitting of titration data using Equilibria. Indicator dye, I, forms complex with host, H. Analyte of interest, G, competitively binds to host, H, displacing indicator dye, I. The system equilibria and binding constant equations are listed below:

$$H + I \rightleftharpoons HI \quad (8)$$

$$K_{HI} = \frac{[HI]}{[H][I]} \quad (9)$$

$$H + G \rightleftharpoons HG \quad (10)$$

$$K_{HG} = \frac{[HG]}{[H][G]} \quad (11)$$

K_{HG} can be determined by measuring the fluorescence of a set of solutions in which host concentration, $[H]_{total}$ and dye concentration, $[I]_{total}$, are both kept constant, with analyte concentration $[G]_{total}$ increasing.

The mass balances for the system are:

$$[H]_{total} = [H] + [HI] + [HG] \quad (12)$$

$$[I]_{total} = [I] + [HI] \quad (13)$$

$$[G]_{total} = [G] + [HG] \quad (14)$$

The fluorescence is proportional to the concentration of the host-dye complex, [HI], with an unquenched baseline fluorescence:

$$F_{calc,\,i} = F_{baseline} + F_{slope}[HI]_i \quad (15)$$

Where $F_{calc,\,i}$ is the fluorescence intensity calculated using Equilibria, and $F_{slope}[HI]_i$ is the measured fluorescence intensity. $F_{baseline}$ is the unquenched baseline fluorescence.

Procedures for preparation of solutions for IDA fluorescence measurement is listed below:

50 μL of 0.01 mM RhB was pipetted into wells of 96-well plate, 50 μL of 0.01 mM CB7 was added. 100 μL of various concentrations of AcAm stock solution was added to the mixture. [RhB] = [CB7] = 2.5 μM. Final concentrations of AcAm ranged from 0 to 10 μM. The excitation wavelength used for RhB was 554 nm. Data was collected at room temperature.

Experiments for berberine were carried out similarly.

2.2.3 Urine preparation

Frozen urine sample was thawed in open air at room temperature. It was centrifuged at 3000 RPM for 30 minutes. Sediment was examined under a light microscope in order to check for bacterial contamination. A few squamous epithelial cells were seen under low power. A few white blood cells were seen but no bacteria were seen under high power. Solid AcAm was added to the supernatant to make AcAm-spiked urine samples for testing. Final values for [AcAm] ranged from 0 to 2000 ng/mL.

2.2.4 PD-10 desalting column protocol

The PD-10 columns (Sample volume 1.0 – 2.5 mL, GE Healthcare) were used according to manufacturer's directions. Gravity flow was used for all loading and elution steps, as follows:

1. Column equilibration. Filled up the column with dH_2O. Repeated 4 times. Discarded the flow-through.
2. Sample application. Added 2.5 ml urine sample to the column. Discarded the flow-through.
3. Elution. Eluted with 3.5 mL dH_2O and collected the eluate.

2.2.5 GC-MS protocol

The GC-MS system used was TRACE DSQ GC/MS. Oven temperature was set at 220 °C, split flow at 20 mL/min, and split ratio at 20. Sample injection volume was 0.5 µL.

AcAm standard solutions were prepared by dissolving solid AcAm in acetone with the final [AcAm] ranged up to 5000 ng/mL.

2.3 Results

Initially, I wanted to have an alternative method to confirm the results obtained using IDA, therefore I used SPE (Strata-X, Phenomenenx, CA) to process the mock urine and human urine (provided by BioMark Technologies, Inc.) and GC-MS to quantify AcAm. The recovery rate of AcAm after SPE from mock urine was 72% and that from human urine 22%. The mock urine was composed of NaCl, KCl, K2SO4, urea, creatinine, Am, AcAm, and corticosterone. The LOD obtained from a standard GC-MS calibration curve (Figure 2.4, LOD for AcAm (739.4 ng/mL)) was much higher than the target value (10 ng/mL). The SPE + GC-MS approach proved to be very time-consuming and labor intensive. These data don't involve development of new analytical methods, and were not explored further during this thesis research.

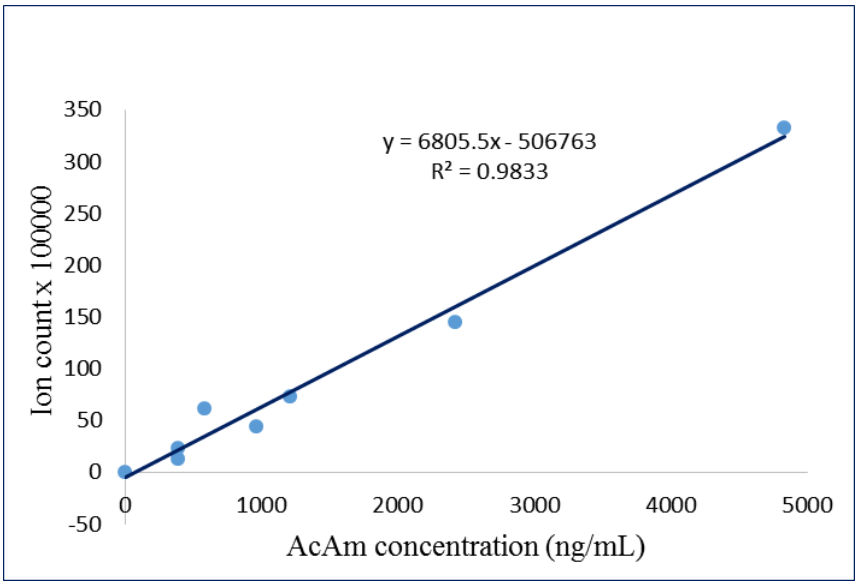

Figure 2.4 AcAm GC-MS standard calibration curve. AcAm was dissolved in acetone. Retention time was 6.54 minute on GC chromatogram.

IDA was attempted in order to get over the shortcomings of this method.

2.3.1 Direct titration of dye and CB7

Direct titration study between the dye molecule and the host molecule, CB7, is needed in order to study the competitive displacement of the dye by the analyte from the CB7 binding cavity leading to the detection of the analyte based on the spectral changes in the process. Experiments were conducted on binding study of two fluorescent dyes, RhB and BER, with CB7.

2.3.1.1 Direct titration of Rhodamine B and CB7

The concentration of RhB in each well was kept constant at 2.5 μM. CB7 concentrations varied from 0 to 10 μM. The equations involved and the method used to obtain the binding constant K_{HI} are discussed in section 2.2.2.1.

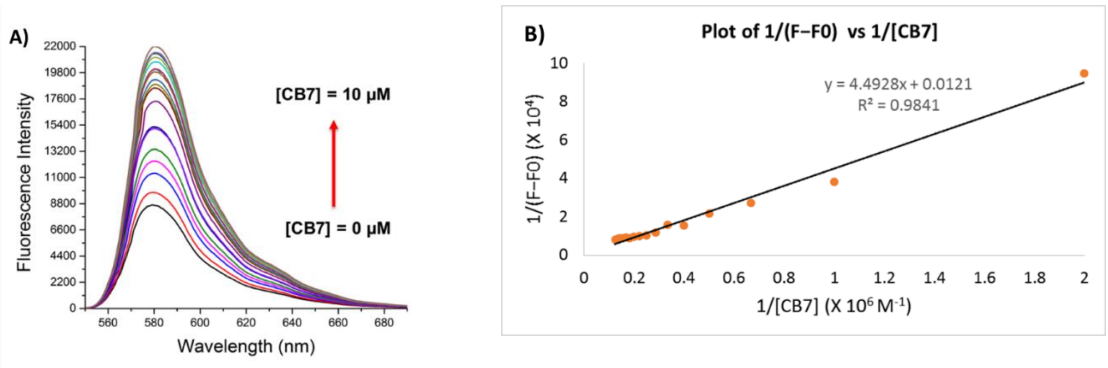

Figure 2.5 Direct titration of RhB and CB7. A) Direct fluorescence titration of RhB (2.5 μM) with host CB7 in dH_2O, λ_{ex} = 554 nm, $\lambda_{max, em}$ = 581 nm. B) Plot of $1/(F-F_0)$ vs 1/[CB7]. Fluorescence intensity was measured at $\lambda_{max, em}$ = 581 nm. Solutions were unbuffered. Measurements were conducted at room temperature.

Fluorescence intensity increases as CB7 concentration increases due to the increasing portion of RhB being encapsulated by CB7. Inclusion of RhB inside CB7 cavity increases the fluorescence intensity of RhB. Slope (4.49 ± 0.05) was obtained from Figure 2.5; binding constant was calculated by applying equation (7). $K_{HI} = 1.68 \pm 0.02 \times 10^5\ M^{-1}$, which is in agreement with the literature value of $1.6 \times 10^5\ M^{-1}$.[119]

RhB contains two N,N-diethylamino groups attached to the xanthene core with one of them included within the CB7 cavity and the other outside when the complex is at the lowest energy configuration (Figure 2.6).[120] Hydrogen bonds involved in the complexation include the one between portal oxygens and the hydrogen atom from the hydroxyl group on RhB and the others formed among portal oxygens and the hydrogen atoms from the encapsulated ethyl group and from the xanthene core.[120] Interactions also exist between the nitrogen cation and the portals through ion-dipole contacts.

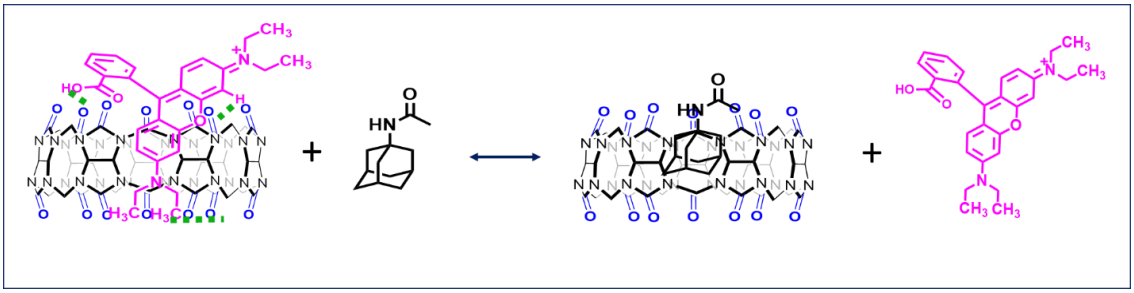

Figure 2.6 Schematic representation of RhB-CB7 complex at the lowest energy configuration and displacement of RhB by AcAm.

As presented subsequently, RhB, the fluorescent dye indicator in IDA assay, is displaced by AcAm, the analyte of interest which has stronger binding affinity with CB7. All the equilibria involved in the system are dynamic.

2.3.1.2 Direct titration of berberine and CB7

The concentration of BER was fixed at 0.5 μM. BER has weak intrinsic fluorescence in dH_2O at 345 nm. The lower the initial BER concentration in the system, the less baseline interference it would cause once displaced, the higher the sensitivity the CB7-BER ensemble would provide for AcAm detection.

CB7 concentrations varied from 0 to 5 μM. The equations involved and the method used to obtain the binding constant K_{HI} are discussed in section 2.2.2.1.

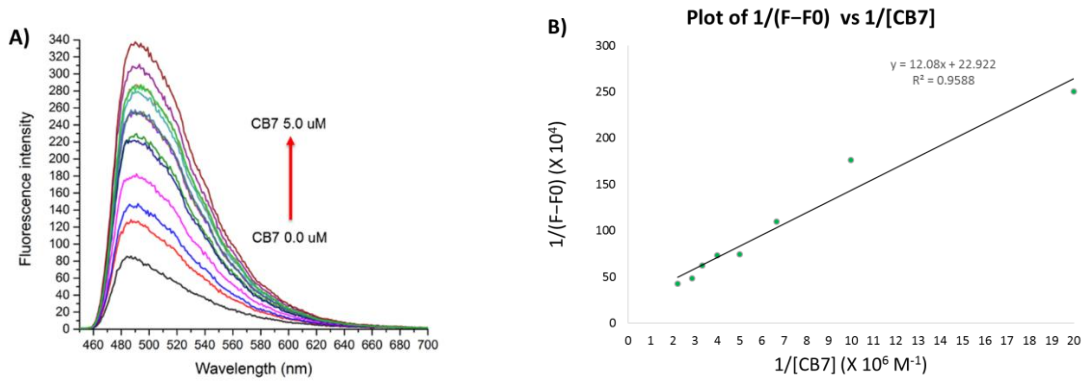

Figure 2.7 Direct titration of BER and CB7. A) Direct fluorescence titration of BER (0.5 µM) with host CB7 in dH_2O, λ_{ex} = 345 nm. B) Plot of 1/(F−F0) vs 1/[CB7]. Fluorescence intensity was measured at $\lambda_{max, em}$ = 485 nm. Solutions were unbuffered. Measurements were conducted at room temperature.

The fluorescence intensity of BER increases as CB7 being introduced to the solution due to the formation of a 1:1 inclusion complex[121] between BER and CB7. The value of the slope (12.08 ± 5.0) was obtained from Figure 2.7; binding constant was calculated by applying equation (7). $K_{HI} = 3.5 \pm 1.0 \times 10^6\ M^{-1}$, which is in agreement with the literature value ($1.6 \times 10^6\ M^{-1}$).[122]

Similar to RhB, BER is partially immersed in the CB7 cavity (Figure 2.8**)**. Inside the CB7 cavity is the isoquinoline ring of BER.[121] Ion-dipole interactions exist between the quaternary nitrogen and the oxygen atoms that make up the CB7 portal.[123] Just like those for RhB, hydrogen bonds would also contribute to the stability of the ensemble.

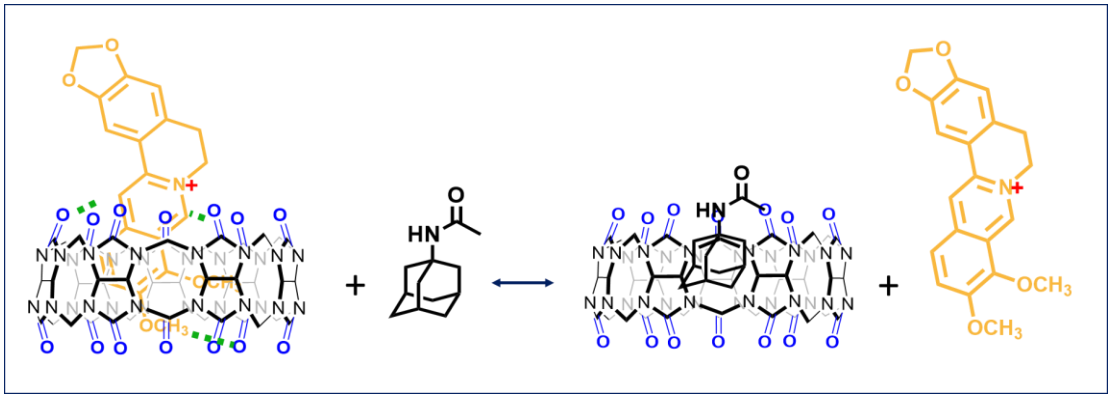

Figure 2.8 Schematic representation of BER-CB7 complex at the lowest energy configuration and displacement of BER by AcAm.

As presented subsequently, BER, the fluorescent dye indicator in IDA assay, is displaced by AcAm, the analyte of interest which has stronger binding affinity with CB7. All the equilibria involved in the system are dynamic.

2.3.2 Fluorescence based IDA with CB7 as receptor for the detection of AcAm in dH_2O

AcAm is non-fluorescent and cannot be detected directly using fluorescent method. Because its precursor, amantadine, has very strong binding affinity with CB7 as mentioned earlier, I predict that the AcAm would possess the same property. AcAm would compete for the binding cavity of CB7 with the dye molecule. The concentration of AcAm would determine the ratio of the dye molecules inside and outside of CB7, which determines the fluorescence intensity of the system accordingly. Therefore there is a correlation between the concentration of AcAm and the fluorescent intensity of the system.

2.3.2.1 RhB-CB7 pair for the detection of AcAm in dH_2O

While the concentrations of both RhB and CB7 were kept constant with each at 2.5 µM (which proves experimentally to provide sufficient sensitivity), those for AcAm varied from 0 to 10 µM. Fluorescence intensity decreases as RhB is being replaced by AcAm from the CB7 binding cavity. Binding constant, $K_{AcAm\text{-}CB7}$ was obtained using Equilibria being 3.2 ± 0.02 X 10^6 M^{-1}, which is much smaller than $K_{Am\text{-}CB7}$. This is because the ion-dipole interaction between NHAc group on AcAm and CB7 is much weaker than that between the NH_3^+ group on Am and CB7. The linear response range for AcAm is between 1 and 200 ng/mL (Figure 2.9). The limit of detection (LOD) is 16.8 ng/mL, which was calculated using Microsoft Excel. The equation used for the calculation is

$$\text{LOD} = \frac{STEYX}{SLOPE} \text{ x } 3.3 \qquad (16)$$

Where STEYX is the standard deviation, SLOPE is the slope of the linear curve.

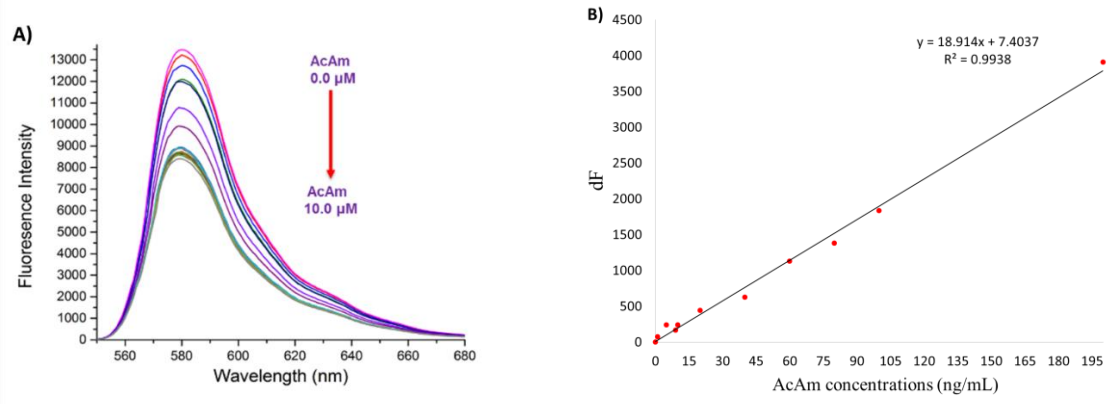

Figure 2.9 Fluorescence based IDA with CB7 as receptor for AcAm detection in dH_2O. Indicator: RhB. A) RhB displacement assay curves. [RhB] = [CB7] = 2.5 µM, [AcAm]: 0.0 – 10.0 µM, λ_{ex} = 554 nm, λ_{em} = 580 nm. B) The change of fluorescence intensity at 580 nm vs [AcAm]. Solutions were unbuffered. Measurements were conducted at room temperature.

RhB was used as a fluorescent signaling probe, therefore setting it at proper concentration was critical for the detection of analyte. If [RhB] was set too low, the sensitive of the sensing device would be too low (Figure 2.10); if set two high, the detection limit of the analyte would be compromised.[39] Figure 2.10 shows an example of the noisy fluorescence emission data that resulted when the [CB7] and [RhB] were set too low. The optimal concentration of RhB and CB7 for the experiment was both at 2.5 μM. dF = F(RhB-CB7) – F(AcAm-CB7).

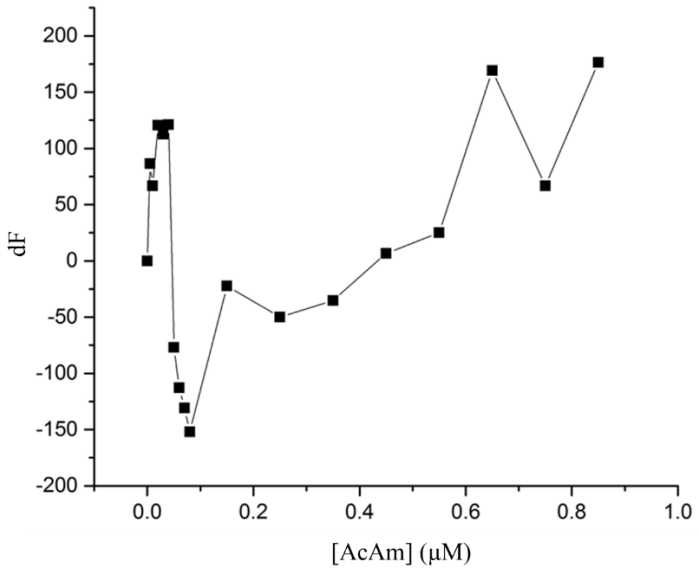

Figure 2.10 The relationship between the change of fluorescence intensity and [AcAm]. [RhB] = [CB7] = 0.5 μM. λ_{ex} = 554 nm. The plot represents noise. dF is the change of fluorescence intensity, which was measured at $\lambda_{max, em}$ = 581 nm. Solutions were unbuffered. Measurements were conducted at room temperature.

2.3.2.2 BER-CB7 pair for the detection of AcAm in dH_2O

While the concentrations of both BER and CB7 were kept constant 2.5 μM, those for AcAm varied from 0 to 4000 ng/ml. Addition of AcAm quenched the fluorescence

intensity of system. Fluorescence intensity decreased as [AcAm] increased due to BER being replaced by AcAm. BER goes to H_2O solution where it displays low fluorescence in a polar environment. The limit of detection (LOD) for AcAm calculated using Excel is 14.8 ng/ml in dH_2O (Figure 2.11).

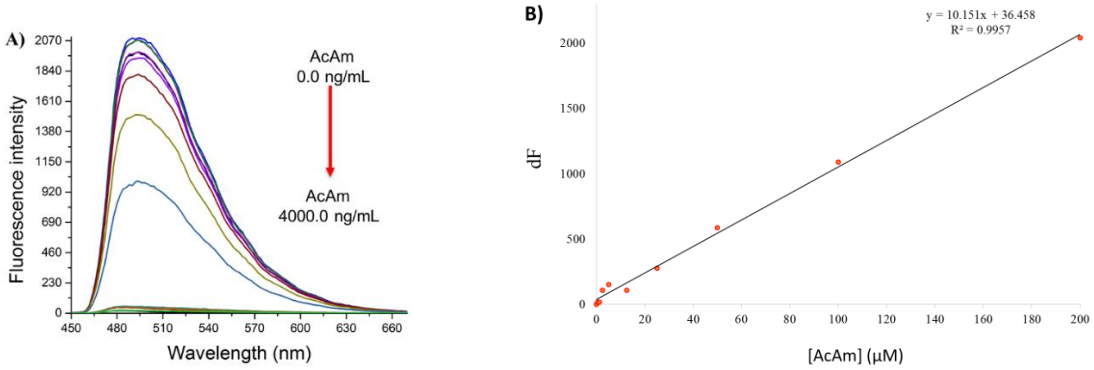

Figure 2.11 Fluorescence based IDA with CB7 as receptor for AcAm detection in dH_2O. Indicator: BER. A) BER displacement assay curves. [BER] = [CB7] = 2.5 µM, [AcAm]: 0.0 – 4000.0 ng/mL, λ_{ex} = 345 nm, λ_{em} = 485 nm. B) The change of fluorescence intensity at 485 nm vs [AcAm]. Solutions were unbuffered. Measurements were conducted at room temperature.

In deionized water, the fluorescence intensity increases 45 fold when BER is encapsulated by CB7, while that for RhB is only 1.5 fold (Figure 2.12**)**. Therefore BER was used as the indicator for all of the subsequent experiments.

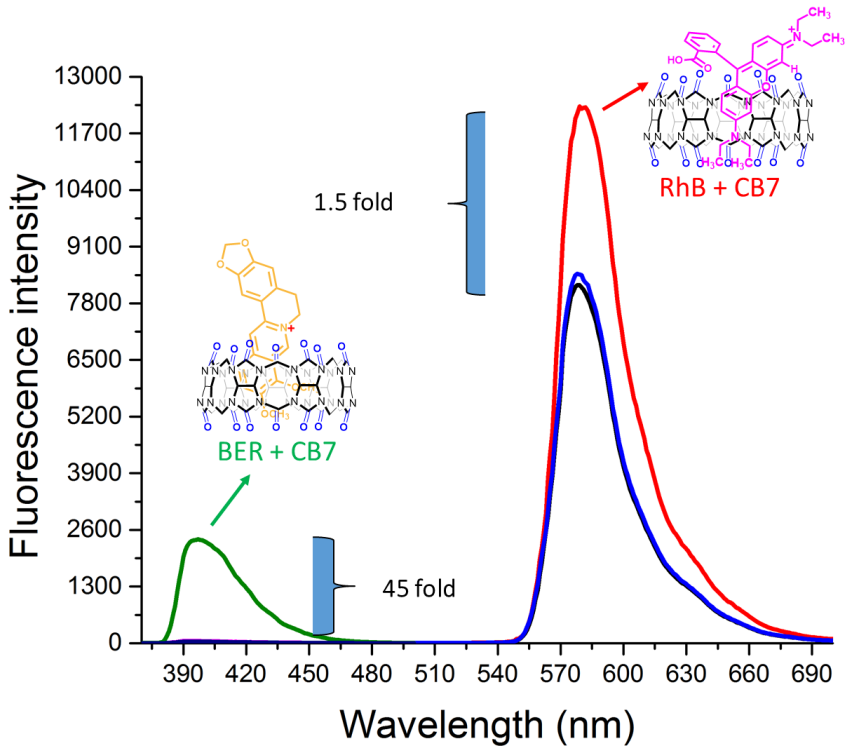

Figure 2.12 **Fluorescence intensity enhancement of BER and RhB by CB7. For BER, λ_{ex} = 345 nm, and for RhB, λ_{ex} = 554 nm. [BER] = [RhB] = [CB7] = 2.5 µM.**

2.3.3 Fluorescence based IDA with CB7 as receptor for the detection of AcAm in urine

2.3.3.1 Detection of AcAm in urine using IDA

For IDA approaches, AcAm stock solutions in urine were prepared by adding AcAm to the urine at various concentrations; in parallel, AcAm stock solutions in dH_2O were prepared as well.

Testing solutions were prepared directly in the wells of the 96-well plate. The concentration of BER was kept at 2.5 µM in each well, so was that of CB7. AcAm stock solutions in urine were added into each of the testing wells. Run in parallel was the same set of experiment but with AcAm stock solutions made in dH_2O instead of in urine.

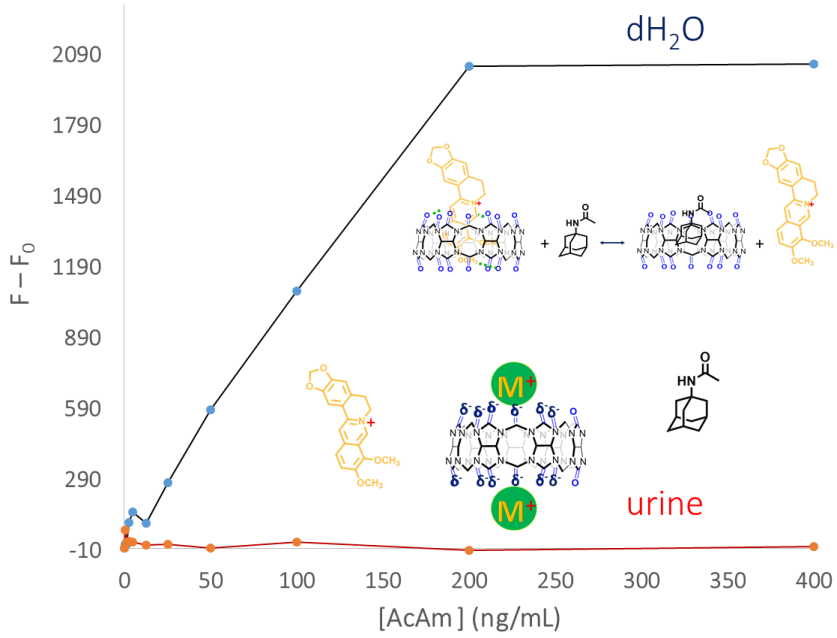

Figure 2.13 Detection of AcAm in urine using IDA. Plot in black: the change of fluorescence intensity vs [AcAm] in dH_2O; plot in orange: the change of fluorescence intensity vs [AcAm] in urine. Indicator: BER. λ_{ex} = 345 nm, λ_{em} = 485 nm. Solutions were unbuffered. Measurements were conducted at room temperature. [BER] = [CB7] = 2.5 μM.

The change of fluorescence intensity increased as [AcAm] increased in dH_2O but showed little differences in urine (Figure 2.13). The addition of AcAm to the BER-CB7-urine system did cause much change of fluorescence intensity. It is reasonable to state that the addition of AcAm did not trigger any noticeable redistribution of BER between the cavity of CB7 and the solvent (urine) because BER-CB7 complex did not exist. What prevents the encapsulation of BER by CB7?

2.3.3.2 Salt effects on guest encapsulation by CB7

The oxygen atoms on carbonyl groups are partially negatively charged therefore the carbonyl-made portals have high binding affinity with cations through the ion-dipole interactions.[124] Cations that bind to the portals of a CB molecule act as “lids” to cover the

portals preventing guest molecules from entering the hydrophobic cavity (Scheme 2.1). These findings were first reported in 1996.[125]

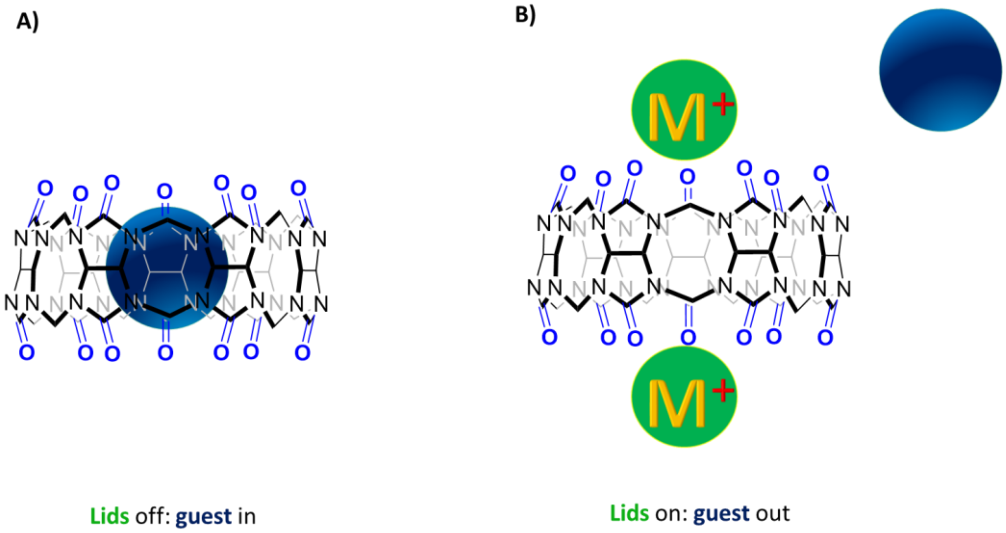

Scheme 2.1 Cations M^+ lining up the CB portals prevent guest binding.

The levels of sodium and potassium in urine depend on the dietary intake and the health state in patients.[126] The reference range for sodium in urine for an adult male is 40 - 220 mmol/L, and that for an adult female is 27 - 287 mmol/L; the reference range for potassium in urine for an adult is 25 - 125 mmol/L.[127]

The following experiments were set up to study the effects of sodium and potassium on the encapsulation of BER by CB7.

The concentrations of both BER and CB7 were kept constant, each at 2.5 μM. Same volume of different concentrations of NaCl in dH_2O was titrated into the BER-CB7 mixtures in the sample wells of a 96-well plate. The same procedures were also applied to

KCl solutions. Fluorescence emission was measured. The fluorescence intensity was plotted against the concentration of NaCl and of KCl (Figure 2.14).

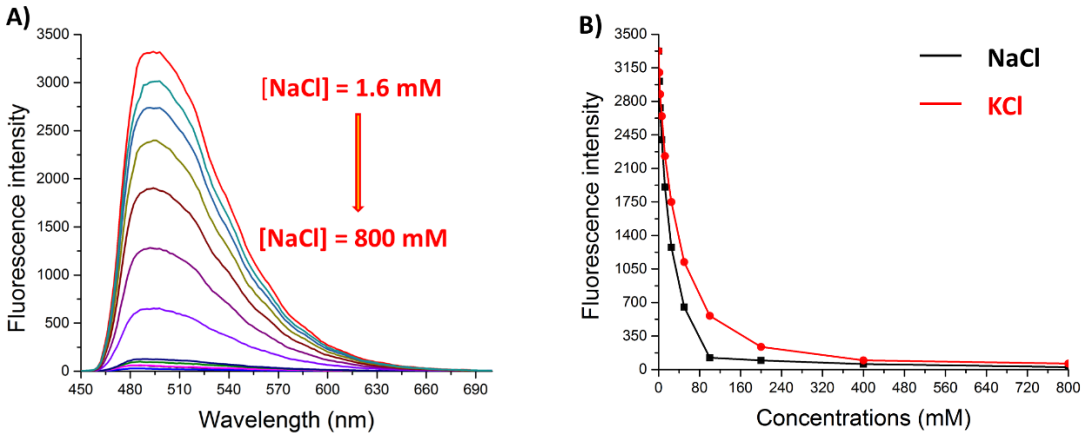

Figure 2.14 Cations acting as "lids" prevent guest encapsulation by CB7. Indicator: BER. A) Emission spectrum: fluorescence intensity decreases as [Na^+] increases. B) Fluorescence intensity vs [Na^+] and [K^+]. λ_{ex} = 345 nm. Fluorescence intensity was measured at λ_{em} = 485 nm. [BER] = [CB7] = 2.5 µM. Solutions were unbuffered. Measurements were conducted at room temperature.

As the concentrations of either sodium or potassium cations increased, the fluorescence intensity decreased which indicates that the portion of BER being encapsulated by CB7 decreased. This finding indicates that that cations act as "lids" covering up the CB7 portals to prevent guest encapsulation by CB7. Cations in urine interact with CB7 molecules by lining up the portals, thus preventing the encapsulation of the indicator dye. The functions of recognition and encapsulation of CB7 are disabled by the cations.

2.3.3.3 Urine treated with disposable PD-10 desalting column

Disposable PD-10 desalting column utilizes the principle of gel filtration chromatography to separate molecules based on their molecular sizes. Molecules that are larger than the largest pores of the filling material are excluded from the matrix and are eluted first; those smaller than the largest pores of the filling material will elute after the large molecules (Scheme 2.2). The matrix is optimized for the removal of mineral salts from aqueous solutions, and as such these columns are routinely used for simple desalting of biological and biochemical samples.

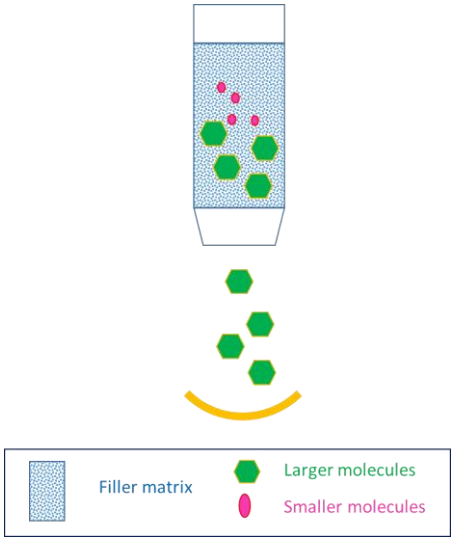

Scheme 2.2 Sample clean-up using PD-10 desalting column

Cations of sodium and potassium are smaller than organic components of urine and are thus retained when samples are run through.

2.3.3.3.1 Urine run through disposable PD-10 column first

I ran urine through a disposable PD-10 column first. I spiked the eluate with AcAm at different concentrations. Emission spectra were collected for the samples with fixed

concentrations of BER and CB7 (each at 2.5 µM). Run in parallel was AcAm solutions in dH_2O with 2.5 µM BER and CB7 µM in each well on plate.

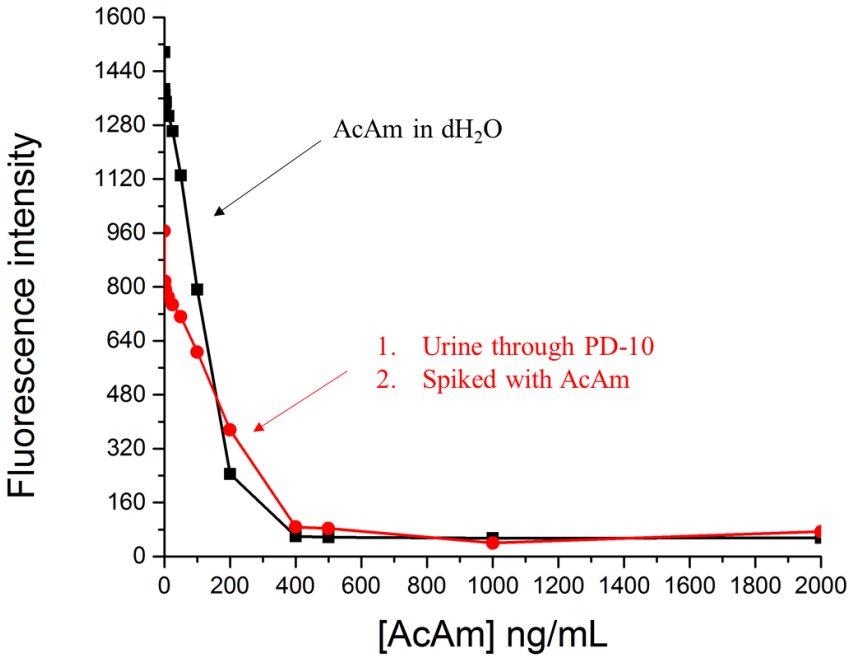

Figure 2.15 PD-10 desalting column to clean up the urine. Plot in black shows fluorescence intensity decreases as [AcAm] in dH_2O increases. Indicator: BER. λ_{ex} = 345 nm, Fluorescence intensity was measured at λ_{em} = 485 nm. Plot in red shows the similar trend as [AcAm] increases in PD-10 treated urine. [BER] = [CB7] = 2.5 µM. Solutions were unbuffered. Measurements were conducted at room temperature.

For urine, as the concentrations of AcAm increased, fluorescence intensity decreased as more BER being displaced. This trend continued up until [AcAm] = 400 ng/ml, when the system got saturated with AcAm and there was no more BER-CB7 complex existed. The trend was very similar to that of AcAm in dH_2O with the maximal fluorescence intensity being smaller, which is most likely due to interferences from other substances in urine (Figure 2.15).

After running through a disposable PD-10 desalting column, the urine was cleaned up. BER was captured by CB7 and AcAm was able to displace BER from CB7 due to its stronger binding affinity, which was reflected by the changes in fluorescence intensity.

2.3.3.3.2 Urine spiked with AcAm first

The realistic scenario is that the urine sample would already contain AcAm when it reaches the lab (because we aim to do AcAm screening for cancer detection). Therefore a set of experiments was conducted to test if AcAm would still be detected after running through PD-10 column.

Figure 2.16 A demonstrates that in dH_2O without the involvement of the PD-10 column, AcAm displaced BER from CB7 binding cavity producing a drop in fluorescence intensity. It also demonstrates that the addition of AcAm solution before running-through PD-10 column did not produce a drop in fluorescence intensity indicating that BER was not displaced from the CB7 binding cavity. The possible explanation is that AcAm was not present in the eluate because it was retained in the column, therefore there was no AcAm to displace BER

Both of Figure 2.16 B and Figure 2.16 C show results for urine. The bar graph in Figure 2.16 B demonstrates that the BER/CB7 ensemble was able to detect AcAm which was added to the urine eluate as already explained in section **2.3.3.3.1.**

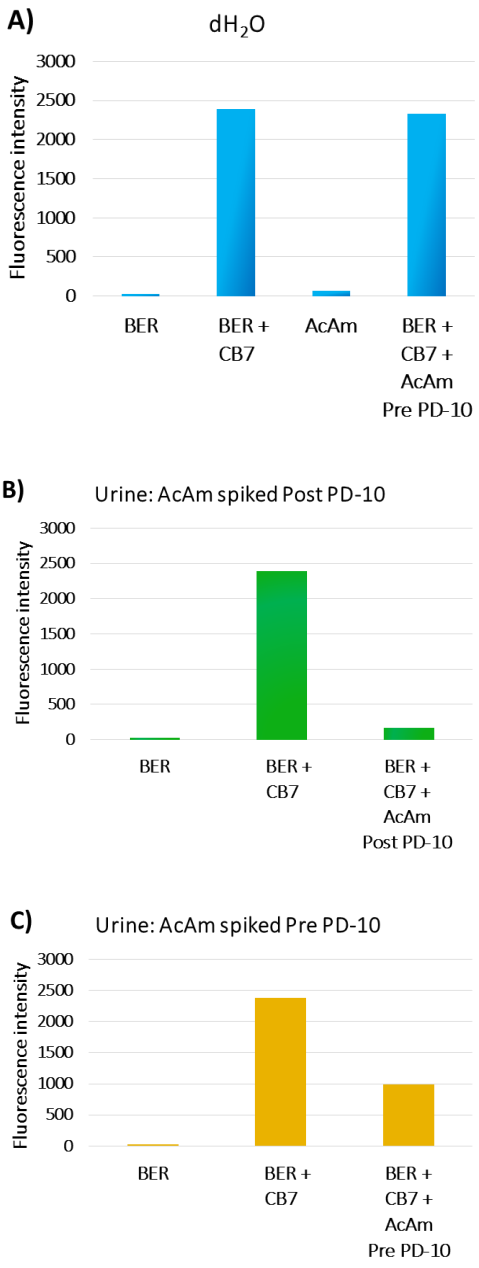

Figure 2.16 Comparison of AcAm displacement of BER from BER-CB7 ensemble. A) Results for AcAm in dH_2O without running through PD-10 desalting column and for AcAm in dH_2O running through PD-10 before applied to BER-CB7 ensemble. B) Urine running through PD-10 first, then spiked with AcAm before applied to BER-CB7 ensemble. C) AcAm spiked urine running through PD-10 before applied to BER-CB7 ensemble. [BER] = [CB7] = [AcAm] = 2.5 µM. λ_{ex} = 345 nm. Fluorescence intensity was measured at $\lambda_{max, em}$ = 485 nm Solutions were unbuffered. Measurements were conducted at room temperature.

Figure 2.16 C shows results for AcAm spiked urine prior to running through PD-10 column. Encapsulation of BER by CB7 did produce enhancement of fluorescence for BER in urine eluate (not spiked with AcAm). When the BER/CB7 ensemble was applied to urine eluate (pre-spiked with AcAm before running through the PD-10 column), fluorescence intensity dropped somewhat but not to the degree compared with the post-spiked urine. AcAm molecules would have been retained in the PD-10 column (Figure 2.16 A), therefore the change of fluorescence intensity must have been caused by a small portion of AcAm that passed through the PD-10 column and some other molecules in urine that displaced BER from CB7 cavity.

To summarize, salts are eliminated from urine after the latter was run through PD-10 column enabling the ability of molecular recognition and inclusion of CB7. Addition of the urine eluate spiked with AcAm after running through the PD-10 column to the BER-CB7 ensemble brought down the fluorescence intensity.

When urine was spiked with AcAm first, then run through a PD-10 desalting column, AcAm would be retained in the column. Application of the eluate to the BER-CB7 ensemble would cause little change in fluorescence intensity.

BER-CB7 ensemble does not work in urine spiked with AcAm first, then treated with PD-10 desalting column. AcAm with molar mass being 193 g/mol is a small molecule and it stays in the PD-10 desalting column together with the salts. PD-10 desalting column cleans up the sample by getting rid of the salts but also the majority of the screening target.

2.3.3.4 Urine treated with lyophilization and UV radiation procedures

Other methods used to clean up urine include lyophilization and UV radiation. Lyophilization method was used in the hope to get rid of the salts in urine; UV radiation procedure was applied to get rid of the inference from urobilin, which is responsible for the yellow color of urine. None of the methods produced expected results.

2.4 Conclusions

The current method for AcAm detection and quantification is LC-MS/MS with detection limit being about 10 ng/mL.[24] The urine sample has to go through SPE first to be cleaned up before being applied to the analytical system. As discussed in Chapter 1, SPE process is laborious and time consuming; LC-MS/MS and GC-MS systems are expensive and the operators need to be highly skilled. The SPE/GC-MS method that I tried on is very time-consuming and labor intensive, and had an inferior LOD of 739.4 ng/mL.

Fluorescence based IDA with CB7 as receptor is sensitive, cost-effective, and easy to use. This method works well for me for the detection and quantification of AcAm in dH_2O, but not in human urine. The values of LOD for AcAm in dH_2O with RhB-CB7 and BER-CB7 ensembles are quite close, with one being 16.8 ng/mL, and the other 14.8 ng/mL, respectively, which are better than LOD by GC-MS and similar to the LOD of 10 ng/mL obtained using the LC-MS/MS method.

On urine sample treatment, I used PD-10 column to process the urine samples as a quicker and easier alternative to SPE. Salts were eliminated together with the analyte AcAm. Therefore PD-10 column is not suitable to use in sample preparation for the detection of AcAm.

2.5 Future work

In order to achieve desirable results for the detection of AcAm in human urine, more extensive sample pre-treatment is unavoidable in order to eliminate or minimize matrix effects in urine. In the meantime, efforts are to be focused on finding different pairs of dye-CB7 ensemble which could provide better sensitivity for AcAm detection.

Chapter 3: Programmed gold nanoparticle disaggregation

3.1 Introduction

This Chapter reports efforts toward detection of AcAm and other small analytes using programmed gold nanoparticle disaggregation.

As described in Chapter 1, AuNPs can be linked by various molecules to form aggregates. They can be linked by DNA sequences, where the known DNA oligonucleotides are chemically bound to AuNPs through base-pairing to create DNA probes.[128] The electrical, optical and structural properties of the DNA-AuNP assemblies should be controllable through the choice of the particle size and the oligonucleotide sequence and length.[129]

AuNPs can be lined by biotin-streptavidin pair as well and the resulting AuNP aggregates are very stable over a wide range of temperature and pH.[130] Similarly, AuNP aggregates can be constructed by antigen-antibody interactions.[131] First, antibodies are chemisorbed onto the particles; the addition of bivalent antigens with appropriate double-headed functionalities into the system would link the particles.[132]

AuNPs can be functionalized with other molecules, such as 15-crown-5 and 11-mercaptoundecanoid acid. Detection of alkali and alkaline earth metal ions, and heavy metal ions can be achieved through colorimetric mechanism as the analytes of interest induce aggregation of the functionalized AuNPs to cause color change.[133]

AuNPs aggregation can be induced by CBs, which bind to gold nanoparticles through their carbonyl groups at the portals.[89] The carbonyls are orientated perpendicularly to the particle surface.[89] The distance from portal to portal for all cucurbit[n]urils is 0.9 nm,

therefore the interparticle spacing produced by CBs is precisely at 0.9 nm. CB molecules are "rigid" enough to create precisely spaced sub-nanometer gaps in between adjacent AuNPs (Scheme 3.1),[98] therefore the plasmonics of the AuNP-CB system is reproducible.[88]

In addition, as stated in Chapter 1, CB7 molecules are able to encapsulate neutral or positively charged molecules where the cationic sites of the guest molecule are positioned along the electronegative portal(s) and its hydrophobic moiety is immersed inside the CB7 cavity. Coupling with the ability of linking AuNPs, analytes of interest can be localized in between the particles because they are recognized by CB7.

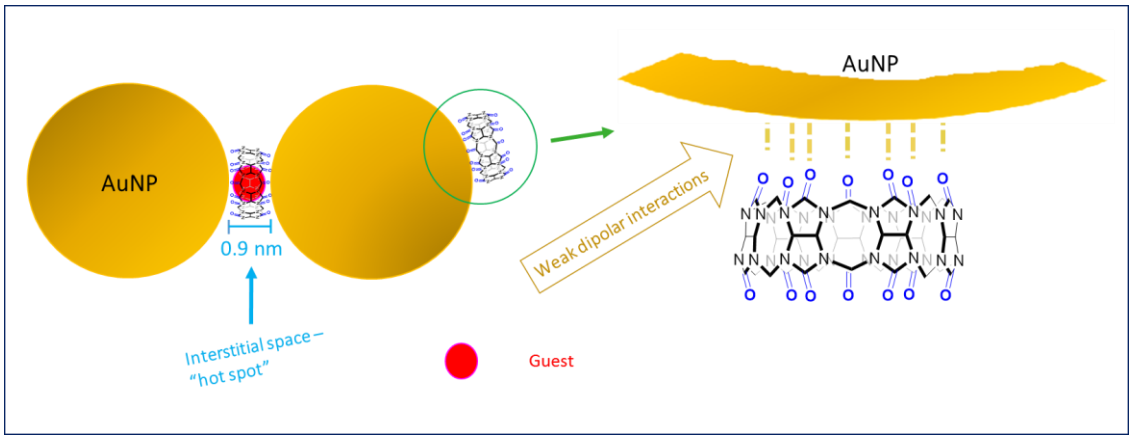

Scheme 3.1 Illustration of linkage among AuNPs provided by CB7 molecules.

The prior work with CB7 and AuNP had focused on trapping guest molecules in a way that enabled their observation by Raman. I was interested instead in how host-guest binding would influence the CB7-induced aggregation of AuNP. In considering both the host-guest binding properties, and AuNP-aggregating abilities of CB7, I had the following questions:

1. Can host-guest chemistry affect AuNP aggregation state in this system? CB7 molecules link AuNPs as stated above and also form inclusion complex with certain guest molecules, such as drug molecules, dyes, amino acids, peptides, saccharides, hydrocarbons, and proteins.[134] Will other host molecules aggregate AuNP? Will inclusion of a specific molecule by CB7 reverse or modify the process of AuNP aggregation so that the particles disaggregate? If it does, will the color of the solution change from purplish blue (AuNPs aggregated) to ruby red (AuNPs dispersed)? Will there be a correlation between the concentration of the guest and the change of absorption intensity?
2. How do analytes that compete directly for AuNP binding affect the system? Some molecules have stronger binding affinities with AuNPs, such as the ones with thiol groups. Will the linkages among AuNPs formed by CB7 molecules be broken so that the aggregation process is reversed, and the disaggregation process proceeds? If such molecules are placed in the AuNP-CB7 system, will the aggregation state change? Will there be a correlation between the concentration of the guest and the change of absorption intensity?

The results of experiments designed to seek the answers to the above questions are reported.

3.2 Experimental methods

Gold nanoparticles were purchased from BBI Solutions (20 nm diameter, 7.00×10^{11} number of particles/mL, catalog number EM.GC20). [CB7] was kept constant at 2.0 μM to study the effect of different guest molecules on AuNP disaggregation. Stock

solutions of guest molecules in dH_2O were prepared at the concentrations being 1.0 mM, 0.5 mM, 0.25 mM, 0.10 mM, 0.05 mM, 0.03 mM, 0.01 mM, 0.005 mM, and 0.001 mM.

Stock solutions of CB7 in dH_2O were prepared at the concentrations being 0.50 mM, 0.25 mM, 0.15 mM, 0.10 mM, 0.05 mM, and 0.01 mM to study the effect of CB7 concentration on AuNP aggregation.

To a 5 ml glass vial added 10 µL 0.1 mM CB7 solution in dH_2O and 10 µL of stock solutions of the analyte. Gentle mixing at room temperature was needed to ensure complete interaction between CB7 and the analyte. 480 µL of 20 nm AuNP colloidal solution was then added to the mixture to bring the total volume of the solution to 500 µL. The final concentration of CB7 was 2.0 µM. Color change of AuNP colloid occurred within seconds.

After pictures of the vials were taken, 200 µL of solution was transferred into wells of a 96-well plate. Absorbance spectra was measured from 450 nm to 800 nm using a SpectraMax® M5 / M5e Microplate Reader.

3.3 Results

3.3.1 Interactions of macrocyclic molecules with AuNPs

In an attempt to expand the list of host molecules, five macrocyclic molecules (4-Sulfocalix[4]arene, 4-Sulfocalix[6]arene, β-cyclodextrin, thiolated β-cyclodextrin, and CB7 (Figure 3.1), were tested to see if they make AuNPs to aggregate.

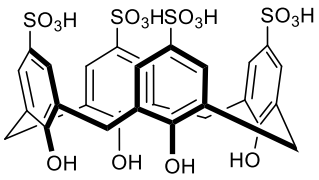

4-Sulfocalix[4]arene

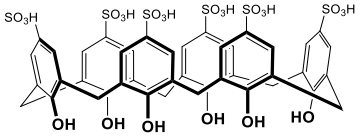

4-Sulfocalix[6]arene

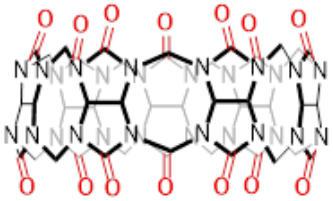

CB7

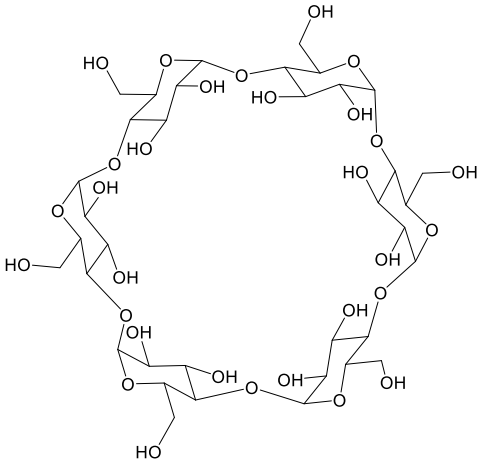

β-Cyclodextrin

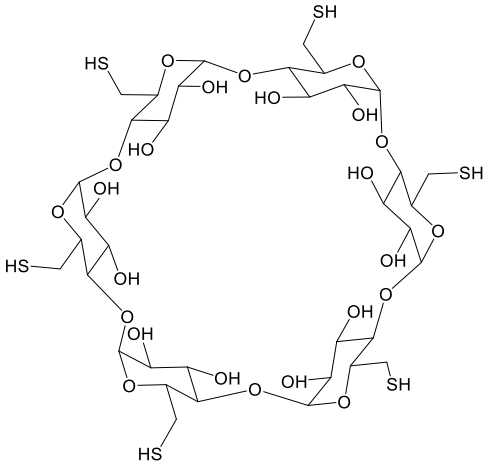

Thiol-β-Cyclodextrin

Figure 3.1 Molecular structures of macrocyclic molecules.

Among all of the macrocyclic hosts tested, only CB7 linked AuNPs under the testing condition (Figure 3.2). The color of the gold colloid changed from ruby red to purplish blue, as had been previously observed.[82] The most likely structural explanation for this aggregation is that oxygen atoms from the carbonyl groups making up the portals of CB7 coordinate to AuNPs to construct a sandwich formation with CB7 in the middle (Scheme 3.1). The other four host molecules do not possess this function because they do not have strong coordinating carbonyl oxygens.

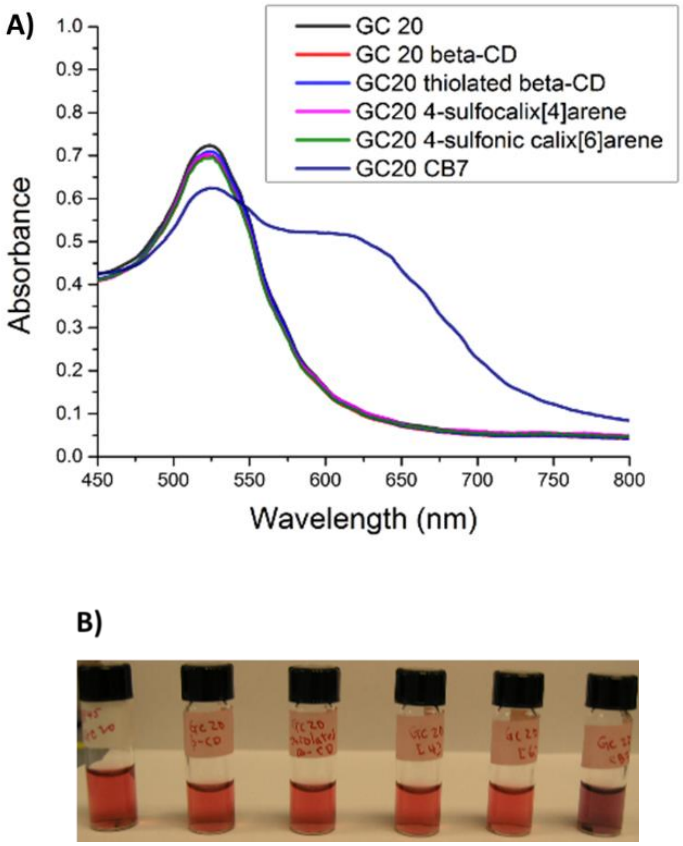

Figure 3.2 Interactions of macrocyclic molecules with AuNPs. A) Absorbance spectrum. B) Photo showing color change caused by the addition of CB7. [macrocycle] = 2.0 µM. Procedures were conducted at room temperature. Solutions in dH_2O were unbuffered. [AuNP] = 6.72×10^{11} particles/mL.

There are two absorption peaks for aggregated AuNP solution. For the reasons discussed in Chapter 1, the intense absorption peak for 20 nm spherical AuNP colloid appears at 520 nm due to interactions of the surface plasmon band of AuNPs with light.[68] The absorption of light at 522 nm (green) renders the AuNPs solution red. CB7 molecules link the AuNPs and reduce the distance between each particles. The decrease of the inter-particle distance produces a strong red shifts of the LSPR frequency around 662 nm due to particle-particle coupling.[77] (Figure 3.2).

3.3.2 Inclusion of AcAm by CB7 does not disrupt AuNP aggregation

Will inclusion of AcAm by CB7 disrupt AuNP aggregation and produce color change? In this experiment, the concentrations of AuNPs and CB7 were kept constant, while AcAm concentration changed from 0.25 ng/ml to 1600 ng/ml. CB7 was mixed with AcAm first, which was to ensure that host-guest interaction occur without the inference from the nanoparticles. The absorbance ratio at 662 nm and 522 nm was calculated and plotted against AcAm concentrations. Absorbance at 662 nm is generated by the aggregated particles; that of 522 nm by the ones still remain in suspension. The absorbance ratio of the two peaks gives more accurate representation of the impacts that AcAm or other analytes may have on the system.

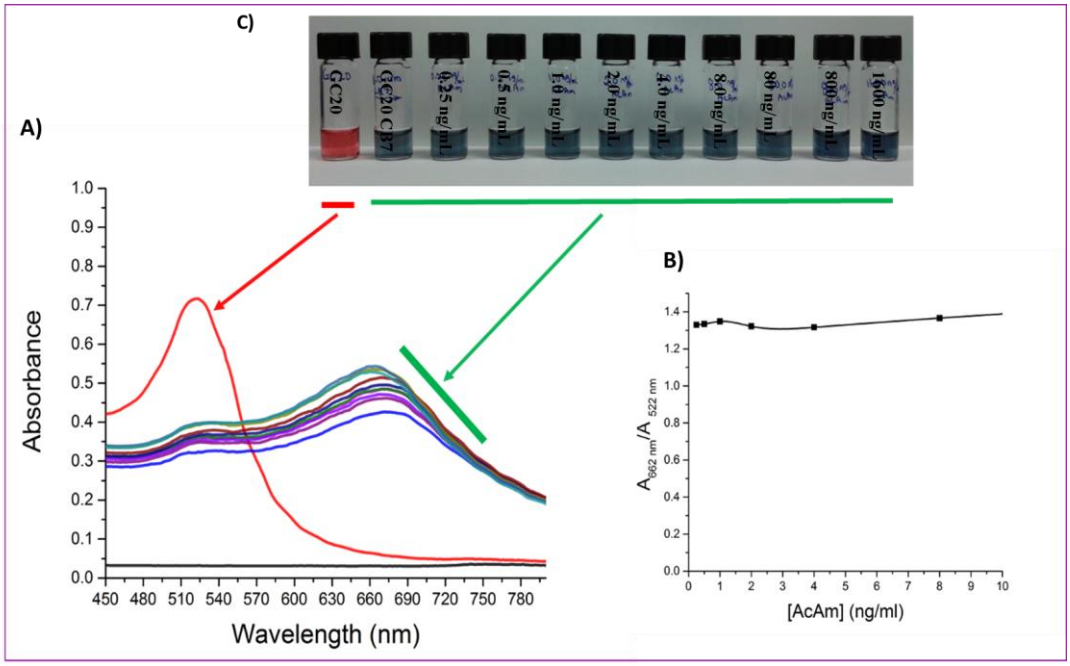

Figure 3.3 **Inclusion of AcAm by CB7 does not disrupt AuNP aggregation. A) Absorption spectrum. B) A662nm/A522nm vs [AcAm]. C) Photo of experiment showing color change. Red: AuNPs; Purplish blue: AuNP + CB7 + AcAm. [CB7] = 2.0 µM. [AcAm] = 0.25 – 1600 ng/mL. Solution was unbuffered in dH_2O. Procedures were conducted at room temperature. [AuNP] = 6.72×10^{11} particles/mL.**

Addition of the same amount of AuNP solution to different glass vials which contained the same concentration of CB7 but different concentration of AcAm did not yield any significant spectral and color change (Figure 3.3 A and C). Solutions remained purplish blue in color; AuNPs were still aggregated. A662nm/A552nm had little variation at various [AcAm] (Figure 3.3 B). The CB7-AcAm complex did not perturb the binding of CB7 with AuNPs. My explanation is that CB7 was still able to link the particles even with AcAm complexed because AcAm is a small molecule.

When encapsulated inside the hydrophobic cavity of CB7, due to its small size, AcAm has no effect on the oxygen atoms on the carbonyl portals to reach out to and therefore to interact with AuNPs (Scheme 3.2). The distance between the two portals, and therefore between the neighboring AuNP, should remain at 0.9 nm. As [AcAm] increased, the absorbance ratio of the two peaks did not change; there was no significant change of optical signal. Because AcAm was mixed with CB7 first before AuNP was added, AcAm interacted with CB7 and formed host-guest complex before the addition of particles. The opportunity for AcAm to stay outside of CB7 cavity before CB7 got saturated with AcAm did not exist. Therefore, AcAm cannot be detected this way.

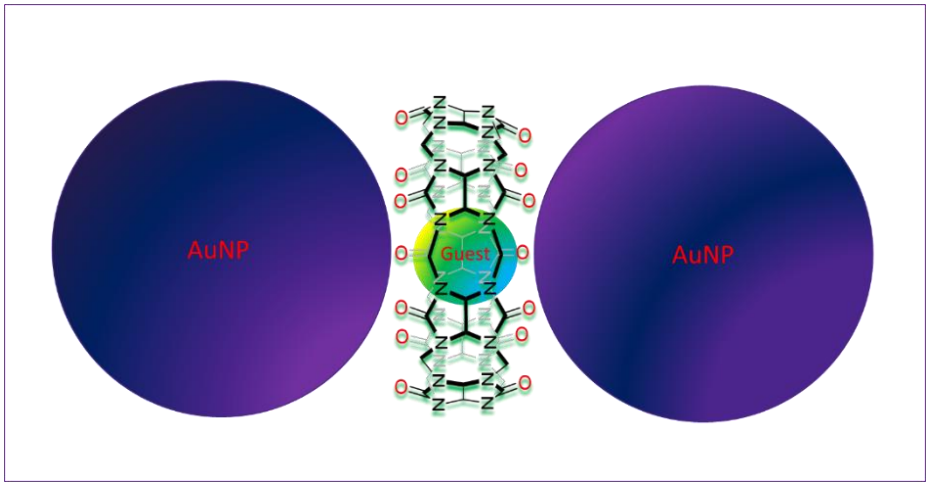

Scheme 3.2 Inclusion of a small guest molecule by CB7 does not disrupt AuNP aggregation. The color of the solution remains purplish blue.

I continued with testing some bigger guest molecules, such as RhB, to find out their effects on AuNP aggregation as guest molecules in the CB7-guest complex.

3.3.3 Inclusion of RhB by CB7 disrupts AuNP aggregation

RhB was added to CB7 first, then ruby red colored AuNP solution was added. The color of the solution remained ruby red. The host-guest complex of RhB with CB7, CB7-RhB, did not cause aggregation of AuNPs as CB7 alone or CB7-AcAm complex did (Figure 3.4). CB7 is disabled from linking AuNPs due to the inclusion of RhB in its hydrophobic cavity. RhB can cause gold nanoparticle to disaggregate.

RhB solutions are red, so in order to rule out the color of RhB itself in driving the optical response, the absorbance of the same concentration of RhB in dH2O was measured as well. The absorbance peaked at 555 nm with the absorbance below 0.1 (Figure 3.4). This indicates that the intrinsic absorbance of RhB should not cause interference to the absorption measurement of the system which absorption peaks are at 522 nm and 662 nm with much stronger absorption.

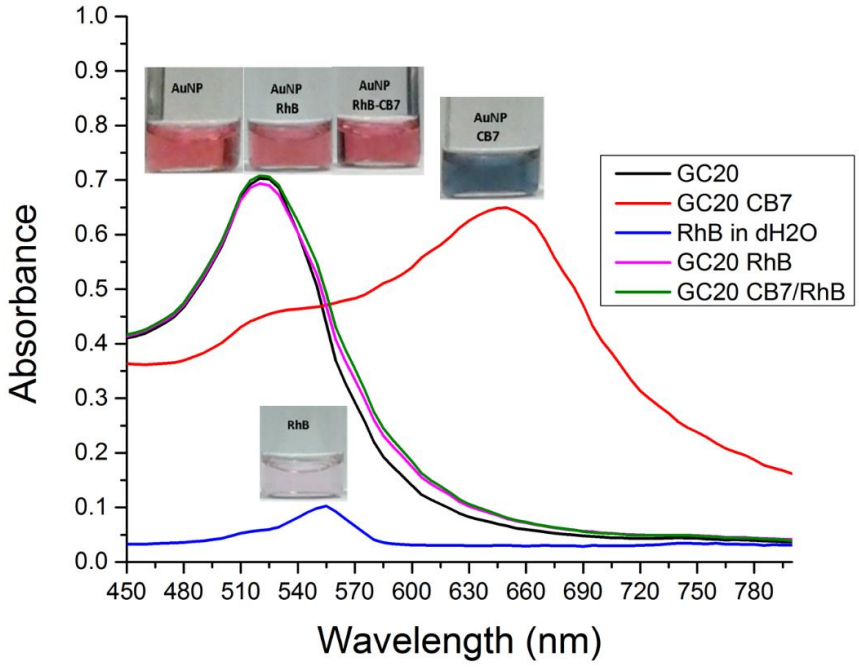

Figure 3.4 Inclusion of RhB by CB7 disrupts AuNP aggregation. [CB7] = [RhB] = 2.0 µM. Solution was unbuffered in dH_2O. Procedures were conducted at room temperature. [AuNP] = 6.72×10^{11} particles/mL. GC20 is 20 nanometer gold nanoparticles and used interchangeably in the thesis with AuNP.

As depicted in Figure 2.5, the portion of RhB that sticks out of the CB7 portal, which is one of the two N,N-diethylamino groups attached to the xanthene core, is bulky enough to prevent the carbonyl oxygens of CB7 from reaching out to and from interacting with the particles.[120] With RhB encapsulated, the two portals of CB7 are not able to connect the AuNPs simultaneously to construct a sandwich configuration with the inter-particle distance being 0.9 nm. AuNPs stay in solution not aggregated; the color of the solution remains ruby red (Scheme 3.3).

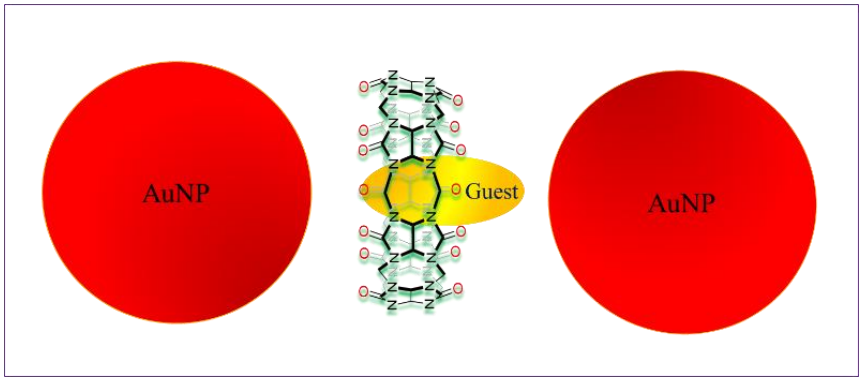

Scheme 3.3 Inclusion of a large guest molecule by CB7 disrupts AuNP aggregation. The color of the solution remains ruby red.

To summarize, addition of CB7 molecules to colloidal AuNPs changes the color of the solution from ruby red to purplish blue due to AuNP aggregation. Inclusion of AcAm by CB7 does not cause AuNPs to disaggregation, but RhB does. RhB is a much bigger molecule than AcAm. Therefore, the idea coming from these experiments was that the size of the CB7 guest molecules play a key role on AuNP disaggregation as illustrated in Scheme 3.4.

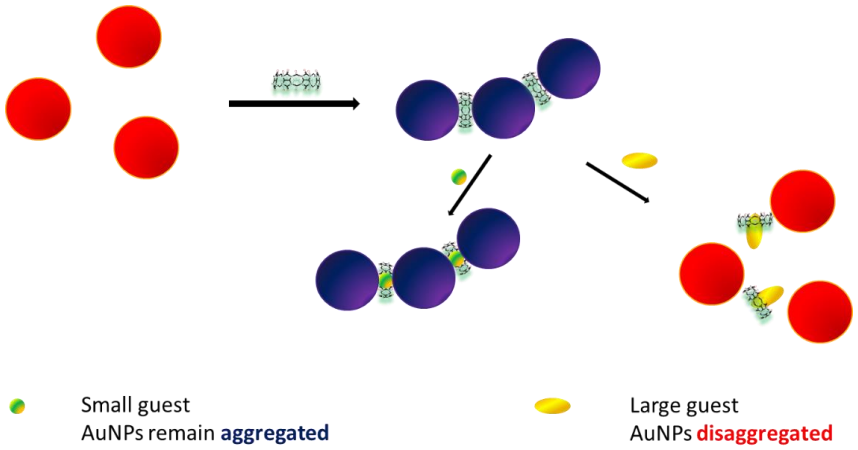

Scheme 3.4 Proposed size effect of CB7 guest molecules on AuNP disaggregation.

3.3.4 Properties of CB7 inclusion molecule on AuNP disaggregation

For AcAm, the acetamide moiety that sticks out of the CB7 portal is too small to maintain a big enough distance between carbonyl oxygens and the particles therefore the inclusion complex can still link the particles.

To test if a bulkier group substituted amantadine would make any difference, I synthesized benzoyl amantadine (BzAm), where acetyl group is replaced by benzoyl group on AcAm. Besides BzAm, together tested were Am, AcAm, phenylalanine, tryptophan, BER, RhB, 1,8-ANS, thiazole orange and methylene blue in this set of experiment (Figure 3.5). RhB was used as a positive control and AcAm as a negative one for AuNP disaggregation.

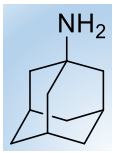

Am

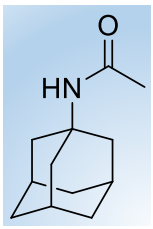

AcAm

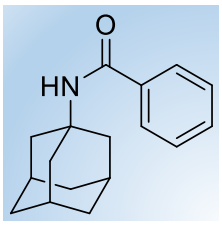

BzAm

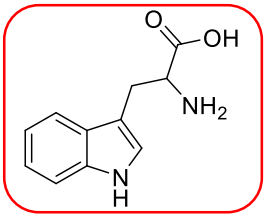

Tryptophan (Trp)

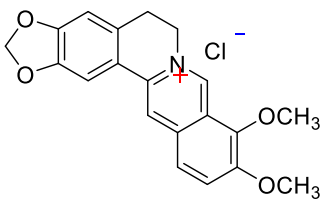

BER

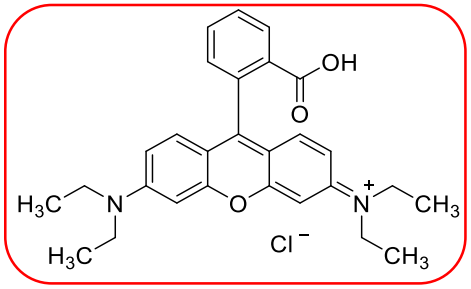

RhB

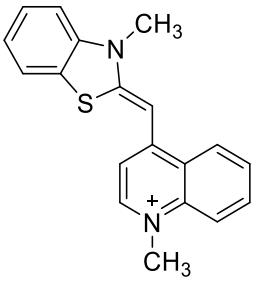

Thiazole orange (TO)

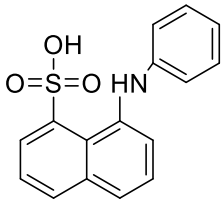

1,8-ANS

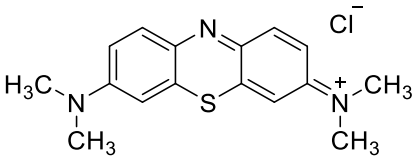

Methylene blue (MB)

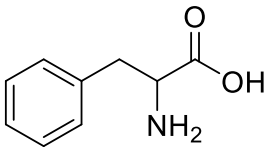

Phenylalanine (Phe)

Figure 3.5 Molecular structures of some guest molecules.

It turned out that CB7-BzAm complex did not cause AuNP to disaggregate. The solution remained purplish blue. BzAm is not big enough? Neither did the rest of the complexes in this group except CB7-RhB and CB7-tryptophan (Figure 3.6). BER is a bigger molecule than tryptophan, yet it does not cause disaggregation. Therefore, the size of the guest molecule for CB7 is not the only contributing factor to cause AuNP disaggregate.

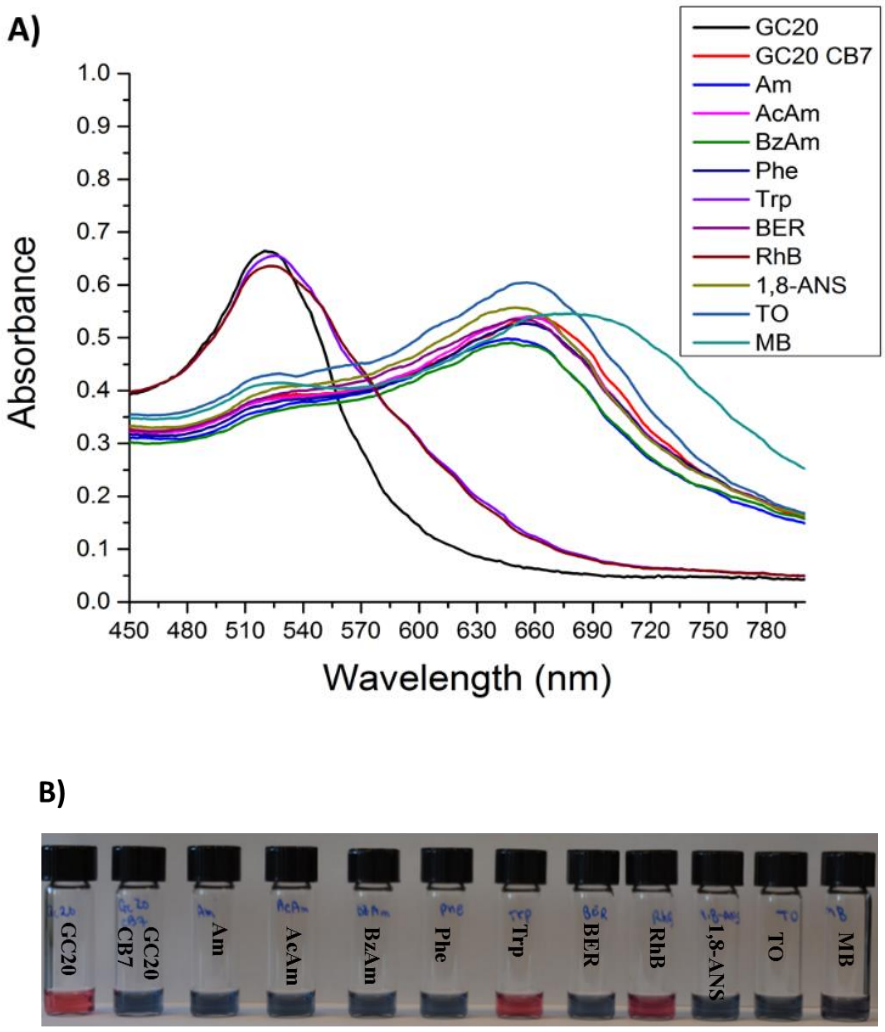

Figure 3.6 Effects of various guest inclusion by CB7 on AuNP disaggregation. A) Absorbance spectrum. B) Photo showing color change caused by the addition of various molecules. [CB7] = [guest] = 2.0 μM. Solution was unbuffered in dH_2O. Procedures were conducted at room temperature. [AuNP] = 6.72×10^{11} particles/mL.

This set of results led me to consider questions other than the size of the guest molecules. What is it so unique about tryptophan? Is it its indole ring?

3.3.5 Tryptophan and its relatives

In this set of experiment, indole and some of its relatives (Figure 3.7) were tested to find out if the indole moiety is the key contributing factor for tryptophan to cause AuNPs to disaggregate.

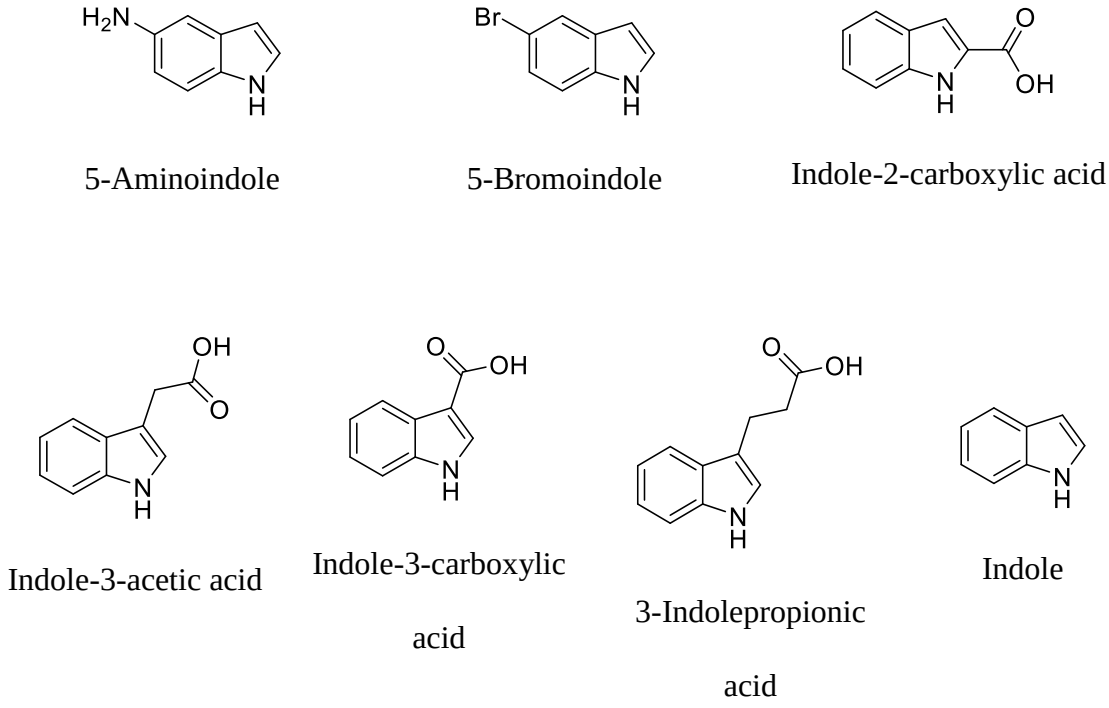

Figure 3.7 Molecular structure of indole and its derivatives.

Tested molecules in this series included AcAm (negative control), RhB (positive control), Trp, 5-Aminoindole, 5-Bromoindole, Indole-2-carboxylic acid, Indole-3-acetic acid, Indole-3-carboxylic acid, 3-Indoproprionic acid, and indole (Figure 3.8), which are represented using numbers from 1 to 10 respectively on the vials in Figure 3.8 B. None of the CB7-guest complexes cause AuNP disaggregation except for CB7-RhB and CB7-Trp. This indicates that the indole rings alone do not disaggregate the AuNPs.

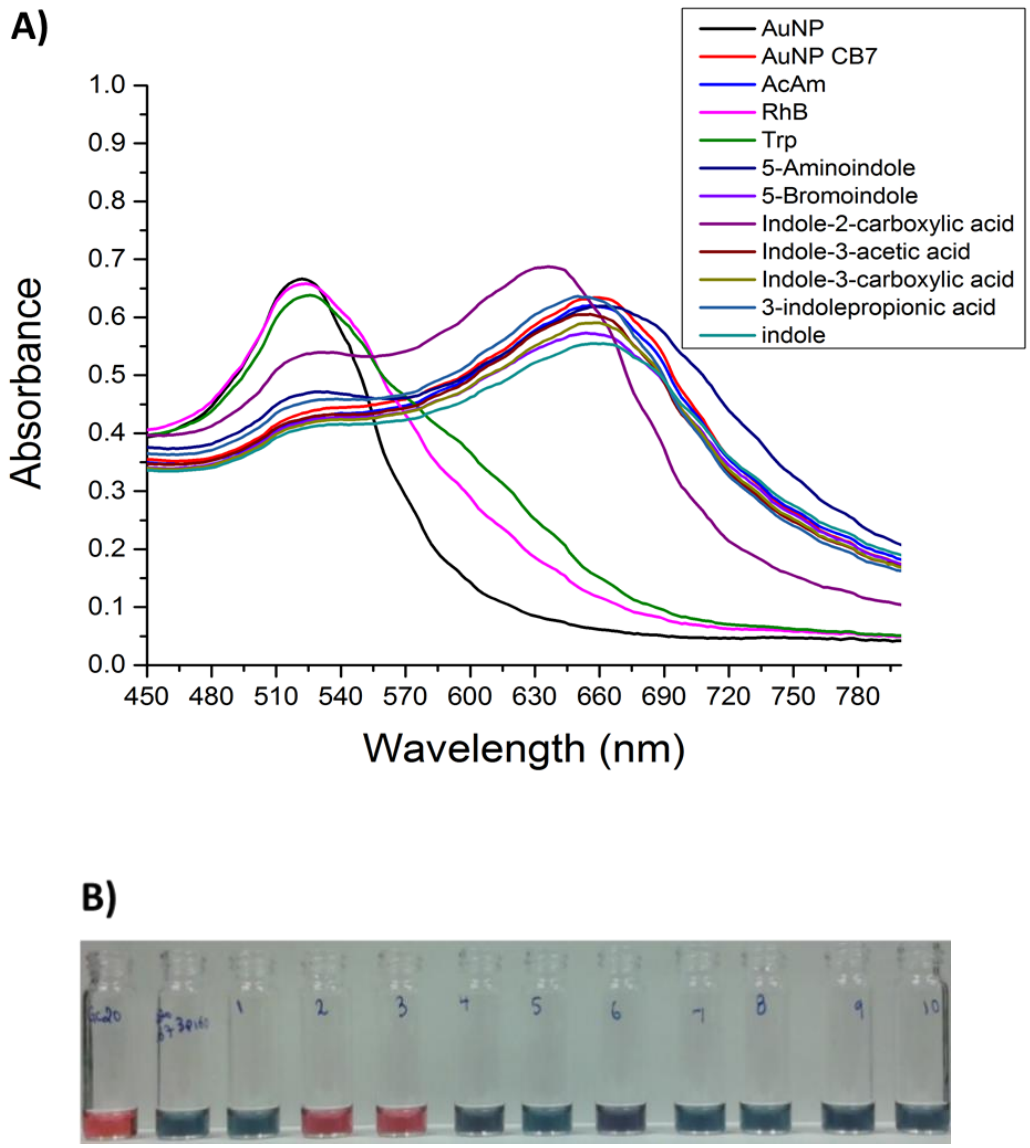

Figure 3.8 Effects of inclusion of indole and its relatives by CB7 on AuNP disaggregation. A) Absorbance spectrum. B) Photo showing color change caused by the addition of various molecules. [CB7] = [guest] = 2.0 μM. Solution was unbuffered in dH_2O. Procedures were conducted at room temperature. 1 = AcAm, 2 = RhB, 3 = Trp, 4 = 5-Aminoindole, 5 = 5-Bromoindole, 6 = Indole-2-carboxylic acid, 7 = Indole-3-acetic acid, 8 = Indole-3-carboxylic acid, 9 = 3-indolepropionic acid, 10 = indole. Guest molecules 1-10 were mixed with CB7 first before the addition of AuNPs. [AuNP] = 6.72 × 10^{11} particles/mL.

3.3.6 Imidazole and hydrophobic compounds

In this set of experiment, tested molecules included menthol, threonine, methionine, arginine, cysteine, serine, corticosterone, imidazole, 1-methyl imidazole, ethyl 4-aminobenzoate, and dextrose. RhB and AcAm were used as positive and negative controls for AuNP disaggregation, respectively. Into glass vials, each of the above compounds was mixed with CB7. Same amount of colloidal AuNPs was added into each vial. In this section, I only discuss about the results for imidazole and hydrophobic compounds (Figure 3.9 and Figure 3.10). Those for the amino acids will be discussed in the following section.

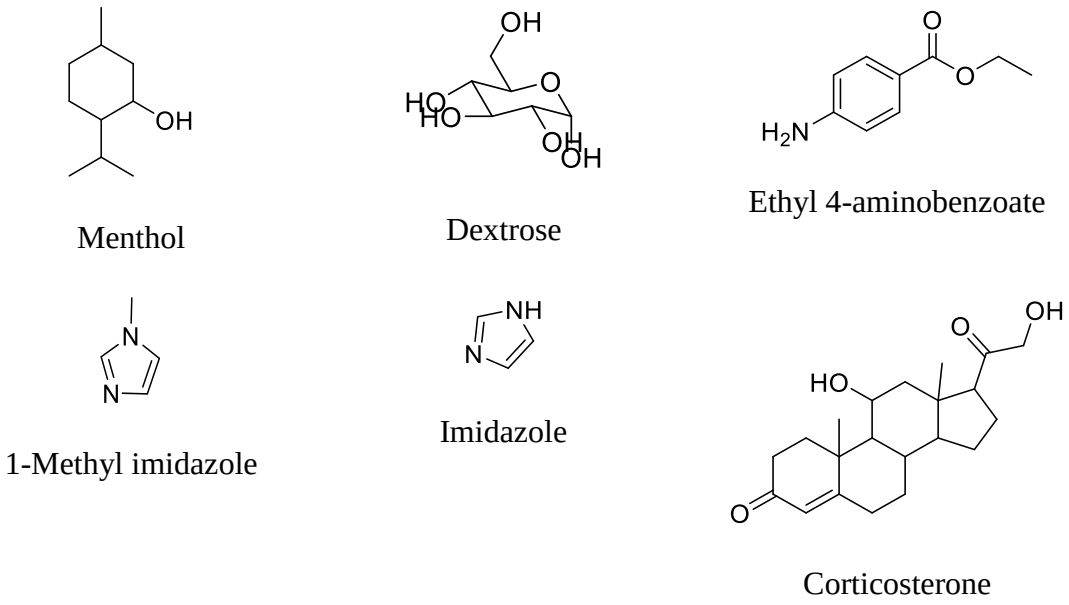

Figure 3.9 Molecule structures of six guest molecules. They are menthol, dextrose, ethyl 4-aminobenzoate, 1-methyl imidazole, imidazole, and corticosterone.

Imidazole and 1-Methyl imidazole do not disrupt AuNP aggregation despite the fact that each of them forms inclusion complex with CB7,[135] neither does menthol even though it forms 1:1 complex with CB7.[136] I think that the three molecules are all too small

to cause AuNP to disaggregate. Addition of dextrose, ethyl 4-aminobenzoate, or corticosterone does not disrupt AuNP aggregation either (Figure 3.10).

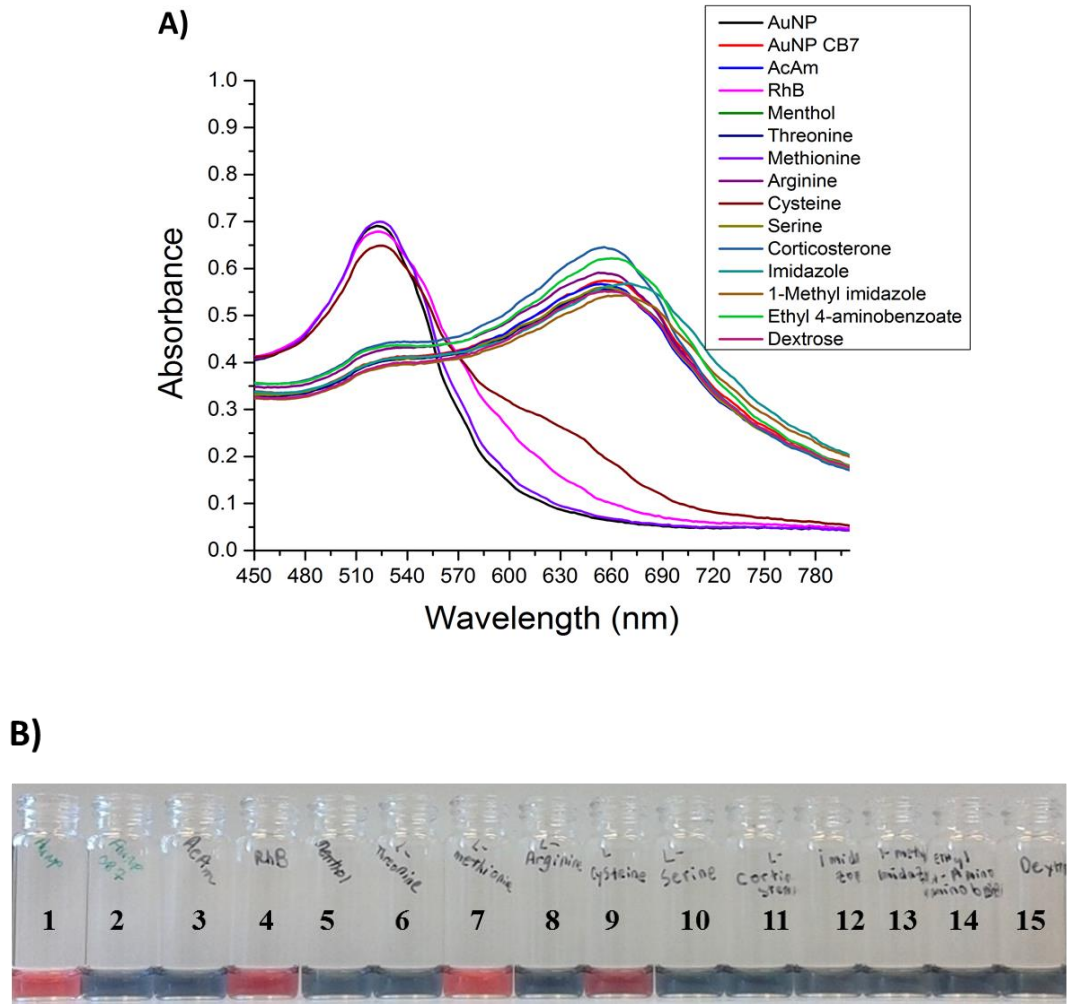

Figure 3.10 Effects of guest molecules in the presence of CB7 on AuNP disaggregation. A) Absorbance spectrum. B) Photo showing color change caused by the addition of various molecules. 1 = AuNP, 2 = AuNP + CB7, Guest molecules were in vials 3 to 15 with constant concentrations of AuNP and CB7. 3 = AcAm, 4 = RhB, 5 = menthol, 6 = threonine, 7 = methionine, 8 = arginine, 9 = cysteine, 10 = serine, 11 = corticosterone, 12 = imidazole, 13 = 1-methyl imidazole, 14 = ethyl 4-aminobenzoate, and 15 = dextrose. [CB7] = [guest] = 2.0 µM. [AuNP] = 6.72 × 10^{11} particles/mL. Solutions were unbuffered. Measurements were conducted at room temperature.

3.3.7 Amino acids

This section discusses the effect of amino acids on AuNP disaggregation. Tested amino acids included phenylalanine, tryptophan (Figure 3.5), threonine, arginine, serine, methionine, cysteine (Figure 3.10 and Figure 3.11), glycine, alanine, valine, leucine, isoleucine, aspartic acid, glutamic acid, asparagine, glutamine, histidine, and proline (Figure 3.11 and Figure 3.13).

Methionine and cysteine caused AuNP disaggregation. Both of them are sulfur-containing amino acids, but none of them form inclusion complex with CB7 as they do not contain aromatic rings, neither do they have long carbon chains as lysine does (Scheme 3.5).[137]

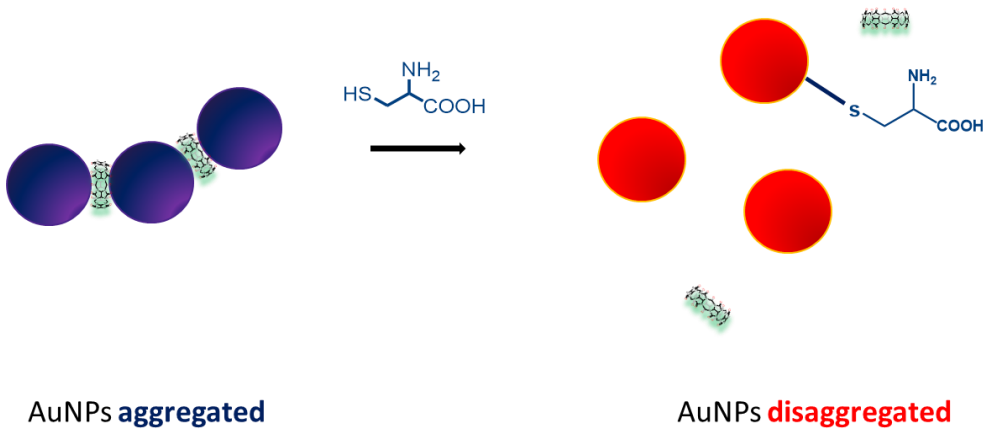

Scheme 3.5 Sulfur-containing amino acids on AuNP disaggregation.

Organosulfur compounds have a strong binding affinity with gold nanoparticles[129,138,139,140] because of the possibility they coordinate very strongly to the particles to form multiple bonds.[141] The interaction between sulfur-containing amino acid

and gold nanoparticles would break the CB7 linkage among AuNPs. The state of AuNPs would change from being aggregated to being disaggregated (Scheme 3.5).

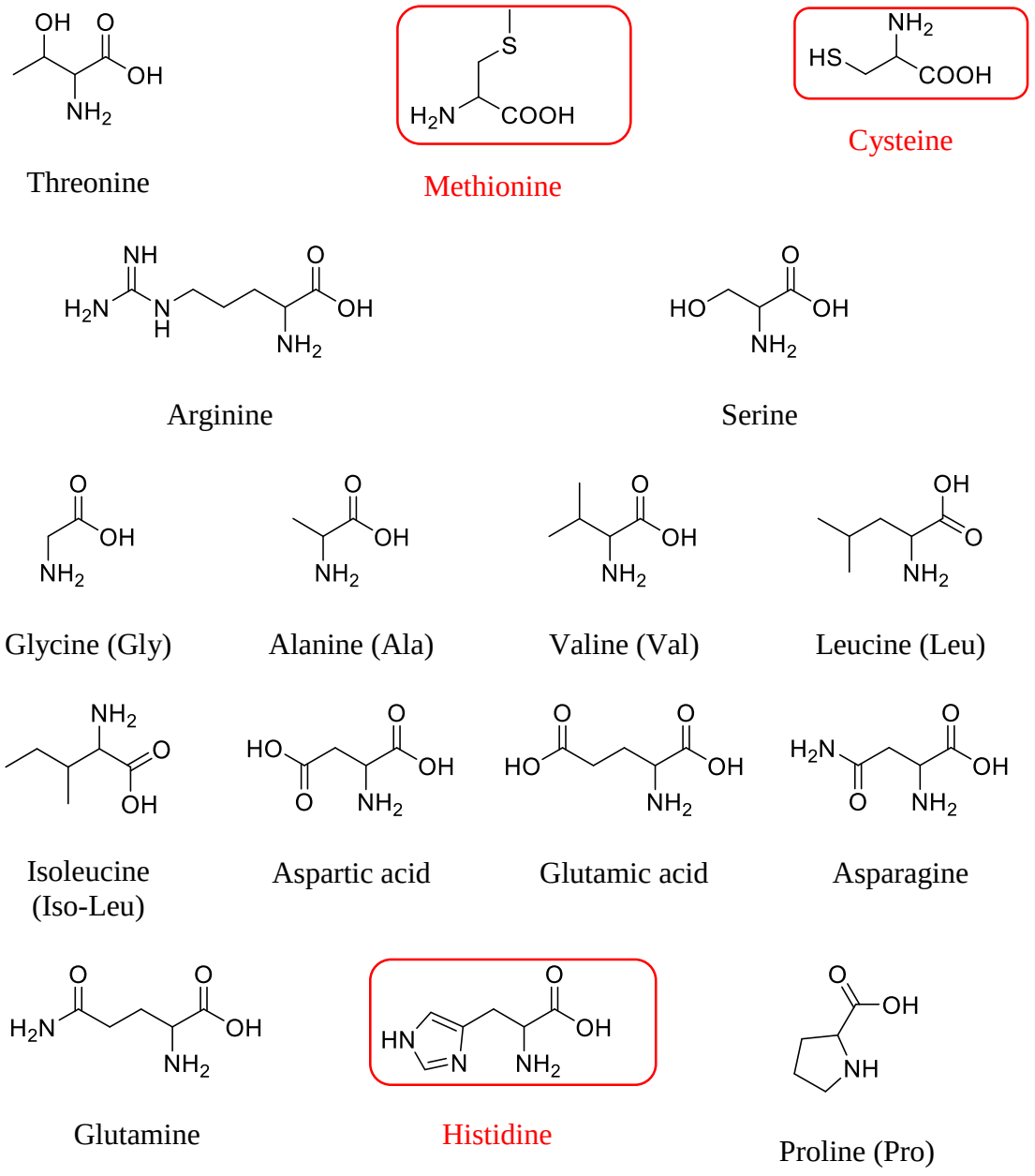

Figure 3.11 Molecule structures of amino acids. Amino acids: glycine, alanine, valine, leucine, iso-leucine, aspartic acid, glutamic acid, asparagine, glutamine, histidine, and proline.

Among all the amino acids tested, besides tryptophan, methionine, and cysteine, histidine also disrupts AuNP aggregation (Figure 3.13). It forms inclusion complex with CB7 just as tryptophan does.[137] In order to see the similarities easier, imidazole, 1-methyl imidazole, histidine, tryptophan, and phenylalanine are placed side by side (Figure 3.12).

Comparing to imidazole and 1-methyl imidazole, histidine has a bulky alanyl group connecting to the imidazole ring. I think it is this group that prevents CB7 from linking AuNPs.

For tryptophan, the alanyl group is connected to an indole ring instead of an imidazole ring (histidine), and both of the indole ring and imidazole rings contain one nitrogen, which could be a very important element here. Phenylalanine is made up of alanyl group and a phenyl group, which does not contain a nitrogen atom. The complex of CB7 and phenylalanine does not disrupt AuNP aggregation.

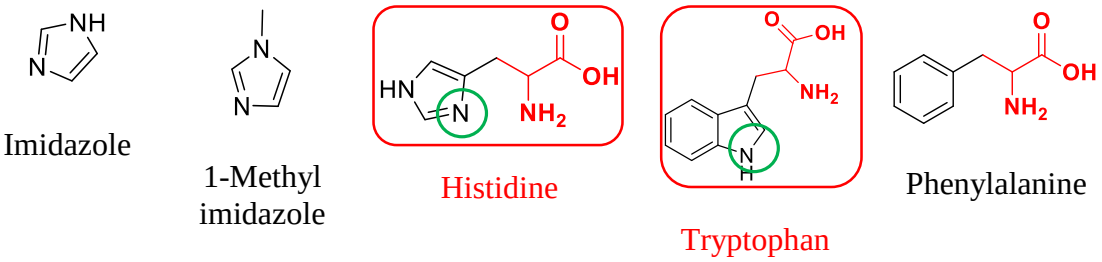

Figure 3.12 Comparison of molecular structures of imidazole and amino acids.

The amino acid guest molecules for CB7 have to have two moieties in order for them to disable CB7 from linking AuNPs: the one that is included in the CB7 cavity has to

have a nitrogen atom in the structure. The other moiety has to be sticking out from the CB7 cavity and it has to have both of amine and carboxylic groups.

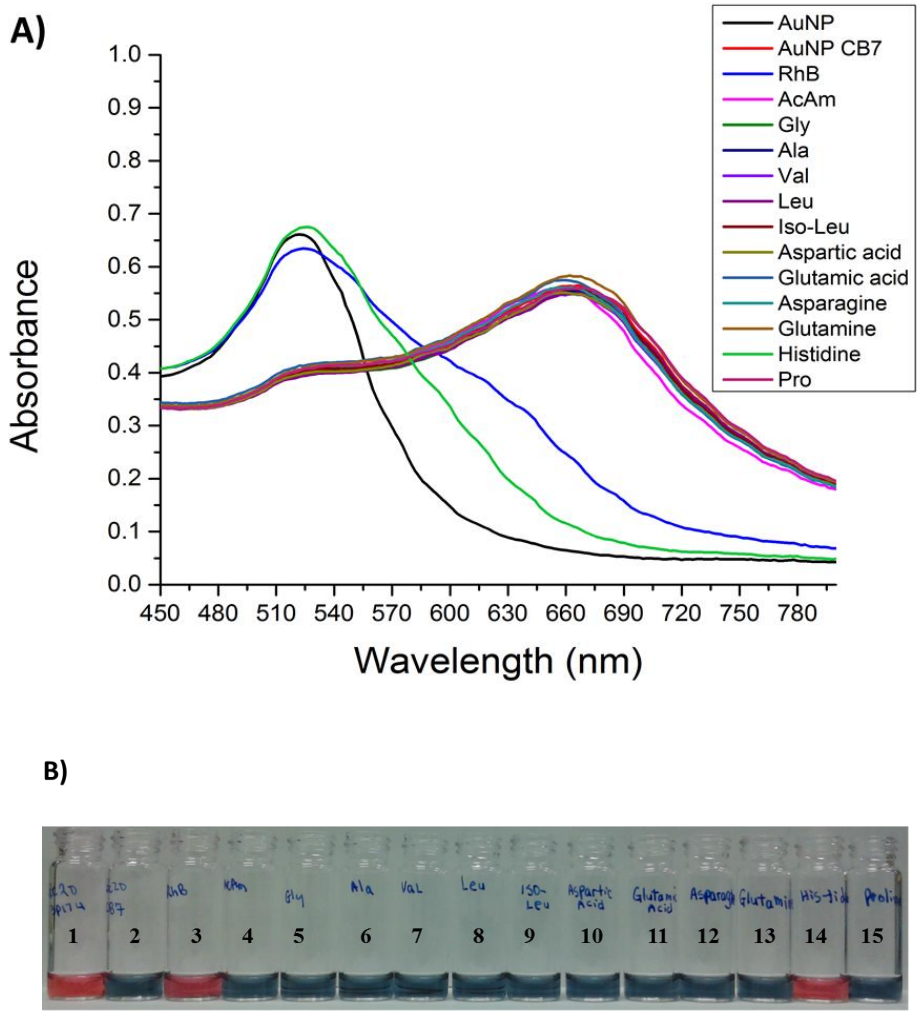

Figure 3.13 Effects of amino acids in the presence of CB7 on AuNP disaggregation. A) Absorbance spectrum. B) Photo showing color change caused by the addition of various molecules. 1 = AuNP, 2 = AuNP + CB7. Guest molecules were in vial 3 to 15. 3 = RhB, 4 = AcAm, 5 = glycine, 6 =alanine, 7 =valine, 8 = leucine, 9 = isoleucine, 10 = aspartic acid, 11 = glutamic acid, 12 = asparagine, 13 = glutamine, 14 = histidine, and 15 = proline. [CB7] = [guest] = 2.0 µM. [AuNP] = 6.72×10^{11} particles/mL. Solutions were unbuffered. Measurements were conducted at room temperature.

3.3.8 Effects of CB7 concentration on AuNP aggregation with and without the presence of methionine

I classify the molecules that disrupt CB7-linked AuNP aggregation into two groups: non sulphur-containing compounds that form inclusion complex with CB7, such as tryptophan; and sulphur-containing compounds that break the linkage through sulphur gold interaction. I conclude through the experiments that the molar ratio between CB7 and AuNP is a very important factor in order for AuNP to aggregate (Figure 3.14). I chose 2.0 μM as CB7 concentration. For a 500 μL solution with 20 nm AuNP being 480 μL and 2.0 μM CB7 being 10 μL, the ratio between the number CB7 molecules and the number of AuNP particles is 3.5 ($7 \text{ X } 10^{11}$ AuNP particles/mL, supplier website).

To test the effect of CB7 concentration on AuNP aggregation, 10 μL of various concentrations of CB7 stock solution were pipetted into class vials; 490 μL of 20 nm AuNP solution was added to CB7. The total volume of the solution was 500 μL making the final concentrations of CB7 to range from 0.2 μM to 20.0 μM. When [CB7] was at 0.2 μM, there was no aggregation indicating that not enough CB7 molecules in solution to link the particles; when [CB7] increased to 1.0 μM and above, aggregation was induced with relatively constant absorbance ratio at 656 nm/522 nm (Figure 3.14) indicating that the system was saturated with CB7 molecules.

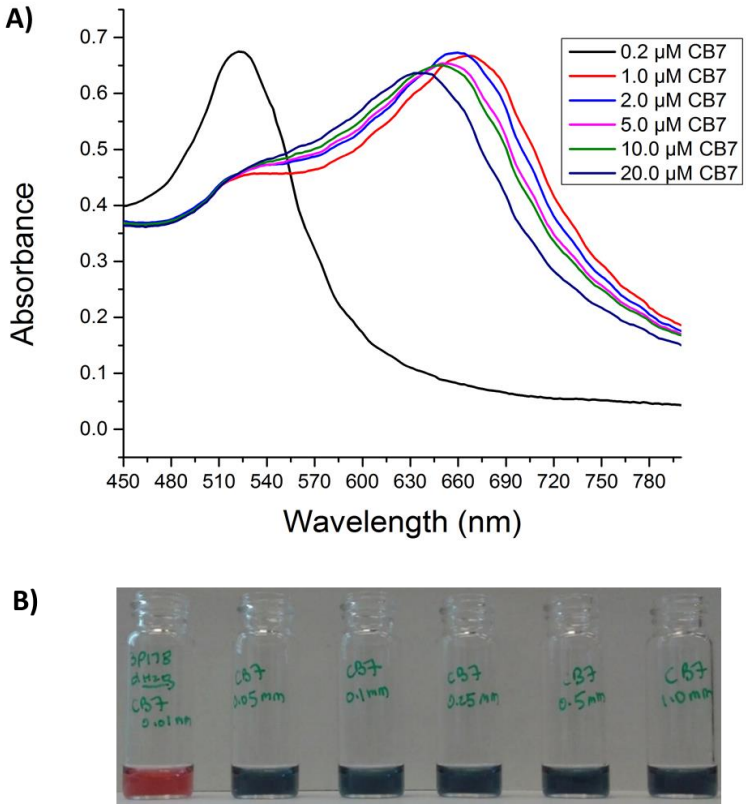

Figure 3.14 Effects of CB7 concentration on AuNP aggregation. [CB7] = 0.2 - 20.0 μM. Solution was unbuffered in dH_2O. [AuNP] = 6.72×10^{11} particles/mL.

For each of the following experiment, [CB7] was fixed at 1.0 μM, 2.0 μM, and 5.0 μM, respectively while [methionine] varied. After a short period of gentle mixing, AuNP was added to the solution. Absorbance was measured and the Abs ratio (656 nm/522 nm) is plotted against [methionine] (Figure 3.15).

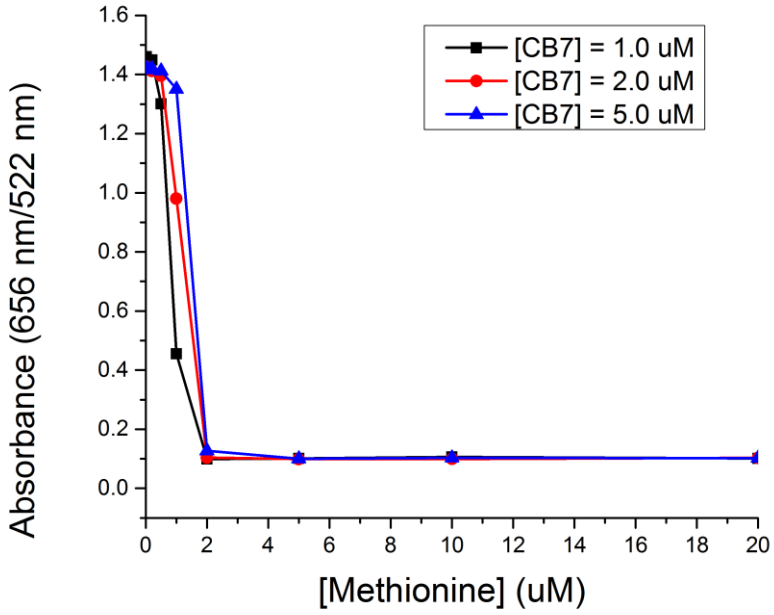

Figure 3.15 Absorbance ratio (656 nm/522 nm) vs [methionine] at different [CB7]. [CB7] = 1.0, 2.0, 5.0 µM. [AuNP] = 6.72×10^{11} particles/mL. Solutions were unbuffered. Measurements were conducted at room temperature.

The absorbance ratio starts to reach a constant value when [methionine] turns to 2 µM despite change of CB7 concentrations. This indicates that the interaction between methionine and CB7, if there is any, would be minimal comparing to the one between methionine and the nanoparticles, which serves as the driving force for the AuNP disaggregation process.

3.3.9 Effects of CB7 concentration on AuNP aggregation with the presence of tryptophan

For each of the following experiment, [CB7] was fixed at 1.0 µM and 3.0 µM respectively while [Trp] varied. After a short period of gentle mixing, AuNP was added to the solution. Absorbance was measured and the Abs ratio (656 nm/522 nm) is plotted against [Trp] (Figure 3.16).

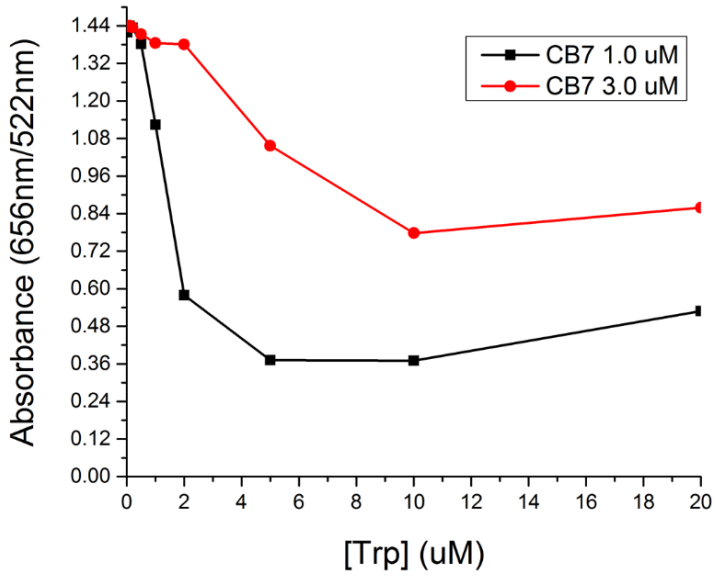

Figure 3.16 Absorbance ratio (656 nm/522 nm) vs [Trp] at different [CB7]. [AuNP] = 6.72 × 10^{11} particles/mL. Solutions were unbuffered in dH_2O.

At any [Trp], the absorbance ratio when [CB7] is at 3.0 μM is bigger than that when [CB7] is at 1.0 μM. This indicates that encapsulation of Trp by CB7 does play a role on AuNP disaggregation, which is different from the methionine-CB7-AuNP system (Figure 3.15), where methionine interacts with the AuNPs directly.

How can we utilize the AuNP disaggregation phenomenon for molecular sensing? The color change during AuNP disaggregation caused by the molecules tested, RhB, tryptophan, cysteine, methionine, and histidine, can be used for the detection of these molecules. To prove this concept, results for the detection of tryptophan, methionine, and histidine in deionized water using AuNP disaggregation are presented in the following sections. Attempts were also made in humane urine, but did not work well due to interferences in the sample. Cations such as Na^+ and K^+ would line up the CB7 portals through ion-dipole interaction preventing CB7 to link AuNPs.

3.3.10 Tryptophan sensing based on AuNP disaggregation

CB7 solution was added to tryptophan solution. After gently mixing, AuNP was added. The concentration of CB7 was 2.0 μM and that of tryptophan varied from 0.02 to 20.0 μM. Tryptophan concentration increases as the numbers on the glass vials increase.

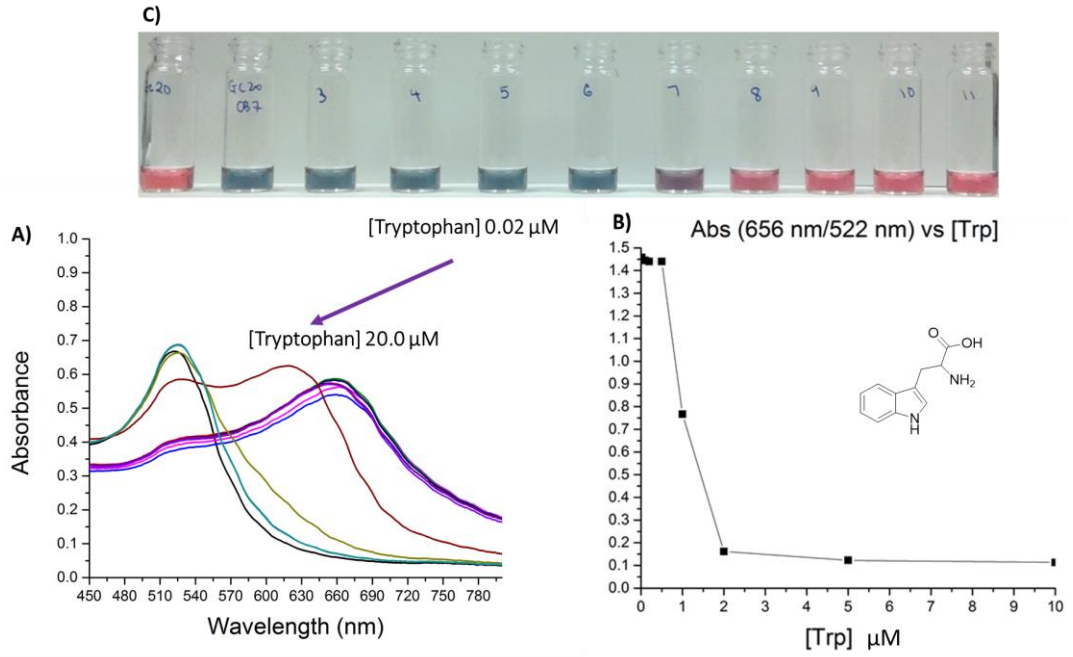

Figure 3.17 Tryptophan sensing based on AuNP disaggregation. A) Absorbance spectrum. B) Relationship between absorbance ratio at 656 nm and 522 nm and [Tryptophan]. C) Photo showing color change caused by the addition of tryptophan of different concentration. Vials 3 to 11 contained constant concentrations of AuNP and CB7. [Tryptophan] in vials 3 to 11 varied from 0.02 – 20.0 μM. [CB7] = 2.0 μM. [AuNP] = 6.72×10^{11} particles/mL. Solutions were unbuffered. Measurements were conducted at room temperature.

When there is no tryptophan in the system, CB7 molecules link AuNPs to form aggregates. The solution is purplish blue and the spectra has two peaks with one at 522 nm produced by colloidal AuNPs, and the other 656 nm produced by aggregated AuNPs. Upon addition of tryptophan into the system, the color of the solution gradually changes from

purplish blue to pinkish red as [Trp] increases. In the meantime, the absorption peak produced by aggregated AuNPs shifts to the left. The absorption peak ratio (656 nm/522 nm) turned to be constant when [Trp] was set at or greater than 2.0 μM, at which point the absorption peak produced by aggregated AuNPs disappeared (Figure 3.17).

When [Trp] is equal or greater than that of [CB7] (2.0 μM), tryptophan molecules occupy all of CB7 hydrophobic cavities. The inclusion of tryptophan disables CB7 from linking AuNPs as discussed in previous section. The increase of tryptophan concentration in the system reduces the number of CB7 molecules available to link AuNPs, therefore less AuNPs are linked and less aggregation is present, the color of the solution returns to ruby red eventually. There is a correlation between the absorbance ratio of 656 versus 522 nm and the tryptophan concentration.

3.3.11 Methionine sensing based on AuNP disaggregation

The concentration of CB7 was 2.0 μM and that of methionine varied from 0.1 to 10.0 μM. Methionine concentration increases as the numbers on the glass vials increase.

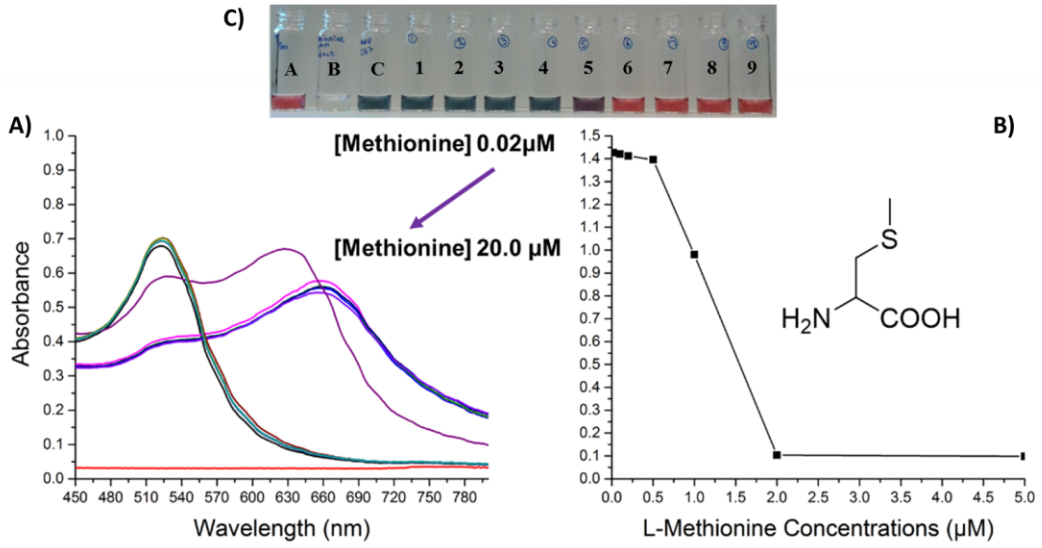

Figure 3.18 Methionine sensing based on AuNP disaggregation. A) Absorbance spectrum. B) Relationship between the absorbance ratio at 656 nm and d522 nm and [methionine]. C) Photo showing color change caused by the addition of methionine of different concentrations ranged from 0.02 – 20.0 μM. Vial A = AuNP, vial B = methionine in dH_2O, vial C = AuNP + CB7, vials 1 to 9 contained constant concentrations of AuNP and CB7, but different concentrations of methionine. [CB7 = 2.0 μM. [AuNP] = 6.72×10^{11} particles/mL. Solution was unbuffered in dH_2O.

When there methionine is absent in the system, CB7 molecules link AuNPs to form aggregates. The solution turns to purplish blue from ruby red and the absorption spectrum has two peaks with one at 522 nm produced by colloidal AuNPs, and the other 656 nm produced by aggregated AuNPs. Upon addition of methionine into the system, the color of the solution gradually changes from purplish blue to pinkish red as the amino acid concentration increases. In the meantime, the absorption peak produced by aggregated AuNPs shifts to the left indicating the amount of aggregated AuNPs is decreasing. The absorption peak ratio (656 nm/522 nm) turned to be constant when methionine concentration was set at or greater than 2.0 μM, at which point the absorption peak produced by aggregated AuNPs disappeared (Figure 3.18).

When the concentration of methionine is equal or greater than that of [CB7] (2.0 μM), methionine molecules break all the linkages formed by CB7 among AuNPs through sulphur-AuNP interaction (Scheme 3.5). The increase of methionine concentration in the system reduces the number of AuNPs aggregated, the color of the solution returns to ruby red eventually. There is a correlation between the absorbance ratio of 656 versus 522 nm and the methionine concentration.

3.3.12 Histidine sensing based on AuNP disaggregation

The concentration of CB7 was set at 2.0 μM and that of histidine varied from 0.1 to 10.0 μM. Histidine concentrations were written on the vials.

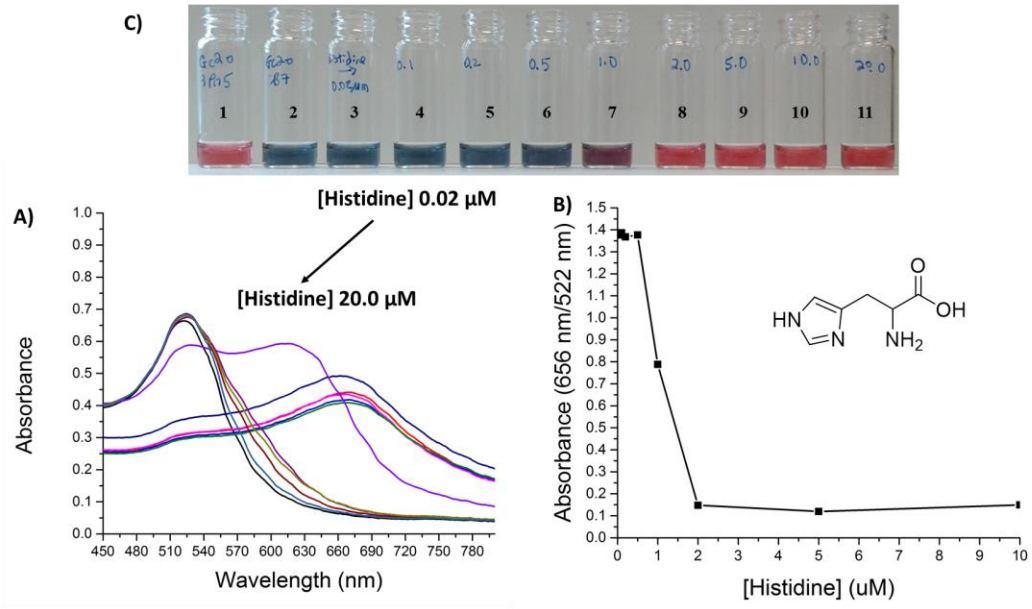

Figure 3.19 Histidine sensing based on AuNP disaggregation. A) Absorbance spectrum. B) Relationship between the absorbance ratio at 656 nm and 522 nm and [histidine]. C) Photo showing color change caused by the addition of histidine at different concentrations ranged from 0.02 – 20.0 μM. 1 = AuNP, 2 = AuNP + CB7, vials 3 to 11 contained constant concentrations of AuNP and CB7 but different concentrations of histidine. [CB7] = 2.0 μM. [AuNP] = 6.72×10^{11} particles/mL. Solution was unbuffered in dH_2O.

The color change and the relationship between absorbance ratio and [Histidine] are similar to those for tryptophan and methionine (Figure 3.19).

3.4 Discussion

One of the factors that have impact on the colors of AuNP colloidal solution is the interparticle spacing.[68] When they are in the dispersed state, the color of the solution is ruby red. Addition of CB7 change the color of the solution to purplish blue due to shortening of the interparticle distance induced by CB7, as the surface plasmon band shifts to longer wavelengths.

Inclusion of AcAm by CB7 does not disrupt the AuNP aggregation because the color of the solution does not change with the presence of AcAm in the system, therefore the programmed gold nanoparticle disaggregation process does not work for AcAm detection. However a few other molecules including RhB, tryptophan, histidine, cysteine and methionine do.

I would propose the following mechanisms for the AuNP disaggregation process:

1. Host-guest complex mechanism: the molecule forms host-guest complex with CB7, which disables CB7 from linking the AuNPs thus causing AuNPs to disaggregate. One factor contributing to the disaggregation is the size of the molecule, the second one is the property of the moiety that is not included by CB7 but has interactions with the portals; the third one is the property of the moiety that is immersed in the CB7 cavity. Complexed with CB7, the guest molecule prevents CB7 from interacting with adjacent AuNPs through carbonyl groups on its portals. The color of the solution is restored to ruby red.

2. Non host-guest complex mechanism: the strong interaction between sulfur-containing amino acids and AuNPs breaks the CB7 linkage among AuNPs. The reverse process of aggregation, disaggregation would occur. The color of the solution changes from purplish blue back to ruby red.

Based on the above proposals, in order to see if a molecule can be detected using AuNP disaggregation method, we can first check if it is a sulphur-containing compound or not. If it is, it could cause AuNP to disaggregate through mechanism 2. If it does not contain sulphur in its structure, but is a good guest of CB7 with the hydrophobic moiety containing nitrogen atom and the sticking out portion containing alanyl group, then this molecule could be a good candidate to cause AuNP to disaggregate through mechanism 1.

3.5 Future work

Future work can be expanded into the following areas.

For the detection of AcAm, attempt on conversion of AcAm to alanyl amantadine could be made. I would hope that alanyl amantadine would cause AuNP to disaggregate for the reasons already discussed.

The following work can be done for the general study of the method:

1. More experiments need to be conducted to prove the proposed mechanisms on this process. Experiments could include trying different sulphur-containing compounds on disaggregating AuNPs. Experiments need to be repeated to confirm the findings of order of addition on AuNP disaggregation.
2. One of the elements that affect LSPR is the size of the particles. I used 20 nm AuNP in this thesis. Next step would be to use a different size of gold particles, for example, 60 nm, to study the LSPR property for molecular sensing needs.

3. I used CB7 to link AuNPs to study disaggregation of the complex with various molecules. We could try to use other cucurbiturils, for example, CB5, to link the particles, to see how the system would behave with the addition of various guest molecules or sulphur-containing compounds. The volume of the hydrophobic cavity is smaller than that of CB7, guest of smaller sizes would fit to it, the sticking-out moiety may cause disaggregation of the gold nanoparticles. This would create a different set of sensing device based on the same concept of disaggregation.

   Study can be expanded to CB8, etc.

4. More work can be done on the selection of metal nanoparticles. I have used gold nanoparticles. This work can be expanded to some other plasmonic particles, such as silver.

3.6 Outlook

The effort of finding a better molecular sensing device for AcAm has resulted in some new findings on AuNP disaggregation. Even though the programmed AuNP disaggregation technique does not work for AcAm detection, it can be used for molecular sensing for the molecules we have tested, and it can be expanded to other molecules including sulphur-containing compounds. Further study is needed.

As introduced at the beginning of this chapter, CB7 molecules link AuNPs and "hot spots" are constructed among the particles with the inter-particle spacing fixed at 0.9 nm, where surface enhanced Raman spectroscopy (SERS) enhancement as high as 10^{10}-10^{14} is achieved. Molecules, such as Rhodamine 6G[88], dopamine, epinephrine, and serotonin

(Figure 3.20) that can be encapsulated by CB7 have been detected using SERS-based multiplexed sensing technique with very low detection limit (< 10^{-9} M).[98]

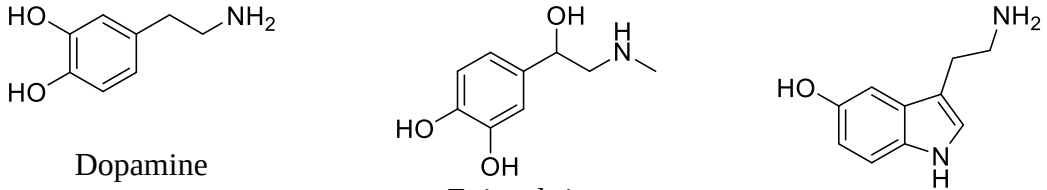

Dopamine Epinephrine Serotonin

Figure 3.20 Structures of neurotransmitters. Neurotransmitters: dopamine, epinephrine, and serotonin.

In order to use SERS for molecular sensing, the following requirements have to be met:

1. The analyte has to be encapsulated by CB7 in order to be placed in the "hot spot".
2. The analyte has to have good Raman signals.

It would be more difficult to make a point-of-care device using SERS due to the complexity of sample preparation and instrument setup and operation.

On the contrary, programmed gold nanoparticle disaggregation can be easily made into a point of care device because it is based on colorimetry technique, like a pregnancy test kit or a serum or urine drug screen test kit. Aggregation and disaggregation of AuNPs can be programmed with CB7 and analyte of interest.

Besides being easy to use and having the possibility of making a point of care device, programmed gold nanoparticle disaggregation has some other strengths including

high sensitivity and low limit of detection. It would be more specific than direct AuNP aggregation based sensing technique as fewer molecules would fit the criteria to either function as the guest of CB7 or to have direct interaction with AuNPs to break the CB7 linkages.

The weaknesses of the technique include sample preparation and the quality requirement of the AuNP solution used. It is the same case for all of the biological sample testing to go through sample processing, such as centrifuge. For our purpose, a general centrifugation of the sample would not be enough, because salts have to be removed in order for CB7 to work. Further sample treatment is necessary.

Because LSPR is dependent on factors such as the size and shape of the particles, uniform size, shape, distribution and dispersion of AuNP particles in solution are required.

When a method is found to remove the matrix inferences but to keep the analyte of interest intact in urine, this technique would make a great sensing device for molecules of biological important, such as tryptophan and cysteine.

Bibliography

1. WHO. http://www.who.int/mediacentre/factsheets/fs297/en/.
2. Canadian Cancer Statistics 2015.
3. Parker, M. S.; Groves, R. C.; Fowler, A. A. I.; Shepherd, R. W.; Cassano, A. D.; Cafaro, P. L.; Chestnut, G. T., Lung Cancer Screening With Low-dose Computed Tomography: An Analysis of the MEDCAC Decision. *Journal of Thoracic Imaging* **2015,** *30* (1), 15-23.
4. Global Burden of Disease Cancer, C., THe global burden of cancer 2013. *JAMA Oncology* **2015**.
5. Brooks, J. D., Translational genomics: The challenge of developing cancer biomarkers. *Genome Research* **2012,** *22* (2), 183-187.
6. He, L.; Long, L. R.; Antani, S.; Thoma, G. R., Histology image analysis for carcinoma detection and grading. *Computer methods and programs in biomedicine* **2012,** *107* (3), 538-556.
7. Azhari, E.-E. M.; Hatta, M. M. M.; Htike, Z. Z.; Win, S. L., Tumor detection in medical imaging: A survey. *International journal of Advanced Information Technology* **2014,** *4*.
8. Hemminki, K.; Liu, H.; Heminki, A.; Sundquist, J., Power and limits of modern cancer diagnostics: cancer of unknown primary. *Annals of oncology* **2012,** *23* (3), 760-764.
9. Wu, L.; Qu, X., Cancer biomarker detection: recent achievements and challenges. *Chemical Society Reviews* **2015,** *44* (10), 2963-2997.
10. Yi, X.; Wang, F.; Qin, W.; Yang, X.; Yuan, J., Near-infrared fluorescent probes in cancer imaging and therapy: an emerging field. *International Journal of Nanomedicine* **2014,** *9*, 1347-1365.
11. Jiang, S.; Gnanasammandhan, M. K.; Zhang, Y., Optical imaging-guided cancer therapy with fluorescent nanoparticles. *Journal of The Royal Society Interface* **2009,** *7* (42), 3-18.
12. Kulasingam, V.; Diamandis, E. P., Strategies for discovering novel cancer biomarkers through utilization of emerging technologies. *Nat Clin Prac Oncol* **2008,** *5* (10), 588-599.
13. Mishra, A.; Verma, M., Cancer Biomarkers: Are We Ready for the Prime Time? *Cancers* **2010,** *2* (1), 190.
14. (a) Andriole, G. L.; Crawford, E. D.; Grubb, R. L.; Buys, S. S.; Chia, D.; Church, T. R.; Fouad, M. N.; Isaacs, C.; Kvale, P. A.; Reding, D. J., Prostate cancer screening in the randomized Prostate, Lung, Colorectal, and Ovarian Cancer Screening Trial: mortality results after 13 years of follow-up. *Journal of the National Cancer Institute* **2012**; (b) Thompson, I. M.; Pauler, D. K.; Goodman, P. J.; Tangen, C. M.; Lucia, M. S.; Parnes, H. L.; Minasian, L. M.; Ford, L. G.; Lippman, S. M.; Crawford, E. D.; Crowley, J. J.; Coltman, C. A., Prevalence of Prostate Cancer among Men with a Prostate-Specific Antigen Level ≤4.0 ng per Milliliter. *New England Journal of Medicine* **2004,** *350* (22), 2239-2246.

15. SchrÖDer, F. H.; van der Cruijsen-Koeter, I.; de Koning, H. J.; Vis, A. N.; Hoedemaeker, R. F.; Kranse, R., PROSTATE CANCER DETECTION AT LOW PROSTATE SPECIFIC ANTIGEN. *The Journal of Urology* **2000,** *163* (3), 806-812.
16. Barry, M. J., Prostate-specific–antigen testing for early diagnosis of prostate cancer. *New England Journal of Medicine* **2001,** *344* (18), 1373-1377.
17. Moyer, V. A., Screening for prostate cancer: US Preventive Services Task Force recommendation statement. *Annals of internal medicine* **2012,** *157* (2), 120-134.
18. Zhang, H.; Cao, J.; Li, L.; Liu, Y.; Zhao, H.; Li, N.; Li, B.; Zhang, A.; Huang, H.; Chen, S.; Dong, M.; Yu, L.; Zhang, J.; Chen, L., Identification of urine protein biomarkers with the potential for early detection of lung cancer. *Scientific Reports* **2015,** *5*, 11805.
19. Pegg, A. E., Spermidine/spermine-N1-acetyltransferase: a key metabolic regulator. *American Journal of Physiology - Endocrinology and Metabolism* **2008,** *294* (6), E995-E1010.
20. Heather M. WALLACE, A. V. F. a. A. H., A perspective of polyamine metabolism. *Biochem. J.* **2003** *376*, 1-14.
21. Wallace, H. M.; Duthie, J.; Evans, D. M.; Lamond, S.; Nicoll, K. M.; Heys, S. D., Alterations in Polyamine Catabolic Enzymes in Human Breast Cancer Tissue. *Clinical Cancer Research* **2000,** *6* (9), 3657-3661.
22. Zhu, Y.-Q.; Zhu, D.-Y.; Yin, L.; Zhang, Y.; Vonrhein, C.; Wang, D.-C., Crystal structure of human spermidine/spermine N1-acetyltransferase (hSSAT): The first structure of a new sequence family of transferase homologous superfamily. *Proteins: Structure, Function, and Bioinformatics* **2006,** *63* (4), 1127-1131.
23. Pegg, A. E.; Hu, R.-H., Effect of polyamine analogues and inhibition of polyamine oxidase on spermidine/spermine N1-acetyltransferase activity and cell proliferation. *Cancer Letters* **1995,** *95* (1–2), 247-252.
24. Danell S. Sitar, A. P. M. B. Method for Assaying Non-Spermine/Spermidine Activity of N1-Acetyltransferase (SSAT), US6811967 B2, 2004.
25. (a) Persson, L.; Rosengren, E., Increased formation of N1-acetylspermidine in human breast cancer. *Cancer Letters* **1989,** *45* (2), 83-86; (b) Murray-Stewart, T.; Applegren, N. B.; Devereux, W.; Hacker, A.; Smith, R.; Wang, Y.; Casero, R. A., Spermidine/spermine N1-acetyltransferase (SSAT) activity in human small-cell lung carcinoma cells following transfection with a genomic SSAT construct. *Biochemical Journal* **2003,** *373* (Pt 2), 629-634.
26. Porter, C. W., Methods for the use of spermidine/spermine N1 - acetyltransferase as a prognostic indicator and/or a tumor response marker. Google Patents: 1996.
27. Ooi, E. E.; Chew, J. S. W.; Loh, J. P.; Chua, R. C. S., In vitro inhibition of human influenza A virus replication by chloroquine. *Virology Journal* **2006,** *3*, 39-39.
28. Bright, R. A.; Shay, D. K.; Shu, B.; Cox, N. J.; Klimov, A. I., ADamantane resistance among influenza a viruses isolated early during the 2005-2006 influenza season in the united states. *JAMA* **2006,** *295* (8), 891-894.

29. Bras, A. P. M.; Jänne, J.; Porter, C. W.; Sitar, D. S., Spermidine/SpermineN 1-Acetyltransferase Catalyzes Amantadine Acetylation. *Drug Metabolism and Disposition* **2001,** *29* (5), 676-680.
30. D. S. Sitar, A. P. B., A. Maksymiuk, K. M. Cheng, and H. Zhou, Progress in the development of SSAT1 activity as a biomarker for diagnosis of cancer. In *BIT Life Sciences' Annual World Cancer Congress*, Beijing, 2009.
31. Sitar, D. S.; Bras, A. P.; Maksymiuk, A.; Pabbies, A.; Brandes, L.; Blakely, B. W., PI-12. *Clinical Pharmacology & Therapeutics* **2006,** *79* (2), P10-P10.
32. Armstrong, J. A., Urinalysis in Western culture: A brief history. *Kidney Int* **2006,** *71* (5), 384-387.
33. Bonifacio, A.; Cervo, S.; Sergo, V., Label-free surface-enhanced Raman spectroscopy of biofluids: fundamental aspects and diagnostic applications. *Anal Bioanal Chem* **2015**, 1-13.
34. Bouatra, S.; Aziat, F.; Mandal, R.; Guo, A. C.; Wilson, M. R.; Knox, C.; Bjorndahl, T. C.; Krishnamurthy, R.; Saleem, F.; Liu, P.; Dame, Z. T.; Poelzer, J.; Huynh, J.; Yallou, F. S.; Psychogios, N.; Dong, E.; Bogumil, R.; Roehring, C.; Wishart, D. S., The Human Urine Metabolome. *PLoS ONE* **2013,** *8* (9), e73076.
35. Strasinger, S. K.; Di Lorenzo, M. S., *Urinalysis and body fluids*. FA Davis: 2014.
36. Burtis, C. A.; Ashwood, E. R.; Bruns, D. E., *Tietz textbook of clinical chemistry and molecular diagnostics*. Elsevier Health Sciences: 2012.
37. Thompsen, J. C.; Mottola, H. A., Kinetics of the complexation of iron(II) with ferrozine. *Analytical Chemistry* **1984,** *56* (4), 755-757.
38. Roškar, R.; Lušin, T. T., *Analytical Methods for Quantification of Drug Metabolites in Biological Samples*. 2012.
39. Wang, G.-Q.; Qin, Y.-F.; Du, L.-M.; Li, J.-F.; Jing, X.; Chang, Y.-X.; Wu, H., Determination of amantadine and rimantadine using a sensitive fluorescent probe. *Spectrochimica Acta Part A: Molecular and Biomolecular Spectroscopy* **2012,** *98* (0), 275-281.
40. Ocampo, A. P.; Hoyt, K. D.; Wadgaonkar, N.; Carver, A. H.; Puglisi, C. V., Determination of tazobactam and piperacillin in human plasma, serum, bile and urine by gradient elution reversed-phase high-performance liquid chromatography. *Journal of Chromatography B: Biomedical Sciences and Applications* **1989,** *496* (0), 167-179.
41. Mei, H.; Hsieh, Y.; Nardo, C.; Xu, X.; Wang, S.; Ng, K.; Korfmacher, W. A., Investigation of matrix effects in bioanalytical high-performance liquid chromatography/tandem mass spectrometric assays: application to drug discovery. *Rapid Communications in Mass Spectrometry* **2003,** *17* (1), 97-103.
42. Taylor, P. J., Matrix effects: the Achilles heel of quantitative high-performance liquid chromatography–electrospray–tandem mass spectrometry. *Clinical Biochemistry* **2005,** *38* (4), 328-334.
43. Marchi, I.; Rudaz, S.; Veuthey, J.-L., Sample preparation development and matrix effects evaluation for multianalyte determination in urine. *Journal of Pharmaceutical and Biomedical Analysis* **2009,** *49* (2), 459-467.

44. Rogers, C. W.; Wolf, M. O., Luminescent molecular sensors based on analyte coordination to transition-metal complexes. *Coordination Chemistry Reviews* **2002,** *233–234* (0), 341-350.
45. Wiskur, S. L.; Ait-Haddou, H.; Lavigne, J. J.; Anslyn, E. V., Teaching Old Indicators New Tricks. *Accounts of Chemical Research* **2001,** *34* (12), 963-972.
46. Martínez-Máñez, R.; Sancenón, F., Fluorogenic and Chromogenic Chemosensors and Reagents for Anions. *Chemical Reviews* **2003,** *103* (11), 4419-4476.
47. Carl A. Burtis, E. R. A., and David E. Bruns, *Tietz textbook of clinical chemistry and molecular diagnostics*. Elsevier Saunders: 2006; Vol. 4th Edition.
48. Richard, J. H., *Clinical Chemistry: Principles and Technics, 2nd Edition*. Harper & Row Publishers, Inc. : New York, 1974.
49. Vo-Dinh, T., SERS chemical sensors and biosensors: new tools for environmental and biological analysis. *Sensors and Actuators B: chemical* **1995,** *29* (1), 183-189.
50. Dudley H. Williams, I. F., *Spectroscopic Methods in Organic Chemistry*. 5 ed.; The McGraw-Hill Companies: 1995.
51. McDonagh, C.; Burke, C. S.; MacCraith, B. D., Optical Chemical Sensors. *Chemical Reviews* **2008,** *108* (2), 400-422.
52. Mirkin, C. A.; Ratner, M. A., Molecular Electronics. *Annual Review of Physical Chemistry* **1992,** *43* (1), 719-754.
53. Nguyen, B. T.; Anslyn, E. V., Indicator–displacement assays. *Coordination Chemistry Reviews* **2006,** *250* (23–24), 3118-3127.
54. Ghale, G.; Nau, W. M., Dynamically Analyte-Responsive Macrocyclic Host–Fluorophore Systems. *Accounts of Chemical Research* **2014,** *47* (7), 2150-2159.
55. Inouye, M.; Hashimoto, K.-i.; Isagawa, K., Nondestructive Detection of Acetylcholine in Protic Media: Artificial-Signaling Acetylcholine Receptors. *Journal of the American Chemical Society* **1994,** *116* (12), 5517-5518.
56. Metzger, A.; Lynch, V. M.; Anslyn, E. V., A Synthetic Receptor Selective for Citrate. *Angewandte Chemie International Edition in English* **1997,** *36* (8), 862-865.
57. Lavigne, J. J.; Anslyn, E. V., Teaching Old Indicators New Tricks: A Colorimetric Chemosensing Ensemble for Tartrate/Malate in Beverages. *Angewandte Chemie International Edition* **1999,** *38* (24), 3666-3669.
58. Tobey, S. L.; Jones, B. D.; Anslyn, E. V., C3v Symmetric Receptors Show High Selectivity and High Affinity for Phosphate. *Journal of the American Chemical Society* **2003,** *125* (14), 4026-4027.
59. Niikura, K.; Anslyn, E. V., Triton X-100 Enhances Ion-Pair-Driven Molecular Recognition in Aqueous Media. Further Work on a Chemosensor for Inositol Trisphosphate. *The Journal of Organic Chemistry* **2003,** *68* (26), 10156-10157.
60. Wiskur, S. L.; Anslyn, E. V., Using a Synthetic Receptor to Create an Optical-Sensing Ensemble for a Class of Analytes: A Colorimetric Assay for the

Aging of Scotch. *Journal of the American Chemical Society* **2001,** *123* (41), 10109-10110.

61. Zhong, Z.; Anslyn, E. V., A Colorimetric Sensing Ensemble for Heparin. *Journal of the American Chemical Society* **2002,** *124* (31), 9014-9015.
62. Zhang, T.; Anslyn, E. V., A Colorimetric Boronic Acid Based Sensing Ensemble for Carboxy and Phospho Sugars. *Organic Letters* **2006,** *8* (8), 1649-1652.
63. Sakakibara, K.; Joyce, L. A.; Mori, T.; Fujisawa, T.; Shabbir, S. H.; Hill, J. P.; Anslyn, E. V.; Ariga, K., A Mechanically Controlled Indicator Displacement Assay. *Angewandte Chemie International Edition* **2012,** *51* (38), 9643-9646.
64. Ghale, G.; Lanctôt, A. G.; Kreissl, H. T.; Jacob, M. H.; Weingart, H.; Winterhalter, M.; Nau, W. M., Chemosensing ensembles for monitoring biomembrane transport in real time. *Angewandte Chemie International Edition* **2014,** *53* (10), 2762-2765.
65. Norouzy, A.; Azizi, Z.; Nau, W. M., Indicator Displacement Assays Inside Live Cells. *Angewandte Chemie International Edition* **2015,** *54* (3), 792-795.
66. Moragues, M. E.; Martinez-Manez, R.; Sancenon, F., Chromogenic and fluorogenic chemosensors and reagents for anions. A comprehensive review of the year 2009. *Chemical Society Reviews* **2011,** *40* (5), 2593-2643.
67. Agasti, S. S.; Rana, S.; Park, M.-H.; Kim, C. K.; You, C.-C.; Rotello, V. M., Nanoparticles for detection and diagnosis. *Advanced Drug Delivery Reviews* **2010,** *62* (3), 316-328.
68. Ghosh, S. K.; Pal, T., Interparticle Coupling Effect on the Surface Plasmon Resonance of Gold Nanoparticles: From Theory to Applications. *Chemical Reviews* **2007,** *107* (11), 4797-4862.
69. Jain, P. K.; Huang, X.; El-Sayed, I. H.; El-Sayed, M. A., Noble Metals on the Nanoscale: Optical and Photothermal Properties and Some Applications in Imaging, Sensing, Biology, and Medicine. *Accounts of Chemical Research* **2008,** *41* (12), 1578-1586.
70. Myroshnychenko, V.; Rodriguez-Fernandez, J.; Pastoriza-Santos, I.; Funston, A. M.; Novo, C.; Mulvaney, P.; Liz-Marzan, L. M.; Garcia de Abajo, F. J., Modelling the optical response of gold nanoparticles. *Chemical Society Reviews* **2008,** *37* (9), 1792-1805.
71. Unser, S.; Bruzas, I.; He, J.; Sagle, L., Localized Surface Plasmon Resonance Biosensing: Current Challenges and Approaches. *Sensors* **2015,** *15* (7), 15684.
72. Link, S.; El-Sayed, M. A., Size and Temperature Dependence of the Plasmon Absorption of Colloidal Gold Nanoparticles. *The Journal of Physical Chemistry B* **1999,** *103* (21), 4212-4217.
73. Kelly, K. L.; Coronado, E.; Zhao, L. L.; Schatz, G. C., The Optical Properties of Metal Nanoparticles: The Influence of Size, Shape, and Dielectric Environment. *The Journal of Physical Chemistry B* **2003,** *107* (3), 668-677.
74. Zeng, S.; Yong, K.-T.; Roy, I.; Dinh, X.-Q.; Yu, X.; Luan, F., A Review on Functionalized Gold Nanoparticles for Biosensing Applications. *Plasmonics* **2011,** *6* (3), 491-506.

75. Liu, X.; Atwater, M.; Wang, J.; Huo, Q., Extinction coefficient of gold nanoparticles with different sizes and different capping ligands. *Colloids and Surfaces B: Biointerfaces* **2007,** *58* (1), 3-7.
76. Jain, P. K.; Lee, K. S.; El-Sayed, I. H.; El-Sayed, M. A., Calculated Absorption and Scattering Properties of Gold Nanoparticles of Different Size, Shape, and Composition: Applications in Biological Imaging and Biomedicine. *The Journal of Physical Chemistry B* **2006,** *110* (14), 7238-7248.
77. Stewart, M. E.; Anderton, C. R.; Thompson, L. B.; Maria, J.; Gray, S. K.; Rogers, J. A.; Nuzzo, R. G., Nanostructured Plasmonic Sensors. *Chemical Reviews* **2008,** *108* (2), 494-521.
78. Cao, X.; Ye, Y.; Liu, S., Gold nanoparticle-based signal amplification for biosensing. *Analytical Biochemistry* **2011,** *417* (1), 1-16.
79. Elghanian, R.; Storhoff, J. J.; Mucic, R. C.; Letsinger, R. L.; Mirkin, C. A., Selective Colorimetric Detection of Polynucleotides Based on the Distance-Dependent Optical Properties of Gold Nanoparticles. *Science* **1997,** *277* (5329), 1078-1081.
80. Aslan, K.; Lakowicz, J. R.; Geddes, C. D., Nanogold-plasmon-resonance-based glucose sensing. *Analytical Biochemistry* **2004,** *330* (1), 145-155.
81. Aslan, K.; Lakowicz, J. R.; Geddes, C. D., Nanogold Plasmon Resonance-Based Glucose Sensing. 2. Wavelength-Ratiometric Resonance Light Scattering. *Analytical Chemistry* **2005,** *77* (7), 2007-2014.
82. Liu, J.; Lu, Y., Fast Colorimetric Sensing of Adenosine and Cocaine Based on a General Sensor Design Involving Aptamers and Nanoparticles. *Angewandte Chemie International Edition* **2006,** *45* (1), 90-94.
83. Liu, J.; Mazumdar, D.; Lu, Y., A Simple and Sensitive "Dipstick" Test in Serum Based on Lateral Flow Separation of Aptamer-Linked Nanostructures. *Angewandte Chemie International Edition* **2006,** *45* (47), 7955-7959.
84. Du, J.; Zhu, B.; Chen, X., Urine for Plasmonic Nanoparticle-Based Colorimetric Detection of Mercury Ion. *Small* **2013,** *9* (24), 4104-4111.
85. Folin, O., Laws governing the chemical composition of urine. *American Journal of Physiology--Legacy Content* **1905,** *13* (1), 66-115.
86. Howes, P. D.; Chandrawati, R.; Stevens, M. M., Colloidal nanoparticles as advanced biological sensors. *Science* **2014,** *346* (6205).
87. Tserkezis, C.; Taylor, R. W.; Beitner, J.; Esteban, R.; Baumberg, J. J.; Aizpurua, J., Optical Response of Metallic Nanoparticle Heteroaggregates with Subnanometric Gaps. *Particle & Particle Systems Characterization* **2014,** *31* (1), 152-160.
88. Taylor, R. W.; Lee, T.-C.; Scherman, O. A.; Esteban, R.; Aizpurua, J.; Huang, F. M.; Baumberg, J. J.; Mahajan, S., Precise Subnanometer Plasmonic Junctions for SERS within Gold Nanoparticle Assemblies Using Cucurbit[n]uril "Glue". *ACS Nano* **2011,** *5* (5), 3878-3887.
89. An, Q.; Li, G.; Tao, C.; Li, Y.; Wu, Y.; Zhang, W., A general and efficient method to form self-assembled cucurbit[n]uril monolayers on gold surfaces. *Chemical Communications* **2008,** (17), 1989-1991.
90. Lagona, J.; Mukhopadhyay, P.; Chakrabarti, S.; Isaacs, L., The Cucurbit[n]uril Family. *Angewandte Chemie International Edition* **2005,** *44* (31), 4844-4870.

91. Herrmann, L. O.; Valev, V. K.; Tserkezis, C.; Barnard, J. S.; Kasera, S.; Scherman, O. A.; Aizpurua, J.; Baumberg, J. J., Threading plasmonic nanoparticle strings with light. *Nat Commun* **2014,** *5*.
92. Chen, J. I. L.; Chen, Y.; Ginger, D. S., Plasmonic Nanoparticle Dimers for Optical Sensing of DNA in Complex Media. *Journal of the American Chemical Society* **2010,** *132* (28), 9600-9601.
93. Nau, W. M., Supramolecular capsules: Under control. *Nat Chem* **2010,** *2* (4), 248-250.
94. Ma, D.; Hettiarachchi, G.; Nguyen, D.; Zhang, B.; Wittenberg, J. B.; Zavalij, P. Y.; Briken, V.; Isaacs, L., Acyclic cucurbit[n]uril molecular containers enhance the solubility and bioactivity of poorly soluble pharmaceuticals. *Nat Chem* **2012,** *4* (6), 503-510.
95. Marquez, C.; Nau, W. M., Polarizabilities Inside Molecular Containers. *Angewandte Chemie International Edition* **2001,** *40* (23), 4387-4390.
96. Kim, J.; Jung, I.-S.; Kim, S.-Y.; Lee, E.; Kang, J.-K.; Sakamoto, S.; Yamaguchi, K.; Kim, K., New Cucurbituril Homologues: Syntheses, Isolation, Characterization, and X-ray Crystal Structures of Cucurbit[n]uril (n = 5, 7, and 8). *Journal of the American Chemical Society* **2000,** *122* (3), 540-541.
97. Werner M. Nau, a. J. M., Taming fluorescent dyes with cucurbituril. *International Journal of Photoenergy* **2005,** *07* (3), 133-141.
98. Kasera, S.; Herrmann, L. O.; Barrio, J. d.; Baumberg, J. J.; Scherman, O. A., Quantitative multiplexing with nano-self-assemblies in SERS. *Sci. Rep.* **2014,** *4*.
99. (a) Márquez, C.; Hudgins, R. R.; Nau, W. M., Mechanism of Host−Guest Complexation by Cucurbituril. *Journal of the American Chemical Society* **2004,** *126* (18), 5806-5816; (b) Biedermann, F.; Uzunova, V. D.; Scherman, O. A.; Nau, W. M.; De Simone, A., Release of High-Energy Water as an Essential Driving Force for the High-Affinity Binding of Cucurbit[n]urils. *Journal of the American Chemical Society* **2012,** *134* (37), 15318-15323.
100. Liu, S.; Ruspic, C.; Mukhopadhyay, P.; Chakrabarti, S.; Zavalij, P. Y.; Isaacs, L., The Cucurbit[n]uril Family: Prime Components for Self-Sorting Systems. *Journal of the American Chemical Society* **2005,** *127* (45), 15959-15967.
101. Isaacs, L., Stimuli Responsive Systems Constructed Using Cucurbit[n]uril-Type Molecular Containers. *Accounts of Chemical Research* **2014,** *47* (7), 2052-2062.
102. Cram, D. J., Molecular container compounds. *Nature* **1992,** *356* (6364), 29-36.
103. Parvari, G.; Reany, O.; Keinan, E., Applicable properties of cucurbiturils. *Israel Journal of Chemistry* **2011,** *51* (5-6), 646-663.
104. Dsouza, R. N.; Pischel, U.; Nau, W. M., Fluorescent Dyes and Their Supramolecular Host/Guest Complexes with Macrocycles in Aqueous Solution. *Chemical Reviews* **2011,** *111* (12), 7941-7980.
105. Chang, Y.-X.; Qiu, Y.-Q.; Du, L.-M.; Li, C.-F.; Guo, M., Determination of ranitidine, nizatidine, and cimetidine by a sensitive fluorescent probe. *Analyst* **2011,** *136* (20), 4168-4173.

106. Yang, J.; Du, L.; Wu, H.; Chang, Y.; Li, C., Determination of L-Cystine by a New Sensitive Cucurbit[7]uril/palmatine Probe. *Chinese Journal of Chemistry* **2011,** *29* (6), 1268-1272.
107. Li, C. F.; Du, L. M.; Wu, H.; Chang, Y. X., Determination of l-phenylalanine by cucurbit[7]uril sensitized fluorescence quenching method. *Chinese Chemical Letters* **2011,** *22* (7), 851-854.
108. Wang, G.-Q.; Du, L.-M.; Guo, Y.-H.; Qin, Y.-F.; Wang, J.-W.; Wu, H., Study on the supramolecular interaction of astemizole with cucurbit[7]uril and its analytical application. *Analytical Methods* **2013,** *5* (1), 173-179.
109. Zhou, Y.; Yu, H.; Zhang, L.; Xu, H.; Wu, L.; Sun, J.; Wang, L., A new spectrofluorometric method for the determination of nicotine base on the inclusion interaction of methylene blue and cucurbit[7]uril. *Microchim Acta* **2009,** *164* (1-2), 63-68.
110. Li, C.; Feng, J.; Ju, H., Supramolecular interaction of labetalol with cucurbit[7]uril for its sensitive fluorescence detection. *Analyst* **2015,** *140* (1), 230-235.
111. Wu, W.-Y.; Yang, J.-Y.; Du, L.-M.; Wu, H.; Li, C.-F., Determination of ethambutol by a sensitive fluorescent probe. *Spectrochimica Acta Part A: Molecular and Biomolecular Spectroscopy* **2011,** *79* (3), 418-422.
112. Li, Y.; Li, C.-F.; Du, L.-M.; Feng, J.-X.; Liu, H.-L.; Fu, Y.-L., A competitive strategy based on cucurbit[7]uril supramolecular interaction for simple and sensitive detection of dibucaine. *Talanta* **2015,** *132* (0), 653-657.
113. Magde, D.; Rojas, G. E.; Seybold, P. G., Solvent Dependence of the Fluorescence Lifetimes of Xanthene Dyes. *Photochemistry and Photobiology* **1999,** *70* (5), 737-744.
114. Ramette, R. W.; Sandell, E. B., Rhodamine B Equilibria. *Journal of the American Chemical Society* **1956,** *78* (19), 4872-4878.
115. Halterman, R. L.; Moore, J. L.; Yakshe, K. A.; Halterman, J. A.; Woodson, K. A., Inclusion complexes of cationic xanthene dyes in cucurbit [7] uril. *Journal of Inclusion Phenomena and Macrocyclic Chemistry* **2010,** *66* (3-4), 231-241.
116. Halterman, R.; Moore, J.; Yip, W., Cucurbit[7]uril Disrupts Aggregate Formation Between Rhodamine B Dyes Covalently Attached to Glass Substrates. *J Fluoresc* **2011,** *21* (4), 1467-1478.
117. Takayama, H.; Takahashi, S.; Moriya, T.; Osada, H.; Iwabuchi, Y.; Kanoh, N., Detection of Cytochrome P450 Substrates by Using a Small-Molecule Droplet Array on an NADH-Immobilized Solid Surface. *ChemBioChem* **2011,** *12* (18), 2748-2752.
118. Li, Y. P.; Wu, H.; Du, L. M., Study on the inclusion interactions of berberine hydrochloride and cucurbit [7] by spectrofluorimetry. *Chinese Chemical Letters* **2009,** *20* (3), 322-325.
119. Halterman, R.; Moore, J.; Yakshe, K.; Halterman, J. I.; Woodson, K., Inclusion complexes of cationic xanthene dyes in cucurbit[7]uril. *Journal of Inclusion Phenomena and Macrocyclic Chemistry* **2010,** *66* (3-4), 231-241.
120. Khedkar, J.; Jagtap, K.; Pinjari, R.; Ray, A.; Gejji, S., Binding of rhodamine B and kiton red S to cucurbit[7]uril: density functional investigations. *J Mol Model* **2012,** *18* (8), 3743-3750.

121. Megyesi, M.; Biczók, L.; Jablonkai, I., Highly Sensitive Fluorescence Response to Inclusion Complex Formation of Berberine Alkaloid with Cucurbit[7]uril. *The Journal of Physical Chemistry C* **2008,** *112* (9), 3410-3416.
122. Wang, G.-Q.; Guo, L.; Du, L.-M.; Fu, Y.-L., Competitive supramolecular interaction of carbachol and berberine with cucurbit[7]uril and its analytical application. *Microchemical Journal* **2013,** *110* (0), 285-291.
123. Dong, N.; Cheng, L.-n.; Wang, X.-l.; Li, Q.; Dai, C.-y.; Tao, Z., Significant fluorescence enhancement by supramolecular complex formation between berberine chloride and cucurbit(n = 7)uril and its analytical application. *Talanta* **2011,** *84* (3), 684-689.
124. Barrow, S. J.; Kasera, S.; Rowland, M. J.; del Barrio, J.; Scherman, O. A., Cucurbituril-Based Molecular Recognition. *Chemical Reviews* **2015,** *115* (22), 12320-12406.
125. Jeon, Y.-M.; Kim, J.; Whang, D.; Kim, K., Molecular Container Assembly Capable of Controlling Binding and Release of Its Guest Molecules: Reversible Encapsulation of Organic Molecules in Sodium Ion Complexed Cucurbituril. *Journal of the American Chemical Society* **1996,** *118* (40), 9790-9791.
126. Payne, S.; Eardley, I.; O'Flynn, K., *Imaging and Technology in Urology: Principles and Clinical Applications*. Springer Science & Business Media: 2012.
127. Tietz, N., *Tietz textbook of clinical chemistry and molecular diagnostics-/[ed. by] Carl A. Burtis, Edward R. Ashwood, David E. Bruns*. St. Louis, Mo: Elsevier Saunders: 2006.
128. Milam, V. T.; Hiddessen, A. L.; Crocker, J. C.; Graves, D. J.; Hammer, D. A., DNA-Driven Assembly of Bidisperse, Micron-Sized Colloids. *Langmuir* **2003,** *19* (24), 10317-10323.
129. Mirkin, C. A.; Letsinger, R. L.; Mucic, R. C.; Storhoff, J. J., A DNA-based method for rationally assembling nanoparticles into macroscopic materials. *Nature* **1996,** *382* (6592), 607-609.
130. Connolly, S.; Fitzmaurice, D., Programmed assembly of gold nanocrystals in aqueous solution. *Advanced Materials* **1999,** *11* (14), 1202-1205.
131. Caruso, F., Nanoengineering of particle surfaces. *Advanced Materials* **2001,** *13* (1), 11-22.
132. Shenton, W.; Davis, S. A.; Mann, S., Directed Self-Assembly of Nanoparticles into Macroscopic Materials Using Antibody–Antigen Recognition. *Advanced Materials* **1999,** *11* (6), 449-452.
133. Saha, K.; Agasti, S. S.; Kim, C.; Li, X.; Rotello, V. M., Gold nanoparticles in chemical and biological sensing. *Chemical reviews* **2012,** *112* (5), 2739-2779.
134. Assaf, K. I.; Nau, W. M., Cucurbiturils: from synthesis to high-affinity binding and catalysis. *Chemical Society Reviews* **2015,** *44* (2), 394-418.
135. Feng, Y.; Xue, S.-F.; Fan, Z.-F.; Zhang, Y.-Q.; Zhu, Q.-J.; Tao, Z., Host–guest complexes of some cucurbit [n] urils with the hydrochloride salts of some imidazole derivatives. *Journal of Inclusion Phenomena and Macrocyclic Chemistry* **2009,** *64* (1-2), 121-131.

136. Kim, K.; Ko, Y. H.; Lee, S. H.; Narayanan, S.; Lee, D. W., Composition for odor removal and fragrance emission comprising complexes of cucurbituril and fragrance. Google Patents: 2014.
137. Lee, J. W.; Lee, H. H. L.; Ko, Y. H.; Kim, K.; Kim, H. I., Deciphering the Specific High-Affinity Binding of Cucurbit[7]uril to Amino Acids in Water. *The Journal of Physical Chemistry B* **2015,** *119* (13), 4628-4636.
138. Fritz, M. C.; Hähner, G.; Spencer, N. D.; Bürli, R.; Vasella, A., Self-Assembled Hexasaccharides: Surface Characterization of Thiol-Terminated Sugars Adsorbed on a Gold Surface. *Langmuir* **1996,** *12* (25), 6074-6082.
139. Grönbeck, H.; Curioni, A.; Andreoni, W., Thiols and Disulfides on the Au(111) Surface: The Headgroup−Gold Interaction. *Journal of the American Chemical Society* **2000,** *122* (16), 3839-3842.
140. Jain, P. K.; Qian, W.; El-Sayed, M. A., Ultrafast cooling of photoexcited electrons in gold nanoparticle-thiolated DNA conjugates involves the dissociation of the gold-thiol bond. *Journal of the American Chemical Society* **2006,** *128* (7), 2426-2433.
141. Ulman, A., Formation and structure of self-assembled monolayers. *Chemical reviews* **1996,** *96* (4), 1533-1554.

Appendices

Appendix 1 AcAm NMR spectrum

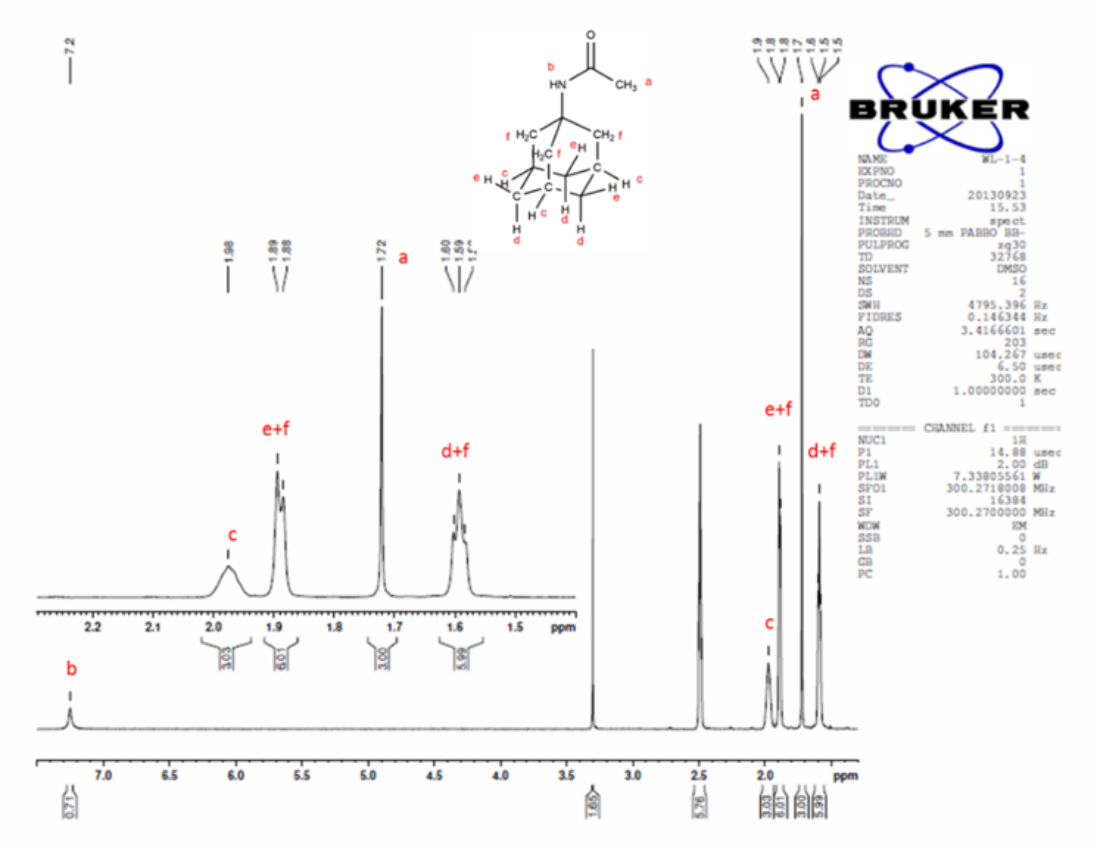

Appendix 2 AcAm MS spectra compared with that of NIST library.

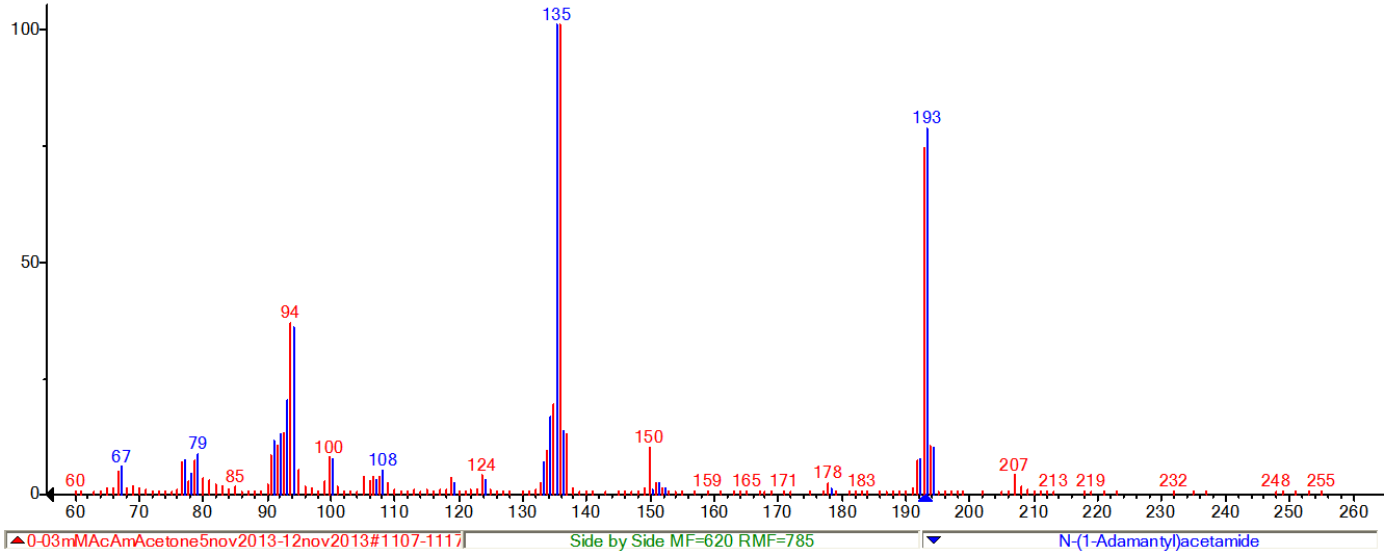

Spectra in red: synthesized AcAm; Spectra in blue: AcAm from NIST library.